UILU-ENG-98-0409

DYNAMIC HYBRID ELECTRIC VEHICLE SIMULATION
Version 1.0

DANIEL L. LOGUE
PHILIP T. KREIN

Power Affiliates Program
Department of Electrical and Computer Engineering
University of Illinois at Urbana-Champaign
Urbana, Illinois 61801

PAP-TR-98-6
December 1998

Table of Contents

List of Figures

1 Introduction

This report discusses a dynamic Hybrid Electric Vehicle (HEV) simulator developed within the MATLAB/SIMULINK programming language. The word hybrid refers to there existing two onboard energy sources, an Internal Combustion Engine (ICE) and a battery pack. The ICE is sized to provide the average road power required by the vehicle and the battery pack provides the necessary transient power for acceleration. The battery pack also absorbs the vehicle's kinetic energy through regeneration during braking.

The ICE, along with a generator and rectifier, form what is referred to as the Auxiliary Power Unit (APU). The generator converts the mechanical energy from the ICE to electrical energy. The rectifier then converts the ac current provided by the generator into dc current which is utilized to charge the battery pack.

Traction power is provided by an induction motor. The motor torque and speed are scaled by the transmission to values applicable to driving the wheels. The motor torque is controlled by using a Pulse Width Modulated (PWM) electronic drive. The drive provides the necessary motor terminal voltages to give the desired shaft torque.

The HEV modeled here is of the series type. The word series refers to the energy provided from the ICE being channeled through all the vehicle components, generator, rectifier, battery pack, drive, motor, transmission, to finally arrive at the wheels. A series HEV uses the battery pack to attempt to de-couple the APU dynamics from the drive system dynamics. Another way of saying this is that the battery pack acts as a power filter between the APU and the drive system. If the transient power requirements of the drive system were imposed on the APU, the result would be very poor ICE efficiency. The APU should track the average load power slowly enough so that ICE efficiency is maintained at an acceptable level.

In reality, these two can not be completely de-coupled from one another because of the dependency of battery pack voltage on loading. During vehicle acceleration the battery pack voltage will tend to decrease because of increased motor current, and during braking the voltage will increase. If the rectifier doesn't act, the variation in battery pack voltage will create a variation in loading torque on the ICE. To prevent this, the rectifier attempts to maintain a constant current output.

A block diagram of the overall HEV system is shown in Figure 1. This figure shows explicitly what is meant by a series hybrid; the battery pack is positioned right in between the APU and the electronic drive. The next section will discuss the simulation models of each of these components.

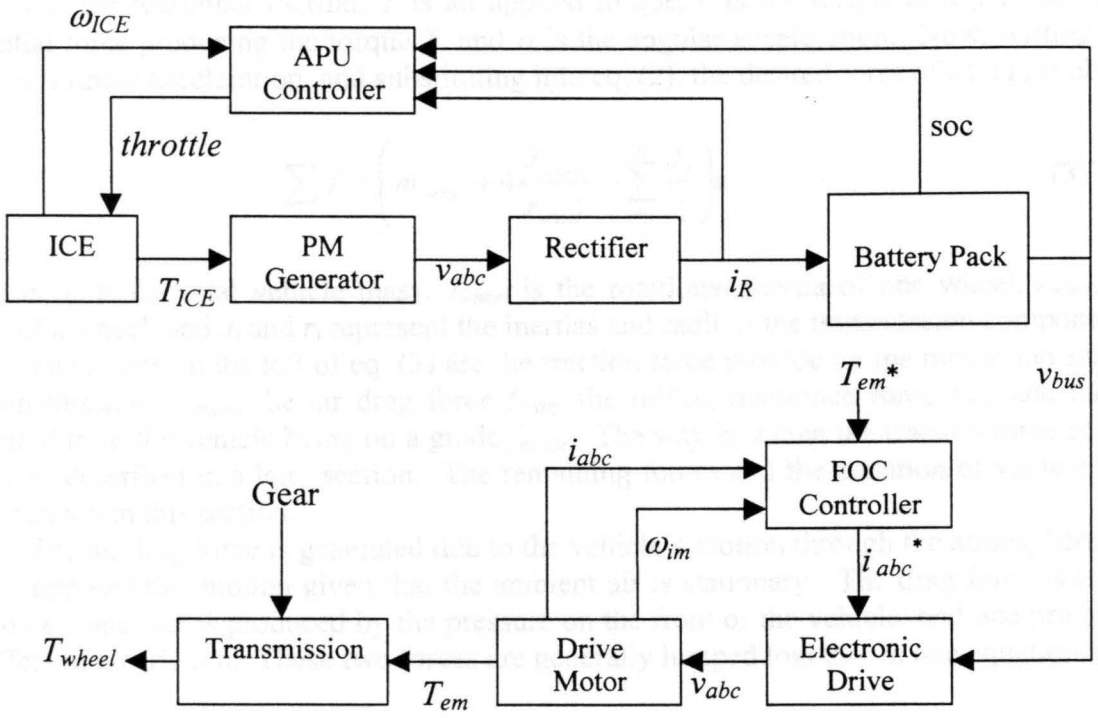

Figure 1: Block diagram of HEV structure.

2 Simulation Models

This section details the component models used in the HEV simulation. First, the model will be discussed and then its implementation into the simulation will be explained. In addition, simulation results from most of the individual subsystem components are provided.

2.1 Vehicle Road Dynamics

The vehicle dynamics model describes how the vehicle's motion is related to the transmission driving torque as well as to external forces such as tire resistance and air drag. The vehicle's acceleration is determined from Newton's second law

$$\sum f_{vehicle} = m_{equivalent} a \tag{1}$$

where $m_{equivalent}$ is the equivalent lumped inertia of the vehicle's total mass and the rotating mass of the wheels and the transmission. The equivalent translational inertial of the rotating mass is found by first writing

$$T = J\alpha = fr \Rightarrow f = \frac{J\alpha}{r} \tag{2}$$

where J is the rotational inertial, T is an applied torque, r is the torque arm, f is the applied tangential force producing the torque T, and α is the angular acceleration. Now, writing α=a/r, where a is linear acceleration, and substituting into eq. (2), the desired form of eq. (1) is obtained

$$\sum f = \left(m_{totoal} + 4\frac{J_{wheel}}{r_{wheel}} + \sum_{i=1}^{N} \frac{J_i}{r_i} \right) a \tag{3}$$

where m_{total} is the total vehicle mass, J_{wheel} is the rotational inertia of one wheel, r_{wheel} is the radius of a wheel, and J_i and r_i represent the inertias and radii of the transmission components.

The forces on the left of eq. (3) are the traction force provide by the motor and scaled by the transmission $f_{traction}$, the air drag force f_{drag}, the rolling resistance force f_{tire}, and the force generated from the vehicle being on a grade f_{grade}. The way in which the traction force is arrived at will be described in a later section. The remaining forces and the equation of vehicle motion are described in this section.

The air drag force is generated due to the vehicle's motion through the atmosphere, and it always opposes this motion given that the ambient air is stationary. The drag force is a sum of two forces, one that is produced by the pressure on the front of the vehicle, and one produced by the effect of air friction. These two forces are generally lumped together in one equation as [1]

$$f_{drag} = \frac{1}{2} C_d \rho A_f v^2 \tag{4}$$

where C_d is what is known as the drag coefficient, ρ is the ambient air density, A_f is the frontal area of the vehicle, and v is the vehicle's velocity. The drag coefficient for the UI HEV was experimentally determined in [2] to be 0.34.

The force from rolling resistance is created due to the continual tire deformation as the rotates under the weight of the vehicle. This force always opposes the vehicle's motion and is independent of vehicle speed up to a certain limit. The rolling resistance is heavily dependent on the tire pressure because the tire pressure determines the severity of tire deformation. Assuming that the tire pressure is constant, the rolling resistance may be expressed as [1]

$$f_{tire} = R_{tire} m_{total} g \tag{5}$$

where R_{tire} is an experimentally determined constant, and g is the gravitational acceleration constant equal to 9.81 m/s^2. The value of R_{tire} for the UI HEV was experimentally determined in [2] to be 0.00993.

When the vehicle encounters a non-zero road grade, there is a gravitational force component in line with the vehicle's motion. This force can oppose or assist vehicle motion depending on whether the slope is positive or negative. Consider the situation depicted in Figure 2. The mass of the vehicle is represented by the block labeled m, f_g is the gravitational force in line with the vehicle, v is the vehicle's velocity, and θ is the road grade angle. The force f_g is then given by

$$f_g = mg\cos(90^\circ - \theta) = mg\sin(\theta) \tag{6}$$

The force f_g shown in Figure 2 opposes the vehicle's motion. If the grade angle had been negative, the force f_g would aid in the vehicle's motion.

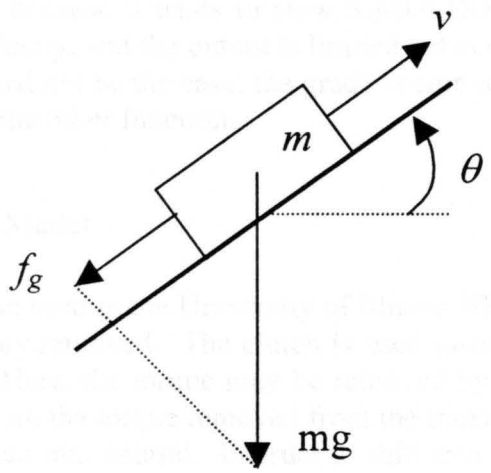

Figure 2: Vehicle on a grade.

Given these forces, the equation of motion for the vehicle is given by

$$m_i a = f_{traction} - \frac{1}{2} C_d \rho A_f v^2 - R_{tire} mg - mg \sin(\theta) \tag{7}$$

where m_i is the equivalent mass given in eq. (3), a is the vehicle acceleration, v is the vehicle velocity, θ is the road grade angle, and $f_{traction}$ is the traction force provide by the transmission. The SIMULINK block representing this equation of motion is shown in Figure 3.

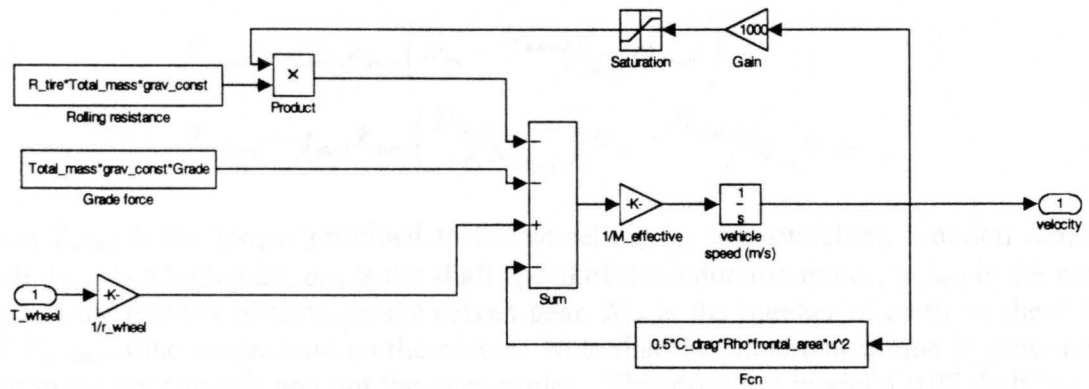

Figure 3: Vehicle dynamics block.

The wheel torque supplied by the transmission is converted to a force by dividing by the wheel radius. This force and the forces described above are summed, scaled by the equivalent mass, and integrated to provide the vehicle velocity. To provide correct operation, the rolling resistance force must be multiplied by the sign of the velocity. This force always opposes vehicle motion. In addition, it must be multiplied by zero when the velocity is zero. A sign block is not used here because it tends to slow SIMULINK down incredibly. Instead, a very high gain scales the velocity, and the output is limited between –1 and +1. The grade is assumed to be constant. This need not be the case; the grade vector could be supplied as a function of the distance traveled, or some other function.

2.2 Transmission Model

The transmission used in the University of Illinois HEV (UI HEV) is a five speed manual with the clutch assembly removed. The clutch is used to remove the motor driving torque in a conventional vehicle. Here, the torque may be removed by simply commanding zero torque to the electronic drive. With the torque removed from the transmission input shaft, the transmission can be shifted out of gear into neutral. In order to shift into another gear, the two meshing gears must be synchronized in some way. In a conventional vehicle this is done using so called synchronizing rings. The synchronizers produce friction between the two gears, bringing their speeds into synchronization.

The UI HEV uses an entirely different approach. The driving gear is brought to synchronous speed by the motor. This is done by using a Proportional-Integral (PI) control loop with the speed error of the two gears as the input. Once the driving gear is at synchronous speed, the two may easily mesh. After the gears have meshed, torque control of the motor is returned to the driver. This type of synchronization is possible because of the fast response of the induction motor driving the HEV. A conventional ICE is much too slow and too difficult to control in this manner.

The transmission is modeled as two gears connected by a torsional damper. The equations governing the transmission are

$$\begin{aligned} T_{wheel} &= q_{mesh} k_{trans} \left(\omega_{im} - N_{wheel} / N_{im} \, \omega_{wheel} \right) \\ T_{im\ load} &= q_{mesh} k_{trans} \left(N_{im} / N_{wheel} \right) \left(\omega_{im} - N_{wheel} / N_{im} \, \omega_{wheel} \right) \end{aligned} \tag{8}$$

where T_{wheel} is the torque provided to the wheels, q_{mesh} is a switching function indicating gear mesh, k_{trans} is a high gain, ω_{im} is the shaft speed of the induction motor, ω_{wheel} is the wheel speed, N_{wheel} is the number of teeth on the driven gear, N_{im} is the number of teeth on the driving gear, and $T_{im\ load}$ is the torque load on the motor. Note that the constraint torque is generated from an error in the gear speeds and not the gear angles. This does not model a stiff shaft but is suitable the purposes here so long as the gain k_{trans} is high. The variable q_{mesh} is one when the gears are meshed and zero when they are free. The block diagram modeling these equations is shown in Figure 4.

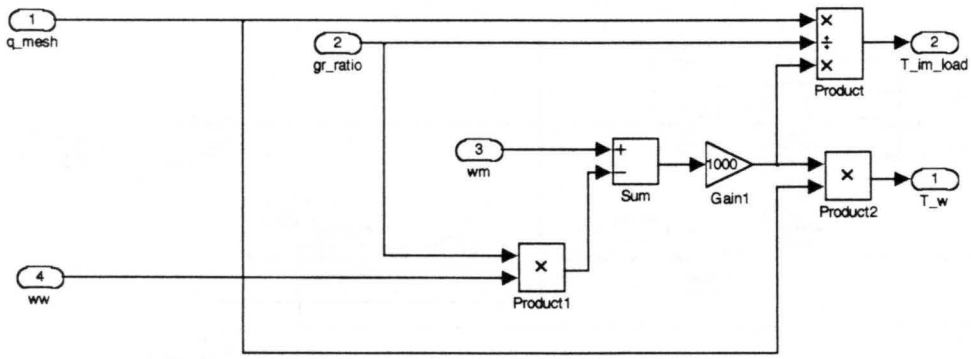

Figure 4: Model of transmission gear mesh.

The block that handles the shifting process is shown in Figure 5. The shifting block is used to determine the gear. It places a vehicle speed dependence on when the gears are shifted. By double clicking on this block, the speed at which each gear is shifted may be set. The backlash block places some hysteresis on this process. This is necessary because the vehicle speed will drop slightly while the shifting process occurs. Hysteresis prevents cycling between adjacent gears.

The flip-flop is a state machine that determines whether or not the gears are meshed. The inverted output of the flip-flop is used to indicate mesh. When the flip-flop is active, the shifting process is taking place. The flip-flop is clocked high when a change in gear ratio is detected. This is done by comparing the present gear ratio signal with a delayed version. The delay is very short, and so it doesn't affect operation.

When the flip-flop is set high, the transmission is immediately shifted to neutral by switch labeled disengagement, and the motor load torque and the traction torque are brought to zero by the multiplicative blocks in Figure 4. The commanded torque signal to the drive T_{em}* is now controlled by a PI controller by activation a switch block. The PI block in Figure 5 is used to control the motor speed to make the speed of the driving gear synchronize with that of the new driven gear. This is done by using a error signal generated by the comparison of the motor speed and the wheel speed scaled by the new gear ratio. The Abs block takes the absolute value of the error signal and compares it to a constant called *gear_eps*. Once the error falls below this value, the gears are assumed to be synchronized and meshing of the gears occurs by resetting the flip-flop. The slight error in the speeds is reduced to zero by resulting motor load torque and wheel torque described by eq. (8). Also, the torque signal to the drive T_{em}* is given back to the driver.

The loss associated with the transmission is dependent on the speed of the gear's rotation in the gear oil and on the current gear value. Transmission losses for the UI HEV were found from a power sink analysis of the vehicle given in [2]. The transmission loss was found in terms of loss power versus input shaft speed and the gear. This is termed the no load loss of the

transmission, and is repeated in Table 1. The power loss corresponding to each speed is converted to a torque in the table.

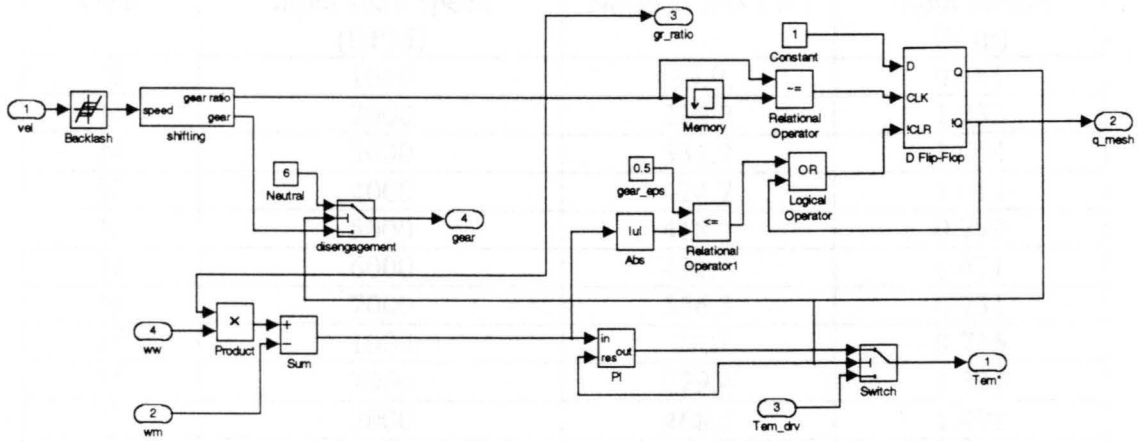

Figure 5: Block diagram of the shifting system.

Look-up tables were created from this data and implemented as shown in Figure 6. The particular loss table used is determined by the current gear. The loss tables give only the no-load loss, and the actual loss is needed. Assuming the transmission has a constant marginal efficiency, the loaded transmission loss can be written as [2]

$$P_{loss} = P_{NL} + (1 - \eta_{trans})(P_{in} - P_{NL}) \tag{9}$$

where P_{NL} is the transmission no-load loss, η_{trans} is the transmission efficiency, and P_{in} is the input power. Since power is a torque-speed product, if eq. (9) is divided by speed the result is

$$T_{loss} = T_{NL} + (1 - \eta_{trans})(T_{in} - T_{NL}) = \eta_{trans} T_{NL} + (1 - \eta_{trans}) T_{in} \tag{10}$$

This torque is added to the motor load torque. During shifting the neutral no-load torque is used, and since there is no transmission of power, T_{in} is taken as zero in eq. (10). The complete transmission block is shown in Figure 7.

Table 1: No-load transmission loss.

Gear	Input shaft speed (RPM)	No-load loss (W)	Input torque (N.m)
N	1000	39.9	0.381
N	2000	216.2	1.032
N	3000	331.2	1.054
N	4000	424.2	1.013
N	5000	418.1	0.799
N	6000	421.6	0.671
N	7000	536.2	0.731
1^{st}	1000	77.0	0.735
1^{st}	2000	279.4	1.334
1^{st}	3000	468.5	1.491
1^{st}	4000	639.0	1.525
1^{st}	5000	634.8	1.212
1^{st}	6000	801.6	1.276
2^{nd}	1000	172.5	1.647
2^{nd}	2000	370.9	1.771
2^{nd}	3000	612.9	1.951
2^{nd}	4000	820.1	1.958
2^{nd}	5000	899.0	1.717
2^{nd}	6000	1055.4	1.680
3^{rd}	1000	165.3	1.578
3^{rd}	1800	418.1	2.218
3^{rd}	3000	733.6	2.332
3^{rd}	4000	982.2	2.345
4^{th}	1000	263.0	2.511
4^{th}	1800	549.0	2.912
4^{th}	3000	972.4	3.095
5^{th}	1800	755.2	4.006
5^{th}	2700	1226.9	4.340

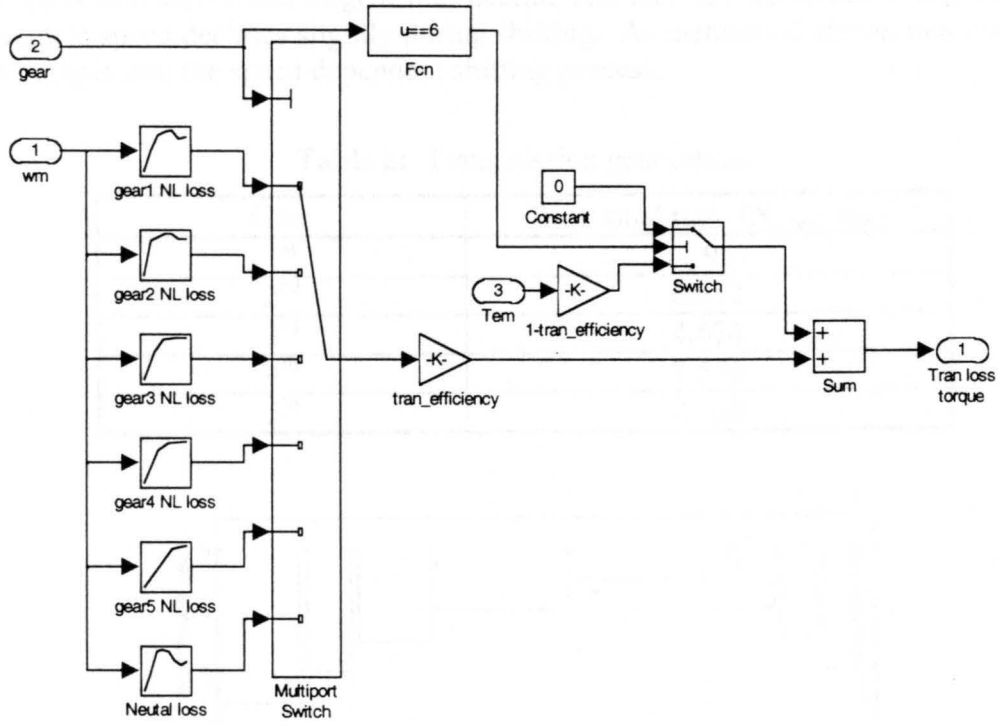

Figure 6: Transmission loss block.

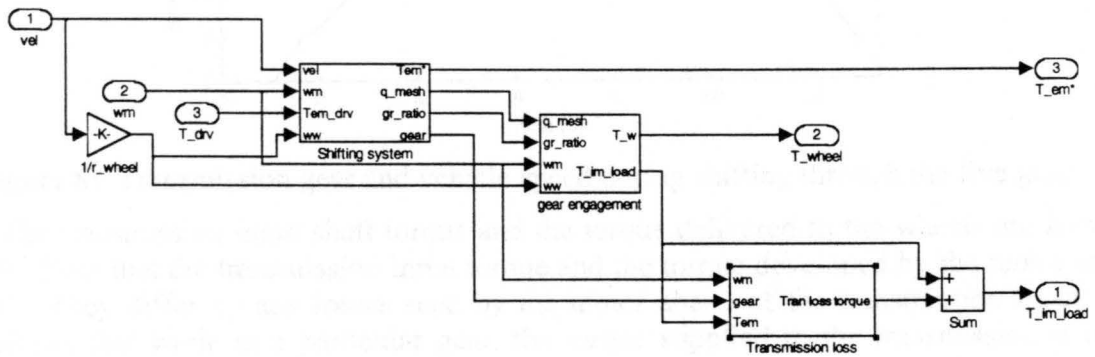

Figure 7: Transmission block.

The transmission gear and the vehicle speed are shown in Figure 8 for an acceleration for 10 s, and then a deceleration. Note that gear six is neutral. Denoting neutral by zero was not done for reasons of indexing in MATLAB. The five gear ratios are given in Table 2. The simulation was done with an equivalent vehicle mass one-tenth that of the actual vehicle mass to

more easily illustrate the shifting process. As shown in the figure, during shifting, the transmission is first shifted out of gear into neutral, and then shifted to the next gear. Also note that the vehicle speed declines slightly during shifting. As mentioned above, this was reason for adding hysteresis into the speed dependent shifting process.

Table 2: Transmission gear ratios.

Gear	Rotational ratio (N_{wheel}/N_{im})
1st	11.957
2nd	6.652
3rd	4.674
4th	3.556
5th	2.638

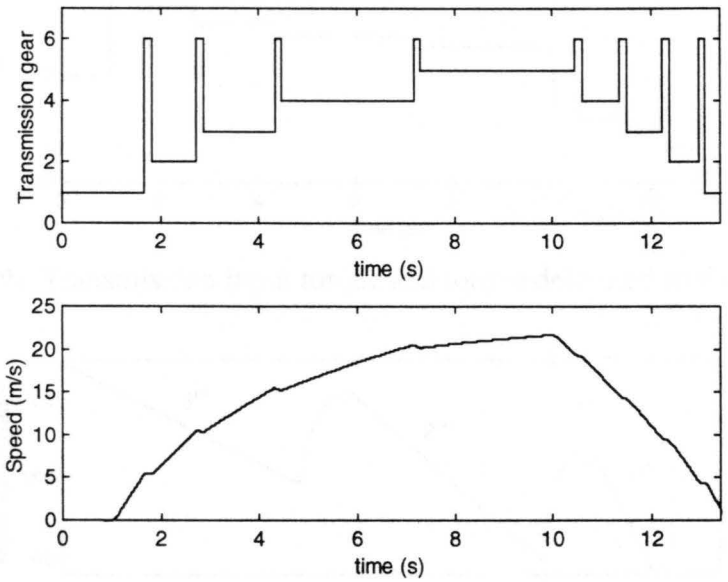

Figure 8: Transmission gear and vehicle speed during shifting through the five gears.

The transmission input shaft torque and the torque delivered to the wheels are shown in Figure 9. Note that the transmission input torque and the torque developed by the motor are not identical. They differ by any losses seen by the motor ahead of the transmission input. The figure shows that while in a particular gear, the torque supplied to the transmission is nearly constant. During shifting, torque control is removed from the driver, and the automatic synchronization controller takes over. Of course, the synchronization torque is negative while shifting to a higher gear. This is because the motor must be slowed in order to synchronize. The opposite is true while shifting to a lower gear. During shifting, the torque to the wheels is zero.

Figure 10 illustrates the process of shifting to a lower gear in detail. Shifting down was chosen because it takes longer than up-shifting. This is because the transmission loss torque tends to help decrease the motor speed. The figure shows that during down-shifting, the transmission input torque is made positive by the PI controller until the motor speed is synchonized, and the shift may be made. In the actual shifting process, depending on the

parameters of the controller, the process of synchronizing the motor speed may be slightly underdamped. In this case, the motor speed would have a settling time before synchronization could occur. Here, it is assumed that the shift is made as soon as the gear speeds are matched to within a certern tolerance. Any remaing error is removed quickly by the system represented by eq. (8), as mentioned earlier.

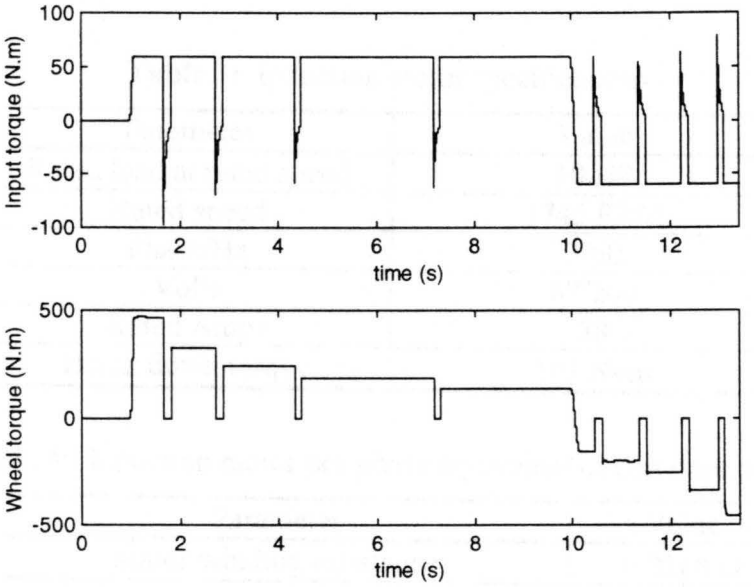

Figure 9: Transmission input torque and torque delivered to the wheels.

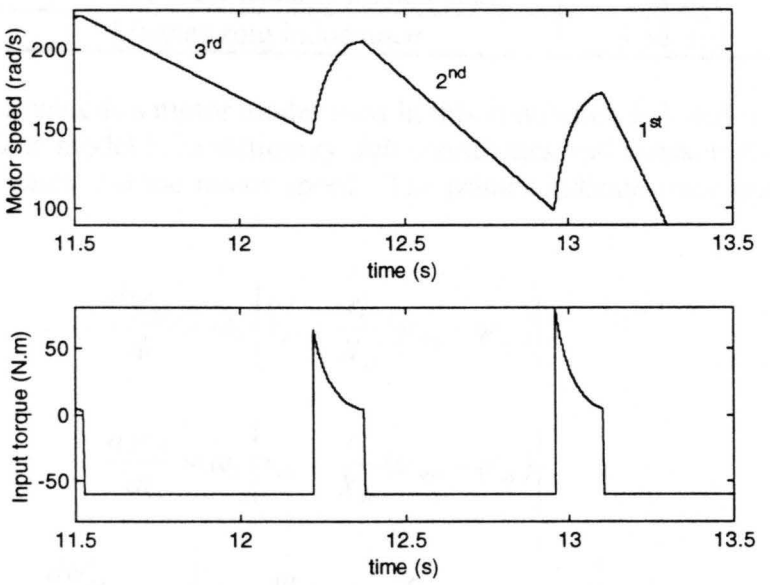

Figure 10: Motor speed and transmission input torque during shifting.

2.3 Induction Motor Model

The traction power for the HEV is supplied by a three-phase induction motor. The motor specifications are listed in Table 3 [3]. The per-phase equivalent circuit parameters are listed in Table 4 [2].

Table 3: Induction motor specifications.

Parameter	Value
Rated load at rated speed	10 HP
Rated speed	1745 RPM
Phase/Hz	3/60
Volts	67/200
Rated Amps	88
Break down torque	103 N•m

Table 4: Induction motor per-phase equivalent circuit parameters.

Parameter	Value
Stator winding resistance	0.0248 Ω
Referred rotor winding resistance	0.01438 Ω
Stator leakage inductance	114 μH
Referred rotor leakage inductance	114 μH
Magnetizing inductance	3.56 mH

The dynamic induction motor model used in this simulation is listed in eqs. (11)-(15) and is taken from [4]. The model is in stationary *dq0* coordinates and contains five states, four flux linkage per second states and the motor speed. The primes indicate rotor quantities referred to the stator.

$$\frac{d\psi_{qs}}{dt} = \omega_b \left\{ v_{qs} + \frac{r_s}{X_{ls}} \left(\psi_{mq} - \psi_{qs} \right) \right\} \tag{11}$$

$$\frac{d\psi_{ds}}{dt} = \omega_b \left\{ v_{ds} + \frac{r_s}{X_{ls}} \left(\psi_{md} - \psi_{ds} \right) \right\} \tag{12}$$

$$\frac{d\psi'_{qr}}{dt} = \omega_b \left\{ v'_{qr} + \frac{\omega_r}{\omega_b} \psi'_{dr} + \frac{r'_r}{X'_{lr}} \left(\psi_{mq} - \psi'_{qr} \right) \right\} \tag{13}$$

$$\frac{d\psi'_{dr}}{dt} = \omega_b \left\{ v'_{dr} - \frac{\omega_r}{\omega_b} \psi'_{qr} + \frac{r'_r}{X'_{lr}} \left(\psi_{md} - \psi'_{dr} \right) \right\} \tag{14}$$

$$\frac{d\omega_{im}}{dt} = \frac{1}{J_{im}}\{T_{em} - T_{im\ load}\} \tag{15}$$

The reactances X_{ls}' and X_{lr}' are found by multiplying the base speed ω_b by the stator and referred rotor leakage inductances respectively. The quantities r_s and r_r' are the stator and referred rotor winding resistances. The developed electric torque is denoted T_{em}, $T_{im\ load}$ is the load torque imposed on the motor, and J_{im} is the total rotational inertia seen by the motor.

The quantities ψ_{mq} and ψ_{md} are defined as

$$\psi_{mq} = X_M\left(\frac{\psi_{qs}}{X_{ls}} + \frac{\psi'_{qr}}{X'_{lr}}\right) \tag{16}$$

$$\psi_{md} = X_M\left(\frac{\psi_{ds}}{X_{ls}} + \frac{\psi'_{dr}}{X'_{lr}}\right) \tag{17}$$

where X_M is defined as

$$X_M = \left(\frac{1}{X_m} + \frac{1}{X_{ls}} + \frac{1}{X'_{lr}}\right)^{-1} \tag{18}$$

where X_m is the magnetizing reactance of the motor given by the base speed multiplied by the magnetizing inductance. These equations are implemented into SIMULINK exactly as they are written [5]. Figure 11 shows the induction motor block diagram. The Q-axis block implements eqs. (11) and (13), in addition to using eq. (16). The D-axis block implements eqs. (12) and (14) with eq. (17). These two blocks also produce the respective currents i_{qs} and i_{ds} by using

$$i_{qs} = \frac{1}{X_{ls}}\{\psi_{qs} - \psi_{mq}\} \tag{19}$$

$$i_{ds} = \frac{1}{X_{ls}}\{\psi_{ds} - \psi_{md}\} \tag{20}$$

The remaining zero-sequence current i_{0s} is implemented separately by

$$\frac{di_{0s}}{dt} = \frac{\omega_b}{X_{ls}}\{v_{0s} - r_s i_{0s}\} \tag{21}$$

These currents are used as feedback for the electronic drive that will be explained later. The motor torque is computed using

$$T_{em} = \frac{3P}{4\omega_b}\left\{\psi_{ds} i_{qs} - \psi_{qs} i_{ds}\right\} \tag{22}$$

where P is the number of motor poles. The majority of the loss due to friction is caused by the cooling fan. This torque is subtracted from that given by eq. (22) to find the input torque to the transmission.

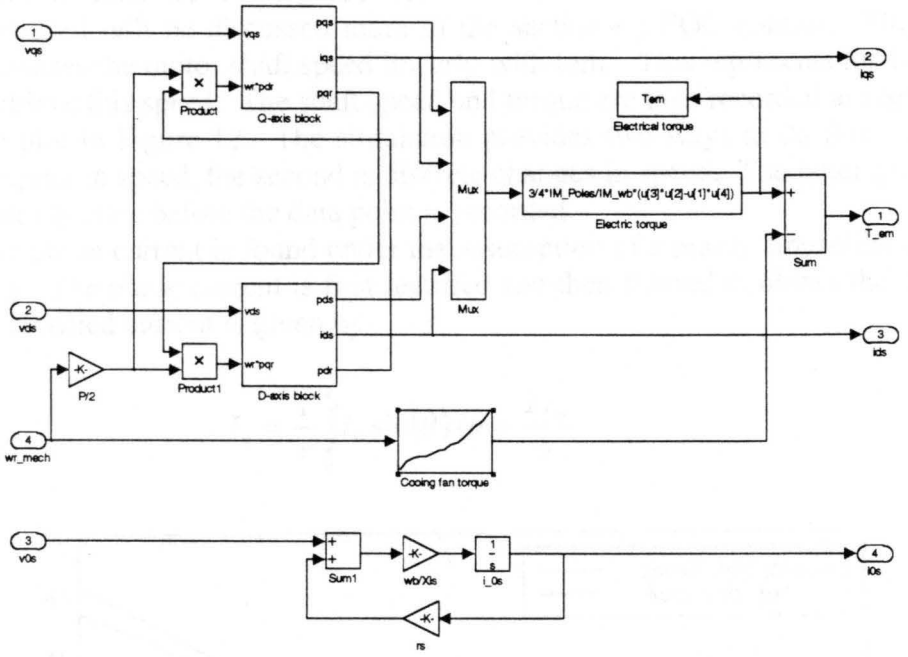

Figure 11: Induction motor SIMULINK model.

The motor model was tested in SIMULINK against the motor data [3] supplied by the manufacturer. The motor is supplied with the rated voltage of 67 $V_{l\text{-}l}$. The data points of shaft torque vs. speed are recorded. The simulated shaft torque and actual shaft torque vs. shaft speed are shown in Figure 12. Note that as the motor is more heavily loaded, the simulation torque exceeds the actual motor torque. This is expected because the motor used in the simulation based on a linear model. As the motor load is increased, the actual torque values fall below the simulated torque values because of the effects of magnetic saturation.

The simulated motor rms input current and the actual motor rms input current vs. shaft speed are shown in Figure 13. The simulated current is calculated based on the assumption of a purely sinusoidal current. The real motor has additional current harmonics due to inverter switching and magnetic saturation effects. This is why the actual current is always higher than the simulated current.

The SIMULINK file used for the simulated motor test is shown in Figure 14. The motor is modeled in *dq0* coordinates and excited by

$$v_{qs} = \frac{67}{\sqrt{3}}\sin(120\pi t)$$
$$v_{ds} = \frac{67}{\sqrt{3}}\sin(120\pi t - \tfrac{\pi}{2})$$
$$v_{0s} = 0$$

which represent a balanced three-phase set when transformed to abc coordinates. The transformations used will be discussed more in the section on FOC control. The shaft speed ramp block increases the motor shaft speed linearly with time. This represents loading the motor to a point to achieve this speed. The shaft speed and torque are then recorded at regular intervals to produce the plot in Figure 12. The simulation provides two ways to do this. The first is a continuous ramping in speed, the second is discrete changes in speed. The latter gives the motor time to reach steady state before the data point is recorded.

The rms phase current is found under the assumption of a purely sinusoidal current at the input frequency. The phase current is first rectified and then filtered to obtain the average. The average of the rectified current is given by

$$I_a = \frac{1}{\pi}\int_0^{\pi} I_0 \sin(\theta)d\theta = \frac{2I_0}{\pi}$$

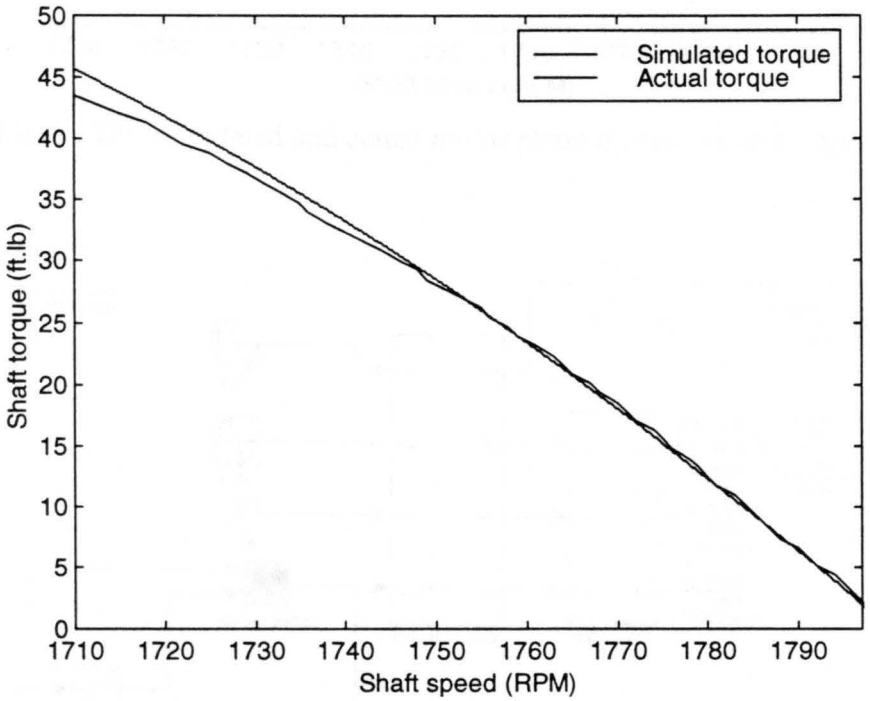

Figure 12: Simulated and actual motor shaft torque vs. shaft speed.

This average current, assuming it is sinusoidal, can be related to the rms phase current by

$$I_{rms}\frac{\pi}{2\sqrt{2}}I_a$$

The plot in Figure 13 was generated this way.

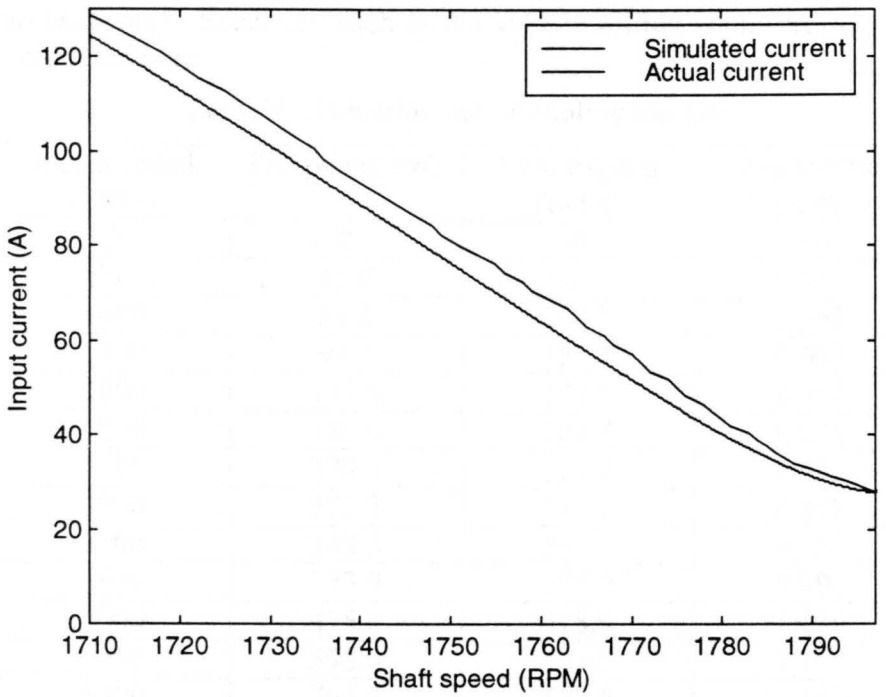

Figure 13: Simulated and actual motor phase current vs. shaft speed.

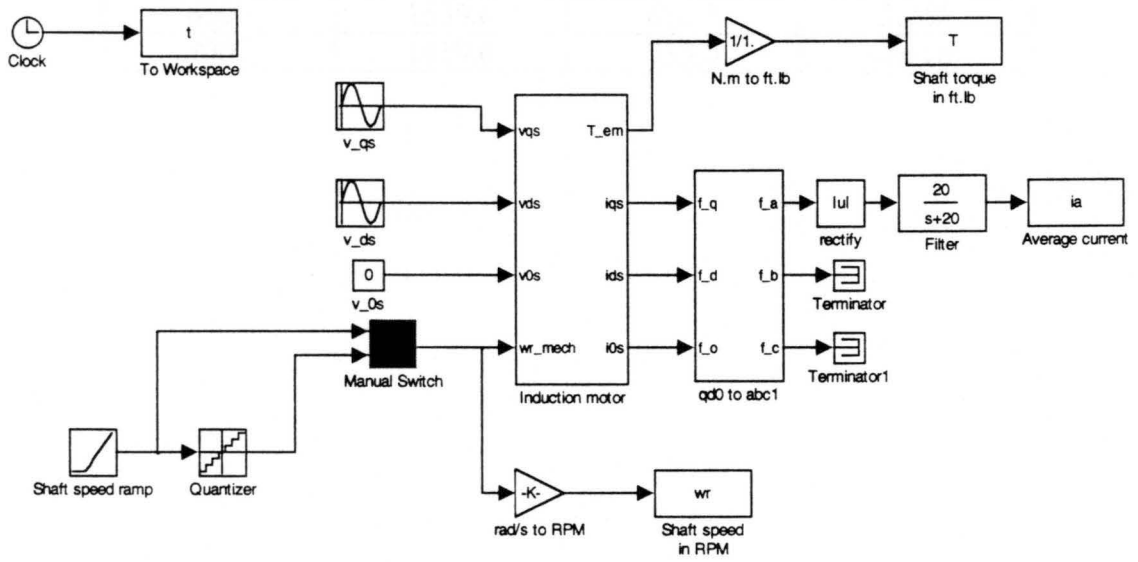

Figure 14: SIMULINK file used for motor tests.

The power loss due to the cooling found was found experimentally in [2] and is repeated in Table 5. The motor speed in rad/s and the fan torque are also given in the table. A plot of the fan torque vs. motor speed is given in Figure 15. A look-up table is created in SIMULINK using this data as shown in Figure 11. Note that the look-up table needs only have values for the motor speed greater than or equal to zero. The UI HEV has a reverse gear, and so the induction motor needs never go backward. Scenarios such as the vehicle rolling backward on a grade while in gear are not considered here.

Table 5: Induction motor cooling fan loss.

Motor speed (RPM)	Fan power (W)	Motor speed (rad/s)	Fan torque (N.m)
0	0	0	0
500	19.0	52.4	0.363
1000	58.8	104.7	0.561
1500	94.7	157.1	0.603
1800	115.8	188.5	0.614
2000	130.0	209.4	0.621
2500	178.7	261.8	0.683
3000	272.7	314.2	0.868
3500	348.3	366.5	0.950
3600	373.9	377.0	0.992
4000	475.0	418.9	1.134
4500	598.0	471.2	1.269
5000	764.3	523.6	1.460
5400	961.2	565.5	1.700
5500	1008.2	576.0	1.750
6000	1284.4	628.3	2.044
6500	1539.6	680.7	2.262
7000	1919.0	733.0	2.618

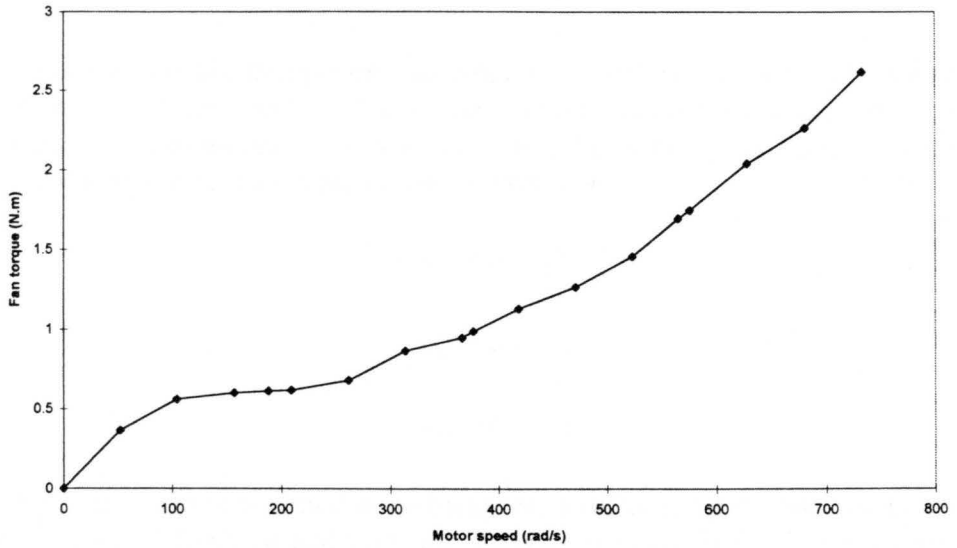

Figure 15: Induction motor cooling fan torque vs. motor speed.

2.4 Electronic Drive

The induction motor in the UI HEV is driven by a three-phase PWM electronic drive using Insulated Gate Bipolar Transistors (IGBTs) as switches. The circuit diagram of the drive and the induction motor are shown in Figure 16. The IGBTs switch at frequency at a frequency much higher than the fundamental of the desired motor terminal voltages. The duty ratio of the switches is modulated such that the time averaged terminal voltages v_{ap}, v_{bp} and v_{cp} are sinusoidal and displaced by $2\pi/3$ radians.

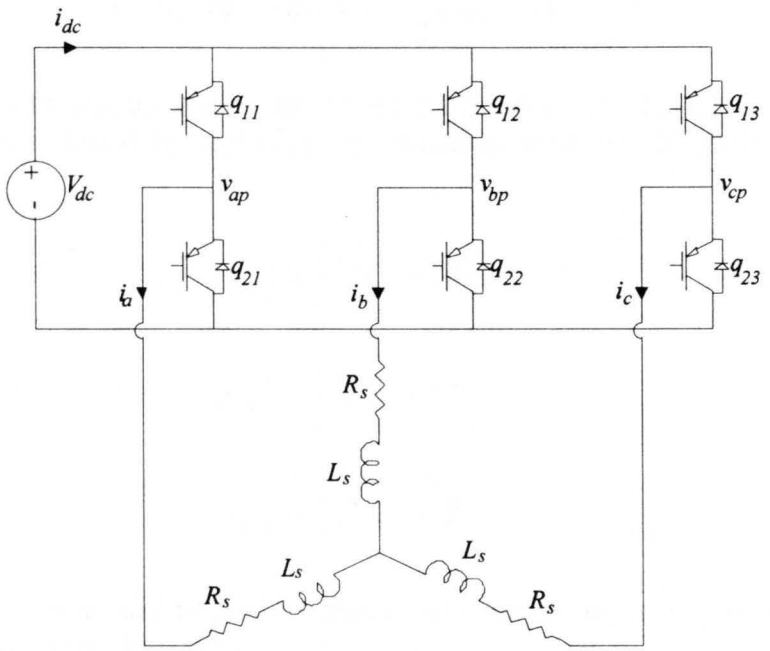

Figure 16: Electronic drive and induction motor.

In order to avoid component damage, the switches must be operated such that the input source is never shorted and so the phase currents always have a path to take. Define the switching function q_{ij} as being equal to one when the switch q_{ij} is on and equal to zero when it is off. The switching constraints may now be written as

$$q_{11} + q_{12} = 1 \tag{23}$$

$$q_{12} + q_{22} = 1 \tag{24}$$

$$q_{13} + q_{23} = 1 \tag{25}$$

Since the load is assumed to be balanced, a reference point may be placed at the center of the wye connected load. In addition, for analysis reasons, if the input source is split into two equal sources in series, the voltage at the node where the sources connect is equal to the center of the wye load. This allows the voltages v_{ap}, v_{bp} and v_{cp} to be written in terms of the switching functions as

$$v_{ap} = \frac{1}{2}(q_{11} - q_{21})V_{dc} = \frac{1}{2}(2q_{11} - 1)V_{dc} \tag{26}$$

$$v_{bp} = \frac{1}{2}(q_{12} - q_{22})V_{dc} = \frac{1}{2}(2q_{12} - 1)V_{dc} \tag{27}$$

$$v_{cp} = \frac{1}{2}(q_{13} - q_{23})V_{dc} = \frac{1}{2}(2q_{13} - 1)V_{dc} \tag{28}$$

where substitutions for q_{21}, q_{22} and q_{23} have been made using eqs. (23)-(25). The time average of the phase voltages is found by replacing the switching functions by their corresponding duty ratios to obtain

$$\langle v_{ap} \rangle = \frac{1}{2}(2d_{11} - 1)V_{dc} \tag{29}$$

$$\langle v_{bp} \rangle = \frac{1}{2}(2d_{12} - 1)V_{dc} \tag{30}$$

$$\langle v_{cp} \rangle = \frac{1}{2}(2d_{13} - 1)V_{dc} \tag{31}$$

The duty ratio function needed to produce sinusoidal phase voltages may be found by solving the following equation for the duty ratio

$$V_0 \cos(\omega t) = \frac{1}{2}(2d - 1)V_{dc} \tag{32}$$

to obtain

$$d(t) = \frac{V_0}{V_{dc}} \cos(\omega t) + \frac{1}{2} \tag{33}$$

where V_0 is the desired amplitude of the phase voltages. Therefore, in order to produce sinusoidal phase voltages at frequency ω and amplitude V_0, the duty ratios of the switches q_{11}, q_{12} and q_{13} should be

$$d_{11}(t) = \frac{V_0}{V_{dc}} \cos(\omega t) + \frac{1}{2} \tag{34}$$

$$d_{12}(t) = \frac{V_0}{V_{dc}} \cos(\omega t - \tfrac{2\pi}{3}) + \frac{1}{2} \tag{35}$$

$$d_{13}(t) = \frac{V_0}{V_{dc}} \cos(\omega t + \tfrac{2\pi}{3}) + \frac{1}{2} \tag{36}$$

The ratio $k_d = 2V_0/V_{dc}$ is termed the depth of modulation and lies between zero and one. Looking at eq. (32) it can be seen that the maximum value for V_0 is $V_{dc}/2$.

The simulation presented here assumes that the phase voltages produced by the inverter are perfectly sinusoidal and ignores all higher harmonics. This assumption is validated by the fact that the harmonics produced by the switching are centered about the switching frequency and multiples of the switching frequency [6].

The SIMULINK inverter model is shown in Figure 17. The inverter is placed in the stationary abc coordinate frame. The input variables to the drive are the motor phase currents i_a*, i_b*, and i_c* which are supplied by the FOC controller. The inverter supplies the phase voltages to the motor. It must control these voltages in such a way to produce the desired phase currents. The phase voltages are given by [5]

$$v_a = k_{CR}(i_a^* - i_a) \tag{37}$$

$$v_b = k_{CR}(i_b^* - i_b) \tag{38}$$

$$v_c = k_{CR}(i_c^* - i_c) \tag{39}$$

where v_a, v_b and v_c are the phase voltages produced by the electronic drive, i_a, i_b and i_c are the actual motor phase currents, and k_{CR} is a high gain. If this gain is relatively high, the phase currents will track the commanded values.

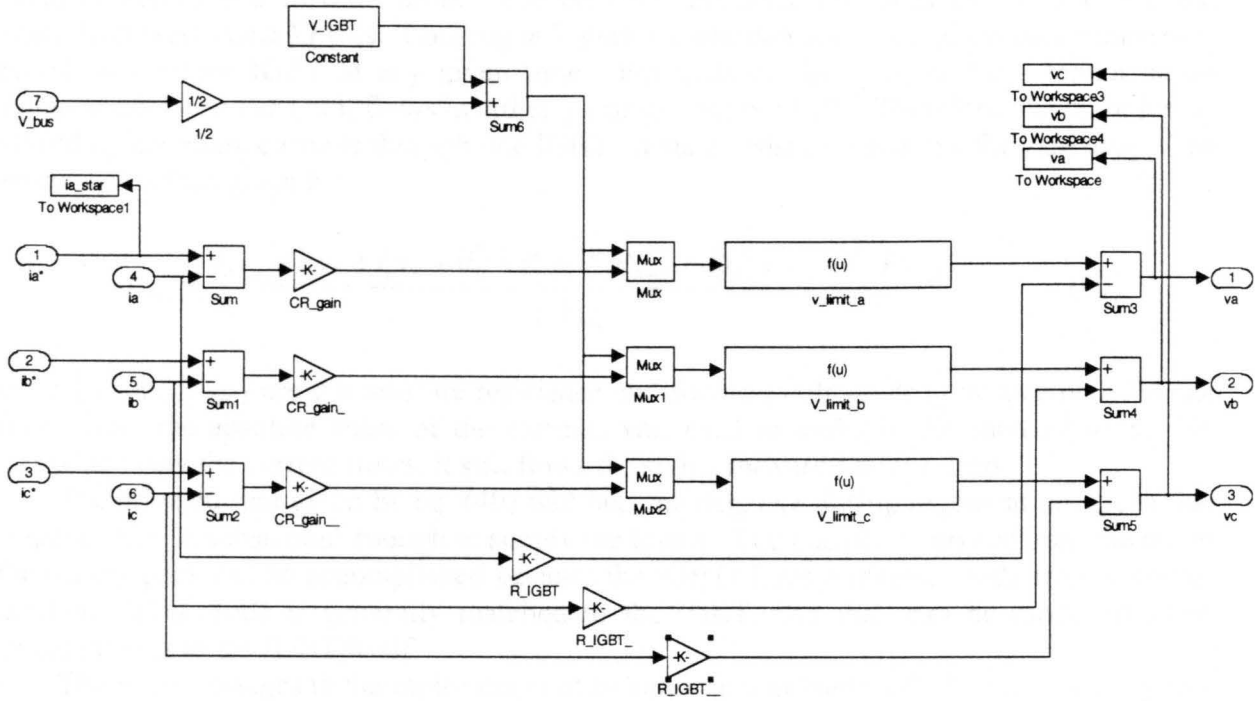

Figure 17: SIMULINK inverter block.

The dc voltage bus for the inverter is supplied by the battery pack. As mentioned above, the peak output voltage of the inverter is no greater than one-half the dc input voltage. Therefore, as shown in the figure, the battery bus voltage is multiplied by one-half. In addition, the forward voltage drop of the IGBTs must be taken into account. The IGBTs used are modeled as a forward voltage drop in series with an on-state resistance [2]. By looking at Figure 16, the voltage drop suffered by each phase is equal to the forward voltage drop of one IGBT. This is because each phase is always connected in series with one IGBT. In addition, the phase voltages must be reduced because of the phase currents flowing through the IGBT on-state resistances. This is done by multiplying the phase currents by the IGBT on-state resistance, and directly subtracting this quantity from the phase voltages.

The voltage limit blocks in Figure 17 limit the phase voltages to the minimum of either the voltage commanded by the current regulator or one-half the battery voltage minus one IGBT forward drop. This mimics a standard PWM inverter, which, after reaching 100% depth of modulation, will go to block modulation, and finally to square-wave operation. The voltage limit blocks simply clip the phase voltages when their amplitude exceed one-half the battery voltage minus an IGBT forward drop.

The current drawn from the battery pack by the inverter must now be determined. This current can be found in more that one way. Whether the current is into or out of the battery is determined by the current direction and the orientation of the switches. The switching action is determined by eqs. (34)-(36). The bus current could be found using the duty ratio information and the phase currents. However, here the power into the electronic drive is found and then divided by the bus voltage to obtain the bus current. The power drawn by the drive is the phase currents multiplied by the phase voltages plus the inverter losses. The losses are due to the IGBT

on-state resistance and forward drop. The on-state resistance produces an I^2R loss and the forward drop produces a VI loss. Looking at Figure 16, one can see that a given phase current is imposed on a single IGBT at any given time. For instance, both q_{11} and q_{21} cannot be on simultaneously. The current i_a flows in either q_{11} or q_{21}, but not both. Therefore, the drive loss is produced by the phase currents through one IGBT on-state resistance and one forward drop. The drive current is then given by

$$i_{drive} = \frac{i_a v_a + i_b v_b + i_c v_c + \left(i_a^2 + i_b^2 + i_c^2\right) R_{IGBT} + \left(|i_a| + |i_b| + |i_c|\right) V_{IGBT}}{V_{bus}} \tag{40}$$

where R_{IGBT} and V_{IGBT} are the on-state resistance and forward voltage drop, respectively, of the IGBTs. Note the absolute value of the currents was used to multiply the forward drop. No matter which way the current flows, it still flows through a forward voltage drop.

The drive current given by eq. (40) will become negative during regeneration, given that the regeneration is substantial enough to supply the losses. The transfer of power from the motor to the battery pack can be accomplished because the IGBTs have a reverse diode from collector to emitter. This diode is generally matched to the IGBT, and thus can be modelled in an identical manner to the IGBT itself.

The phase voltages to the motor may not be sinusoidal or balanced. The is especially true when the inverter produces block PWM because a voltage limit is reached. Since the connection to the motor is a 3-wire, the stator neutral is floating. This voltage may be obtained by placing a small fictitious from the stator neutral to the battery bus neutral [5]. Remember, the battery neutral was defined above as the center of the battery voltage. The stator neutral voltage is given by

$$v_g = \frac{1}{C_g} \int \left(i_a + i_b + i_c\right) dt$$

The phase voltages are then given by

$$\begin{aligned} v_{as} &= v_a - v_g \\ v_{bs} &= v_b - v_g \\ v_{cs} &= v_c - v_g \end{aligned}$$

where v_{as}, v_{bs}, and v_{cs} are the actual stator winding voltages, and v_a, v_b, and v_c are the input phase voltages. In a stationary $dq0$ coordinate system, the voltages are

$$\begin{aligned} v_{qs} &= v_q - v_g \\ v_{ds} &= v_d \\ v_{0s} &= v_0 - v_g \end{aligned}$$

So, given the desired voltages, the above equations are used to correct for the voltage imbalance in the stator.

2.5 Field Oriented Control

Field oriented control allows the induction motor torque to be controlled directly by changing the input current. This is very similar to the way the torque is controlled in a dc machine, only the details are more complicated. In an induction machine, the stator and rotor fields are not held electrically orthogonal to one another as they are in the dc machine. Another complication arises from the fact that the rotor field in an induction machine is induced by the stator field. Induction machine field oriented control controls the stator currents in such a way as to mimic the dc machine. Induction machine field oriented control allows the following requirements for torque control to be met [7]

1. independent control of armature current
2. independent control or constant value of field flux
3. orthogonality between the field flux axis and the stator MMF axis to avoid interaction between the flux and MMF

In this section, the equations necessary for torque control of the induction motor will be developed. We start with the motor voltage equations in an arbitrary reference frame. For a more detailed discussion of reference frame transformation and elimination of the time varying inductances associated with the induction motor see [4]. The stator voltage equations for the induction machine in an arbitrary reference frame are

$$v_{ds} = r_s i_{ds} + \frac{d\lambda_{ds}}{dt} - \omega\lambda_{qs} \tag{41}$$

$$v_{qs} = r_s i_{qs} + \frac{d\lambda_{qs}}{dt} + \omega\lambda_{ds} \tag{42}$$

$$v_{0s} = r_s i_{0s} + \frac{d\lambda_{0s}}{dt} \tag{43}$$

where

$$\lambda_{ds} = L_{ls} i_{ds} + L_m \left(i_{ds} + i'_{dr}\right) \tag{44}$$

$$\lambda_{qs} = L_{ls} i_{qs} + L_m \left(i_{qs} + i'_{qr}\right) \tag{45}$$

$$\lambda_{0s} = L_{ls} i_{0s} \tag{46}$$

and for the rotor

$$v'_{dr} = r'_r i'_{dr} + \frac{d\lambda'_{dr}}{dt} - (\omega - \omega_r)\lambda'_{qr} \tag{47}$$

$$v'_{qr} = r'_r i'_{qr} + \frac{d\lambda'_{qr}}{dt} + (\omega - \omega_r)\lambda'_{dr} \tag{48}$$

$$v'_{0r} = r'_r i'_{0r} + \frac{d\lambda'_{0r}}{dt} \tag{49}$$

where

$$\lambda'_{dr} = L'_{lr} i'_{dr} + L_m (i_{ds} + i'_{dr}) \tag{50}$$

$$\lambda'_{qr} = L'_{lr} i'_{qr} + L_m (i_{qs} + i'_{qr}) \tag{51}$$

$$\lambda'_{0r} = L'_{lr} i'_{0r} \tag{52}$$

where ω_r is the rotor speed, ω is the reference frame speed, and the primes indicate rotor referred quantities. The model described above in eqs. (11)-(14) can be obtained from these equations setting the reference frame speed to zero and using eqs. (44)-(46) to substitute for the currents in eqs. (41)-(43) and using eqs. (50)-(52) to substitute for the currents in eqs. (47)-(49).

The derivation of field oriented control is best done with the voltage equations placed in the synchronously rotating reference frame. The synchronously rotating frame is found by substituing ω_e for ω in eqs. (41)-(52) as follows

$$v^e_{qs} = r_s i^e_{qs} + \frac{d\lambda^e_{qs}}{dt} + \omega_e \lambda^e_{ds} \tag{53}$$

$$v^e_{ds} = r_s i^e_{ds} + \frac{d\lambda^e_{ds}}{dt} - \omega_e \lambda^e_{qs} \tag{54}$$

$$0 = r_r i^e_{qr} + \frac{d\lambda^e_{qr}}{dt} + (\omega_e - \omega_r)\lambda^e_{dr} \tag{55}$$

$$0 = r_r i^e_{dr} + \frac{d\lambda^e_{dr}}{dt} - (\omega_e - \omega_r)\lambda^e_{qr} \tag{56}$$

where

$$\lambda^e_{ds} = L_{ls} i^e_{ds} + L_m (i^e_{ds} + i^e_{dr}) \tag{57}$$

$$\lambda^e_{qs} = L_{ls} i^e_{qs} + L_m (i^e_{qs} + i^e_{qr}) \tag{58}$$

$$\lambda^e_{dr} = L_{lr} i^e_{dr} + L_m (i^e_{ds} + i^e_{dr}) \tag{59}$$

$$\lambda_{qr}^{e} = L_{lr} i_{qr}^{e} + L_m \left(i_{qs}^{e} + i_{qr}^{e} \right) \tag{60}$$

where the primes indicating referred rotor quantities have been left out for convenience. The superscripted *e*'s indicate the synchronously rotating reference frame. For the purposes here, the motor shaft torque may be expressed as

$$T_{em} = \frac{3PL_m}{4L_{lr}} \left(\lambda_{dr}^{e} i_{qs}^{e} - \lambda_{qr}^{e} i_{ds}^{e} \right) \tag{61}$$

An in depth discussion of induction motor torque control may be found in [7]. The equations necessary for torque control will be presented here, and it will be shown that they perform the desired the function. The rotor flux should be entirely along the d-axis in the synchronously rotating frame. This implies the following

$$\lambda_{qr}^{e} = 0 \tag{62}$$

When substituted in the torque equation, the following is obtained

$$T_{em} = \frac{3PL_m}{4L_{lr}} \lambda_{dr}^{e} i_{qs}^{e} \tag{63}$$

where P is the number of motor poles and $L_r = L_{lr} + L_m$. Now, if the rotor flux along the d-axis is held constant, the motor shaft torque is completely controlled by the current i_{qs}^{e}. A constant rotor flux in the direction of the d-axis implies

$$\frac{d\lambda_{dr}^{e}}{dt} = 0 \tag{64}$$

It is needed to find the stator currents that produce a given shaft torque and flux level in the rotor. The first current is found directly from eq. (63)

$$i_{qs}^{e}{}^{*} = \frac{4L_r}{3PL_m} \frac{T_{em}{}^{*}}{\lambda_{dr}^{e}{}^{*}} \tag{65}$$

where $T_{em}{}^{*}$ is the desired shaft torque, $\lambda_{dr}^{e}{}^{*}$ is the desired rotor flux, and $i_{qs}^{e}{}^{*}$ is the desired stator current. The second stator current is slightly more difficult to obtain. Start by substiting eq. (62) into the rotor voltage eq. (56) to obtain

$$v_{dr}^{e} = 0 = r_r i_{dr}^{e} + \frac{d\lambda_{dr}^{e}}{dt} \tag{66}$$

where the externally applied rotor voltage v_{dr}^{e} is zero. Now, solve eq. (59) for the rotor current i_{dr}^{e} as follows

$$\lambda_{dr}^{e} = (L_{lr} + L_m) i_{dr}^{e} + L_m i_{ds}^{e}$$

$$i_{dr}^{e} = \frac{\lambda_{dr}^{e} - L_m i_{ds}^{e}}{L_{lr} + L_m} = \frac{\lambda_{dr}^{e} - L_m i_{ds}^{e}}{L_r} \tag{67}$$

By substituting eq. (67) into eq. (66), the stator current is obtained

$$i_{ds}^{e}* = \frac{1}{r_r L_m}\left(r_r \lambda_{dr}^{e}* + L_r \frac{d\lambda_{dr}^{e}*}{dt} \right) \tag{68}$$

The derivative of the rotor flux is only necessary in the field weakening region of operation. The field oriented control block as implemented in SIMULINK is shown in Figure 18.

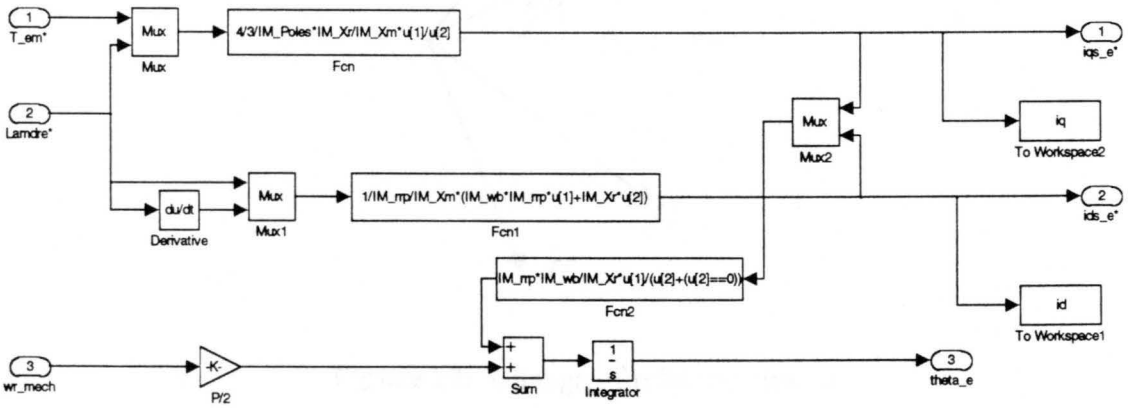

Figure 18: SIMULINK field oriented control block.

We now have the necessary stator currents in the synchronously rotating frame, but they need to be converted to the stationary frame to be used as inputs by the inverter. Figure 19 shows graphically the transformation between two reference frames. Define the following vectors

$$\begin{aligned} \mathbf{f}_{qd0}^{y} &= \begin{bmatrix} f_q^y & f_d^y & f_0^y \end{bmatrix}^T \\ \mathbf{f}_{qd0}^{x} &= \begin{bmatrix} f_q^x & f_d^x & f_0^x \end{bmatrix}^T \end{aligned} \tag{69}$$

where these vectors represent circuit variables such as current or voltage. The x and y indicate the reference frames rotating at speeds ω_x and ω_y, respectively. The two reference frames are related by the transformation [4]

$$\mathbf{f}_{qd0}^{y} = {}^{x}\mathbf{K}^{y}\mathbf{f}_{qd0}^{x} \tag{70}$$

where the matrix ${}^{x}\mathbf{K}^{y}$ is given by

$${}^{x}\mathbf{K}^{y} = \begin{bmatrix} \cos(\theta_y - \theta_x) & -\sin(\theta_y - \theta_x) & 0 \\ \sin(\theta_y - \theta_x) & \cos(\theta_y - \theta_x) & 0 \\ 0 & 0 & 1 \end{bmatrix} \tag{71}$$

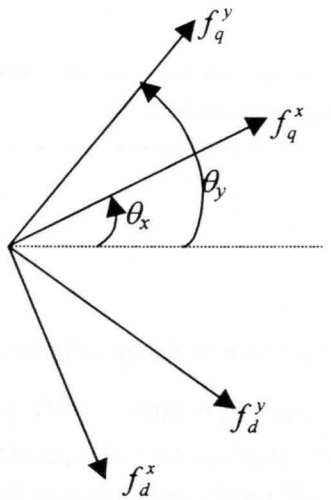

Figure 19: Change of reference frame.

The transformation from the synchronous reference frame to the stationary reference frame is found by substituting zero for θ_y and $\omega_e t$ for θ_x in transformation matrix of eq. (71) where ω_e is the angular velocity of the synchronously rotating reference frame. The SIMULINK block that implements this transformation is shown in Figure 20. The input θ_e is the position of the synchronous frame and given by

$$\theta_e = \int \omega_e dt \tag{72}$$

In order to go back to the stationary reference frame, θ_e must be found. Since we do not have access to the rotor field, it must be found indirectly from the stator currents and the rotor position. The rotor is position is known via an angular resolver attached to the rotor.

Substituting eq. (62) into eq. (55) the slip speed may be found as

$$\omega_e - \omega_{re} = -\frac{r_r i^e_{qr}}{\lambda^e_{dr}} \tag{73}$$

where ω_{re} is the rotor speed in electrical radians per second. The rotor current in eq. (73) is found by substituting eq. (62) into eq. (60), and is given by

$$i^e_{qr} = -\frac{L_m}{L_r} i^e_{qs} \tag{74}$$

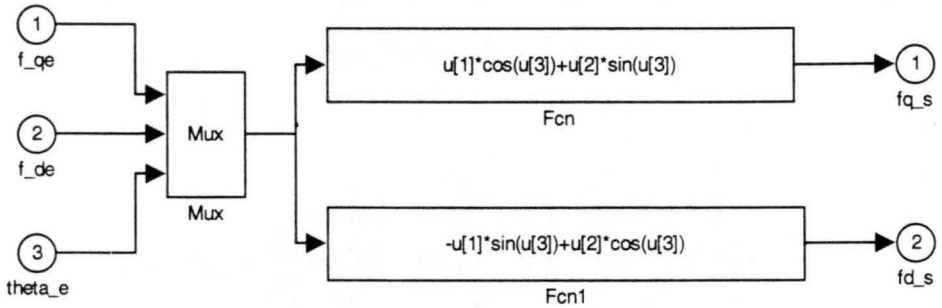

Figure 20: Transformation from the synchronous to the stationary reference frame.

The rotor flux λ^e_{dr} is given by eq. (59). This equation also contains the rotor current i^e_{dr}. However, by substituting eq. (62) into eq. (56) and setting the time derivative of the rotor flux to zero, it can be shown that i^e_{dr} is equal to zero. Equation (59) then becomes

$$\lambda^e_{dr} = L_m i^e_{ds} \tag{75}$$

The desired form for the slip frequency is found by substituting eqs. (74) and (75) into eq. (73) as

$$\omega_e - \omega_{re} = \frac{r_r}{L_r} \frac{i^e_{qs}}{i^e_{ds}} \tag{76}$$

which, when rearranged and integrated gives the rotor synchronous position

$$\theta_e = \int \left(\frac{r_r}{L_m} \frac{i^e_{qs}}{i^e_{ds}} + \omega_{re} \right) dt \tag{77}$$

The implementation of this equation is shown in Figure 18.

The SIMULINK block diagram containing the induction motor, electronic drive, and field oriented controller is shown in Figure 21. Note that since the motor is in *dq0* coordinates, the motor input voltages and the currents must be transformed between the *dq0* and the *abc* coordinate systems. The relationship between the two coordinate frames is depicted graphically in Figure 22 and can be written as [4]

$$\mathbf{f}_{qd0} = \mathbf{K}_s \mathbf{f}_{abc} \tag{78}$$

where

$$\begin{aligned} \mathbf{f}_{qd0} &= \begin{bmatrix} f_q & f_d & f_0 \end{bmatrix}^T \\ \mathbf{f}_{abc} &= \begin{bmatrix} f_a & f_b & f_c \end{bmatrix}^T \end{aligned} \tag{79}$$

and

$$\mathbf{K}_s = \frac{2}{3}\begin{bmatrix} \cos(\theta) & \cos(\theta - \frac{2\pi}{3}) & \cos(\theta + \frac{2\pi}{3}) \\ \sin(\theta) & \sin(\theta - \frac{2\pi}{3}) & \sin(\theta + \frac{2\pi}{3}) \\ 1/2 & 1/2 & 1/2 \end{bmatrix} \tag{80}$$

This matrix makes the transformation from stationary *abc* coordinates to *dq0* coordinates in an arbitrary reference frame. Here the transformation is from stationary *dq0* coordinates to stationary *abc* coordinates. Therefore, the inverse of K_s must be used as in eq. (81).

$$\mathbf{f}_{abcs} = \mathbf{K}_s^{-1} \mathbf{f}_{qd0s} \tag{81}$$

where

$$\mathbf{K}_s^{-1} = \begin{bmatrix} \cos(\theta) & \sin(\theta) & 1 \\ \cos(\theta - \frac{2\pi}{3}) & \sin(\theta - \frac{2\pi}{3}) & 1 \\ \cos(\theta + \frac{2\pi}{3}) & \sin(\theta + \frac{2\pi}{3}) & 1 \end{bmatrix} \tag{82}$$

Since both coordinate frames are stationary, θ is equal to zero in eq. (82). The SIMULINK implementation of this transformation is shown in Figure 23. This transformation is used twice in the simulation. Once to convert the *dq0* reference currents from the field oriented controller to *abc* coordinates for use by the drive, and once to convert the motor currents to *abc* coordinates to be used for feedback.

The remaining block in Figure 21 is the block labeled field weakening. As the motor speed increases, so must the terminal voltage. At a certain speed, the inverter will hit a voltage limit imposed by the battery voltage. At this point, the rotor flux must be reduced or the stator current will fall. The usual scheme employed is to reduce the rotor flux as one over the rotor speed while i_{qs}^e is held constant. As seen by eq. (63), this constitutes a constant power speed

region. In the UI HEV, this region begins at about 5400 RPM given a nominal battery voltage of 312 V.

The motor model used here has a linear magnetic characteristic. This means, in essence, that the shaft torque increases with input voltage without limit. The actual motor will stall when the shaft torque exceeds what is known as the breakdown torque. The breakdown torque limit exists because there is a limit on how intense the machine air gap flux can become due to saturation of the iron. This problem is solved with linear model by limiting the torque reference to the controller to that of the machine breakdown torque.

Figure 24 shows the motor shaft torque, reference torque, and stator currents for a simulation example. The torque reference is left at zero until time equal one second. This is done to allow the flux to build in the rotor. If the flux is not established in the rotor, the field oriented control will not function properly. At time equal to one second, the torque reference is brought to 60 N•m. The current i^e_{qs} climbs to approximately 150 A, and the shaft torque climbs to 60 N•m very nearly tracking on top of the reference. The reference the goes to –60 N•m. Note that the current i^e_{ds} stays constant because it is proportional to λ^e_{dr}.

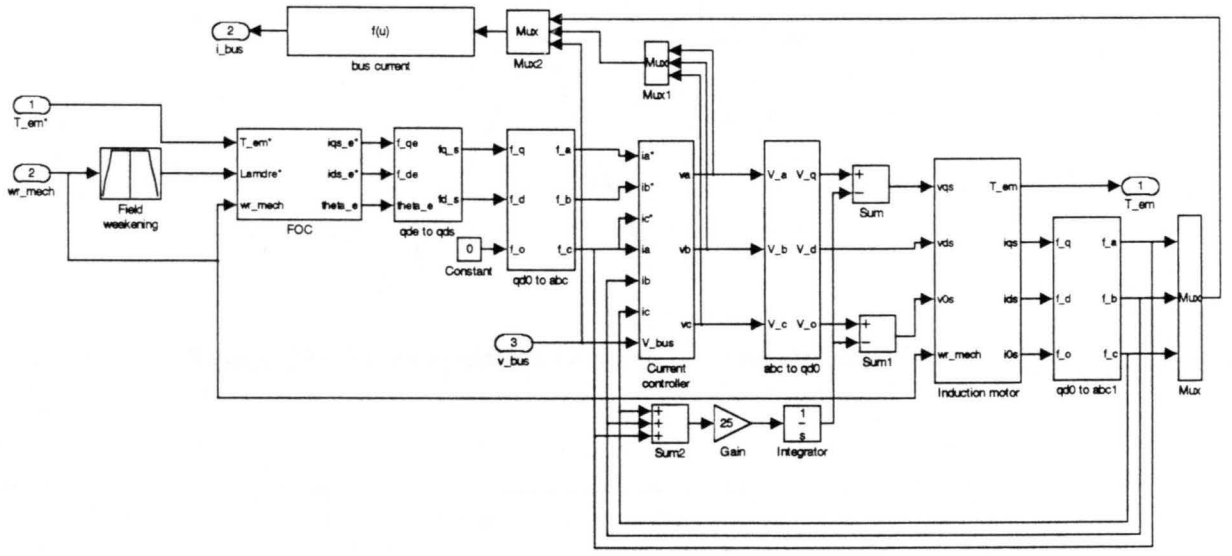

Figure 21: Induction motor, electronic drive and FOC controller.

The next three figures illustrate an example of induction motor operation in the field weakening region. At time equal to one second, the torque reference is set to the motor rated torque of 41 N•m, and the motor inertia is allow to free accelerate. Figure 25 shows the motor shaft speed and the shaft torque. The shaft torque falls off approximately as one over the shaft speed after reaching about 5400 RPM. The motor currents in the synchronous reference frame are shown in Figure 26. Note that as the d-axis current begins to fall due to field weakening, the q-axis current increases. The controller is using the extra dc bus voltage in an attempt to keep the shaft torque at the reference value. The q-axis current increases for a short time until the rated current of the motor is hit. This limit has been set equal to the steady state rated current of

the motor for illustration of the field weakening effect. Once the current limit is hit, the torque begins to fall off.

The d-axis rotor flux and its time derivative are shown in Figure 27. The rotor flux decreases in proportion to one over the shaft speed. Looking at eq. (63), it is immediately obvious why the shaft torque also decreases as one over the shaft speed, considering that i_{qs}^{e} is constant. The shaft power in the field weakening region is approximately constant. It is not exactly constant because the d-axis rotor flux is not constant and proper field orientation is not maintained.

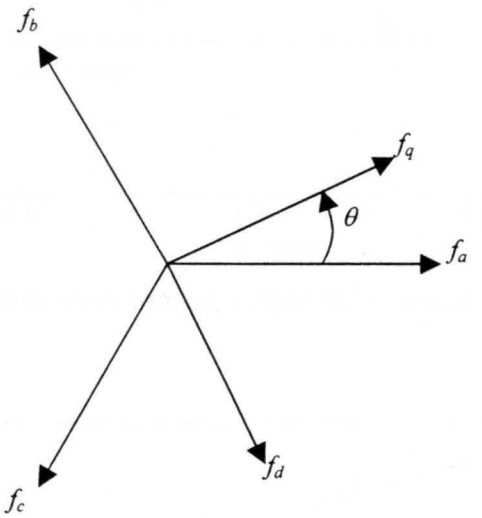

Figure 22: Transformation between *abc* and *dq0* coordinate frames.

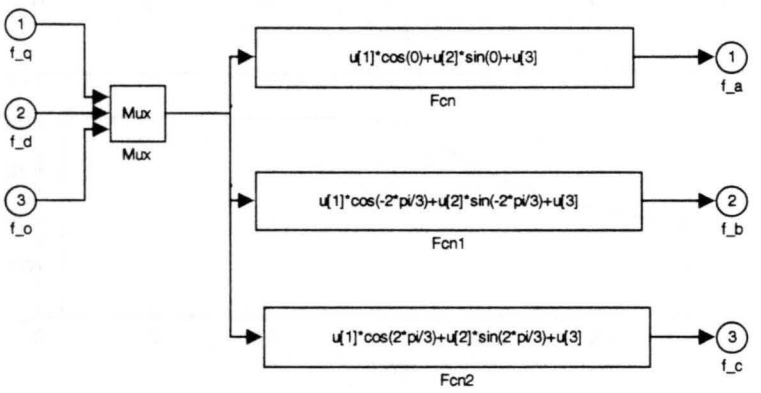

Figure 23: Transformation from stationary *dq0* coordinates to stationary *abc* coordinates.

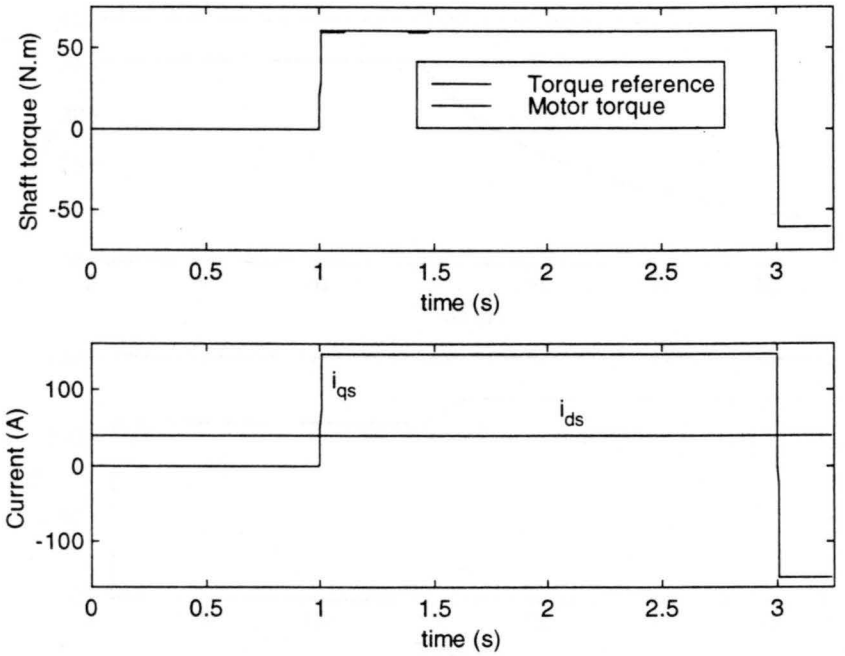

Figure 24: Motor shaft torque, torque reference, and stator currents.

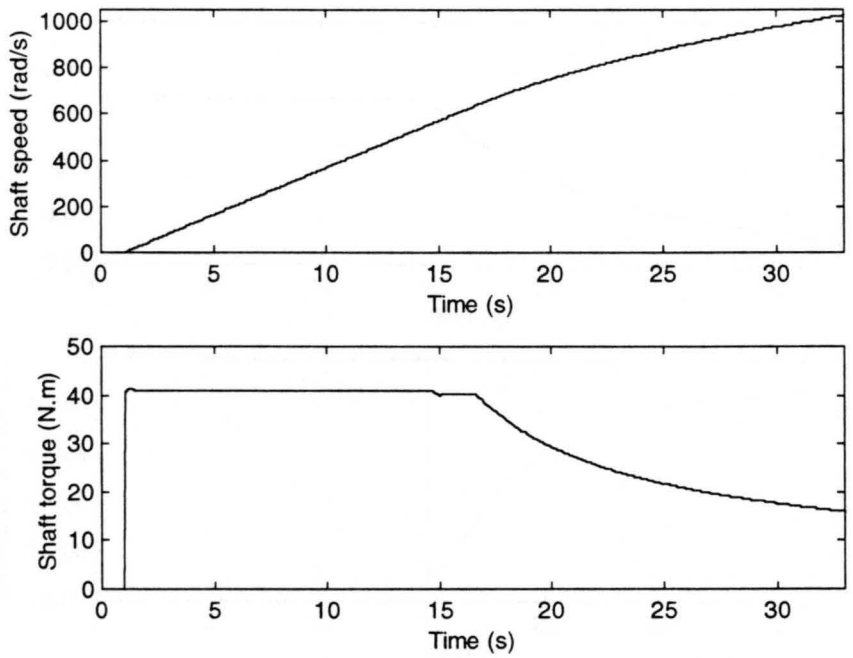

Figure 25: Induction motor shaft speed and torque.

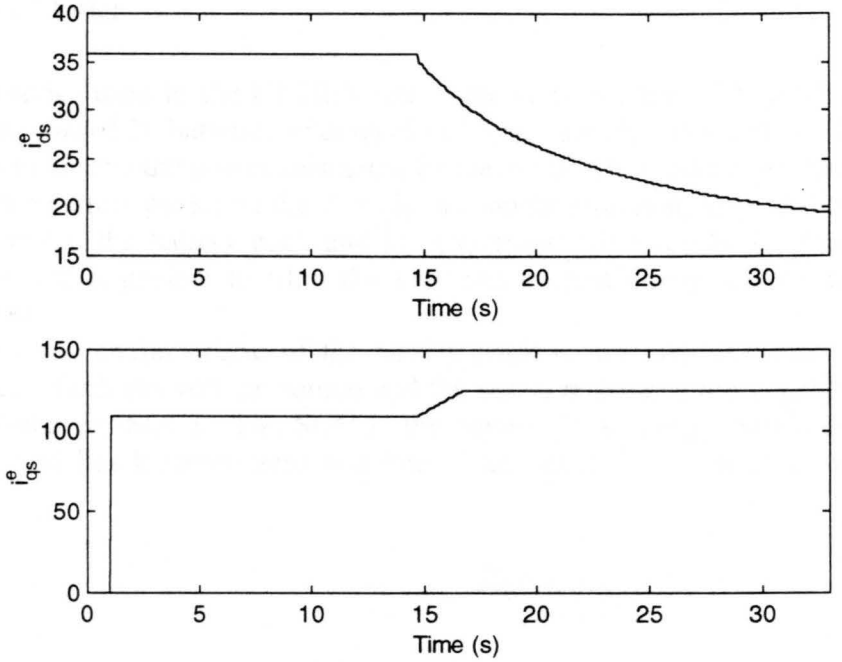

Figure 26: Induction motor stator currents in synchronous reference frame.

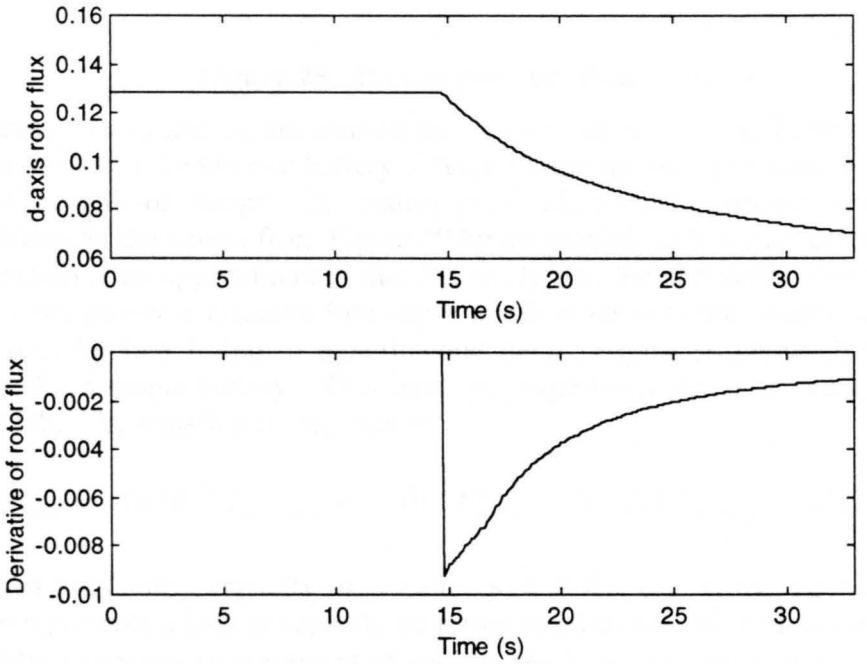

Figure 27: d-axis rotor flux and time derivative of d-axis rotor flux.

2.6 Battery Model

The batteries used in the UI HEV are of the conventional 12 V lead acid variety. The battery pack consists of 26 batteries with an electrolytic capacitor in parallel. The purpose of the battery pack is to absorb the power mismatch between the APU and the electronic drive. Power flow between the battery pack and the APU is in a single direction, toward the battery pack, and power flow between the battery pack and the electronic drive can be in either direction. The parallel capacitance is present to filter the very fast current changes, such as switching noise from the inverter.

The terminal characteristic of the battery pack is modeled as a voltage source with a series resistance. Both the voltage source and the series resistance are dependent on the battery pack's state-of-charge (SOC). The SOC is the battery pack energy normalized by the battery pack capacity, and lies between zero and one. The battery pack terminal model is shown in Figure 28 [1].

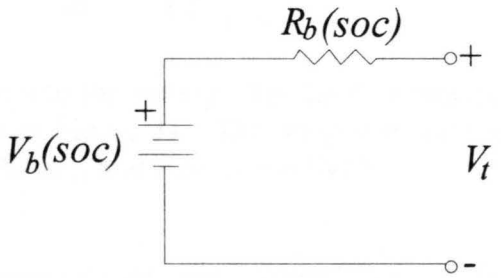

Figure 28: Battery pack terminal model.

In simulation, V_b and R_b are formed by look-up tables with the battery pack SOC as the input. Figure 29 shows the internal battery voltage V_b and the series resistance R_b for one battery as function of the state-of-charge. The battery pack voltage and series resistance are, of course, found by multiplying the values from Figure 29 by the number of batteries comprising the pack.

This model is an approximation that fits easily into the simulation framework. The total battery loss is not purely a resistive loss and a much more accurate model for the battery loss may be obtained by line fitting to experimental data. Figure 30 shows battery capacity vs. discharge rate for a single battery. This data was experimentally obtained by discharging the battery in the lab. The equation for the line fit is

$$E_{battery} = -5\times10^{-10} P_{discharge}^3 + 2\times10^{-5} P_{discharge}^2 - 0.1298 P_{discharge} + 302 \qquad (83)$$

where $E_{battery}$ is the battery capacity in watt-hours, and $P_{discharge}$ is the discharge rate in watts. This equation represents a battery capacity de-rating as a function of the level of discharge.

Consider removing an increment of energy $\Delta E = P_0 \Delta t$ from the terminals of a battery over the time interval Δt at a constant discharge rate P_0. Equation (83) demonstrates that the energy ΔE is less than the change in energy stored in the battery $\Delta E_{battery}$. The change in the amount of energy stored in the battery is given by

$$\Delta E_{battery} = \frac{E_{capacity}}{f(P_0)} P_0 \Delta t \tag{84}$$

where $f(\bullet)$ is defined as eq. (83) and $E_{capacity}$ is maximal battery capacity, 302 W-hr in this instance. Now, consider adding an increment of energy ΔE to the battery terminals. The change stored energy is given by

$$\Delta E_{battery} = \frac{f(P_0)}{E_{capacity}} P_0 \Delta t \tag{85}$$

Note that these equations represent battery losses because $f(P) \leq E_{capacity}$ for all P. Now, letting $\Delta E_{battery}$ and Δt become small, eqs. (84) and (85) can be expressed as

$$\frac{dE_{capacity}}{dt} = \left(\frac{f(P)}{E_{capacity}} \right)^{sign(P)} P \tag{86}$$

where P is defined as positive into the battery. The implementation of the battery pack terminal and storage models is shown in Figure 31. The integrator representing the battery energy has upper and lower limits set to $E_{capacity}$ and zero, respectively.

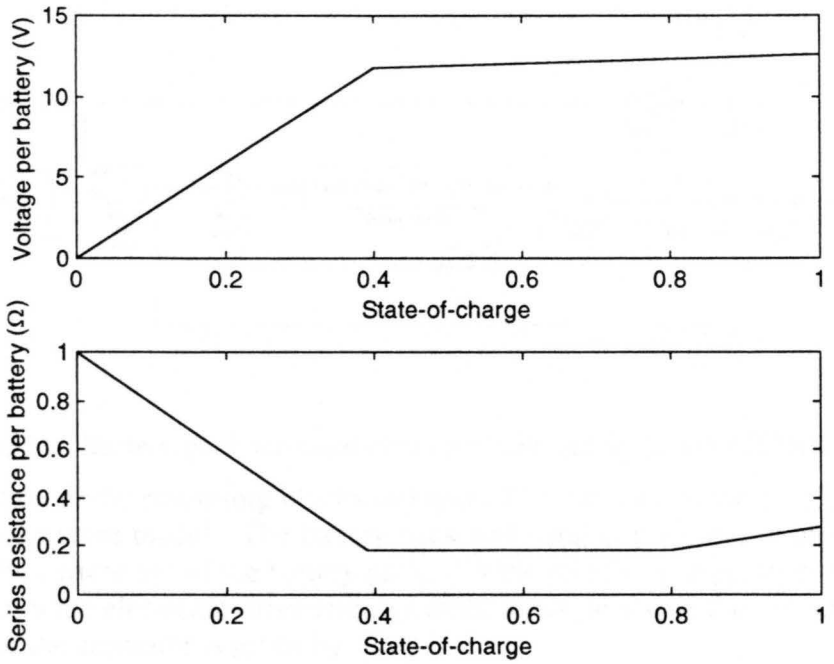

Figure 29: Internal battery voltage and series resistance as a function of SOC.

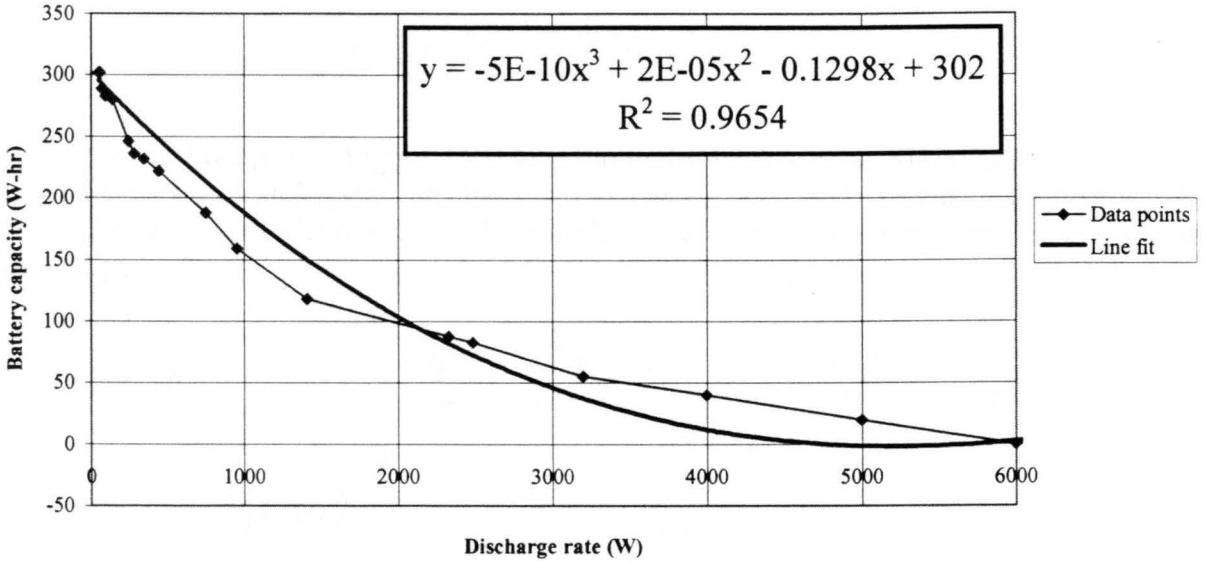

Figure 30: Battery capacity vs. discharge rate.

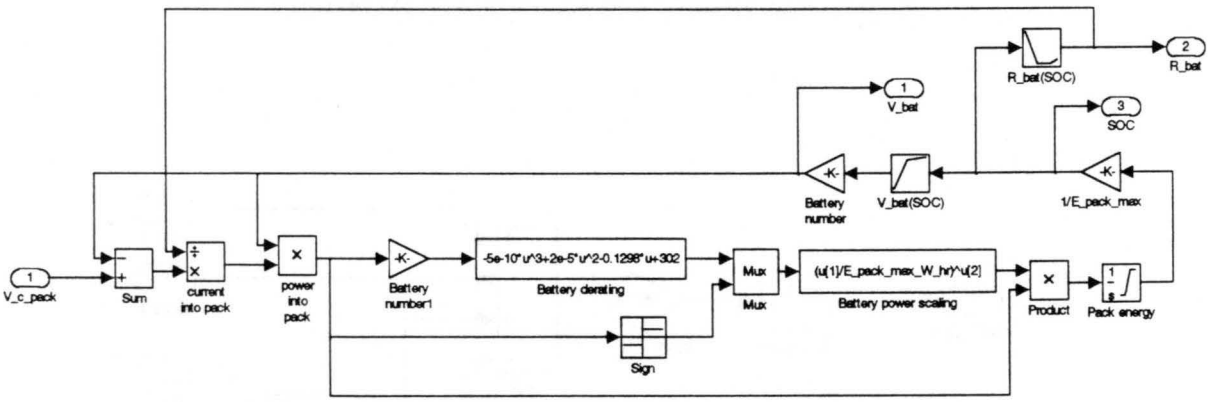

Figure 31: Battery pack terminal characteristic and SOC SIMULINK model.

Explanation of the remaining blocks in Figure 31 requires that we first look at the battery pack parallel capacitance model. The battery pack and parallel capacitance are shown in Figure 32, where i_b is the current out of the battery pack, i_r is the rectifier current from the APU, i_d is the current provided to the electronic drive and any other loads, and v_c is the capacitor voltage. The state equation for the capacitor is given by

$$\frac{dv_c}{dt} = \frac{1}{C_b}(i_r - i_d + i_b) = \frac{1}{C_b}\left(i_r - i_d + \frac{V_b(soc) - v_c}{R_b(soc)}\right) \tag{87}$$

and is implemented in SIMULINK as shown in Figure 33.

The power into the battery pack is calculated as

$$P_{pack} = \left(\frac{v_c - V_b(soc)}{R_b(soc)} \right) V_b(soc) \tag{88}$$

and is shown in Figure 31. Figure 34 shows the entire battery pack SIMULINK model. The input variables i_gen and i_load are the rectifier current and load current, respectively. The output variables vc_pack and soc are the parallel capacitance voltage and the state-of-charge, respectively.

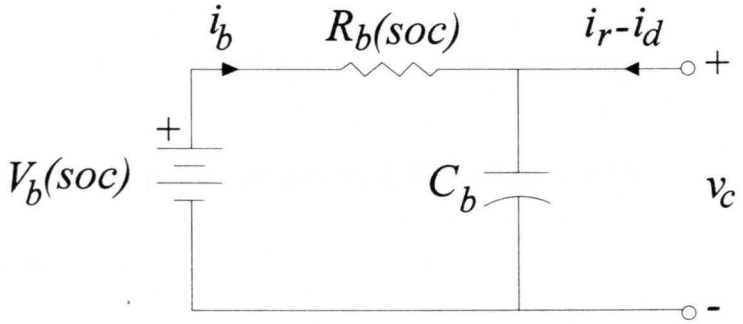

Figure 32: Battery pack and parallel capacitance.

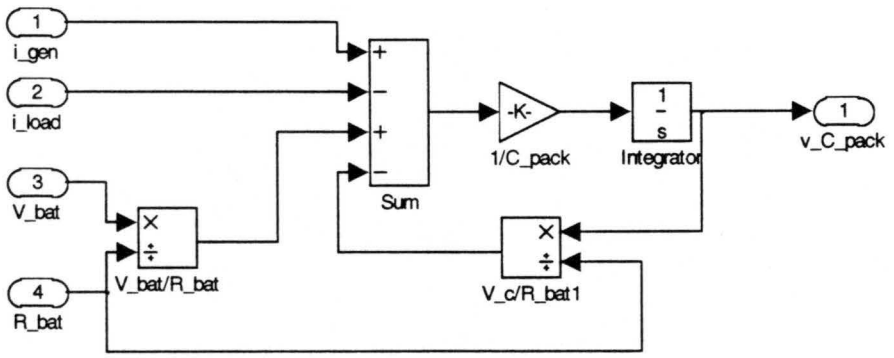

Figure 33: Battery pack capacitance model.

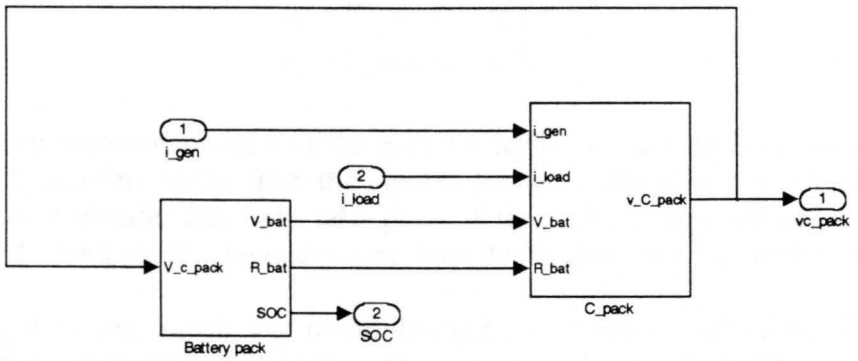

Figure 34: Battery pack SIMULINK model.

2.7 Rectifier Model

The rectifier in the UI HEV is a three-phase bridge consisting of six Silicon Controlled Rectifiers (SCRs), a firing circuit, and a current controller. The rectifier is used to convert the ac current from the generator into a dc current to supply the battery pack. A rectifier circuit diagram is shown in Figure 35. The rectifier in the figure has been simplified for illustration

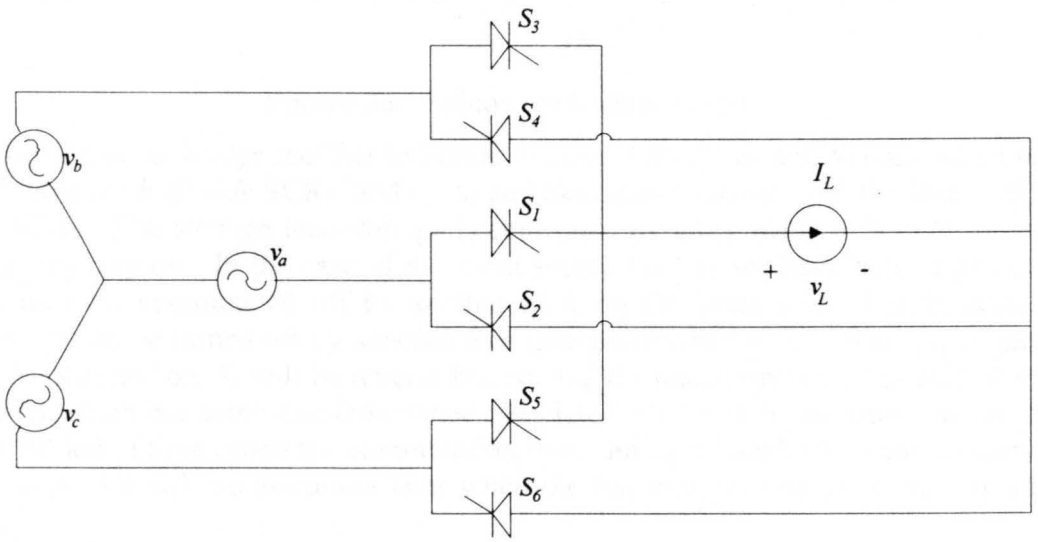

Figure 35: Simplified rectifier model.

purposes. This circuit as three ac input voltage sources, six SCRs and a dc current source load. The voltages of the three input sources form a balanced three-phase set and are

$$
\begin{aligned}
v_a &= V_0 \sin(\omega t) \\
v_b &= V_0 \sin(\omega t - \tfrac{2\pi}{3}) \\
v_c &= V_0 \sin(\omega t + \tfrac{2\pi}{3})
\end{aligned}
\tag{89}
$$

The basic operation of the rectifier is to cyclically connect the input sources to the load in a manner which transfers power from the input to the load. The load is a dc current source. This means that power transfer can only take place if the voltage imposed across the load by the rectifier has a dc component. To understand how this is done, we first look at the operation of a single SCR.

The SCR is very much like a simple diode; it is capable of conducting current in the forward direction and is reverse blocking. The circuit symbol for the SCR is shown in Figure 36. The main difference between the two, is the SCR can also forward block. In fact, if just placed in a circuit, it will block in both directions. Forward conduction of the SCR is initiated by applying a current pulse to the third terminal called the gate. Forward conduction will then commence given that the device was initially forward biased from anode to cathode. At this point, the SCR can be modeled much like a diode [6]. The SCR will continue to conduct until the current flowing through the device goes to zero. This is a very important aspect of the SCR; its turn-on time is directly controllable by when the gate signal is applied, but its turn-off time is determined by the current flow through the device. In essence, turn-off is determined by the circuit in which the SCR resides.

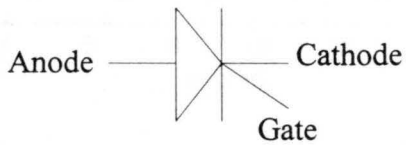

Figure 36: Silicon controlled rectifier.

Looking at the bridge rectifier in Figure 35, the SCRs S_1, S_3 and S_5 conduct current to the load, call these the *high side* SCRs, and S_2, S_4 and S_6 conduct current from the load, call these the *low side* SCRs. The average load voltage is controlled by when these SCRs are turned on and how long they stay on. In the case of a current source load as we have here, a particular SCR will stay on until commutated off by another SCR on the same side. For instance, if S_1 is conducting, it can be turned off by sending S_3 a gate pulse when $v_b > v_a$. Since v_b is greater than v_a, when S_3 is turned on, S_1 will be reverse biased, and the load current will be shifted to v_b. In a real rectifier which has some line inductance associated with each input source phase, there will be a short period of time called the commutation time, during which both S_1 and S_3 carry the load current. This case will be discussed later when the full rectifier and generator are considered together.

Figure 37 shows the phase voltages input to the rectifier. The amplitude of the phase voltages is taken as one for simplicity. For ease of analysis, the time axis has been multiplied by the frequency of the sinusoids to place it in radians. The delay angle α defines the turn-on of the SCRs. The delay angle is defined to be zero for S_1 at $\omega t = \pi/6 + 2k\pi$ and zero for S_2 at $\omega t = \pi/6 + (2k+1)\pi$ for $k = 0,1,2,\ldots$ It may be similarly defined for the remaining SCRs, only shifted by $2\pi/3$ radians for the phase b SCRs, and $4\pi/3$ for the phase c SCRs. The reason $\alpha = 0$ is defined this way is because of the assumption of continuous current conduction due to the current

sourced load. Consider trying to turn on S_3 before the point α=0 as defined above. In this situation, as we attempt to turn on S_3, S_1 is conducting and $v_a > v_b$. Therefore, S_3 is reverse biased and will not conduct. However, if an attempt is made to turn on S_3 after the point α=0, forward bias exists and S_3 will turn-on, taking the current away from S_1.

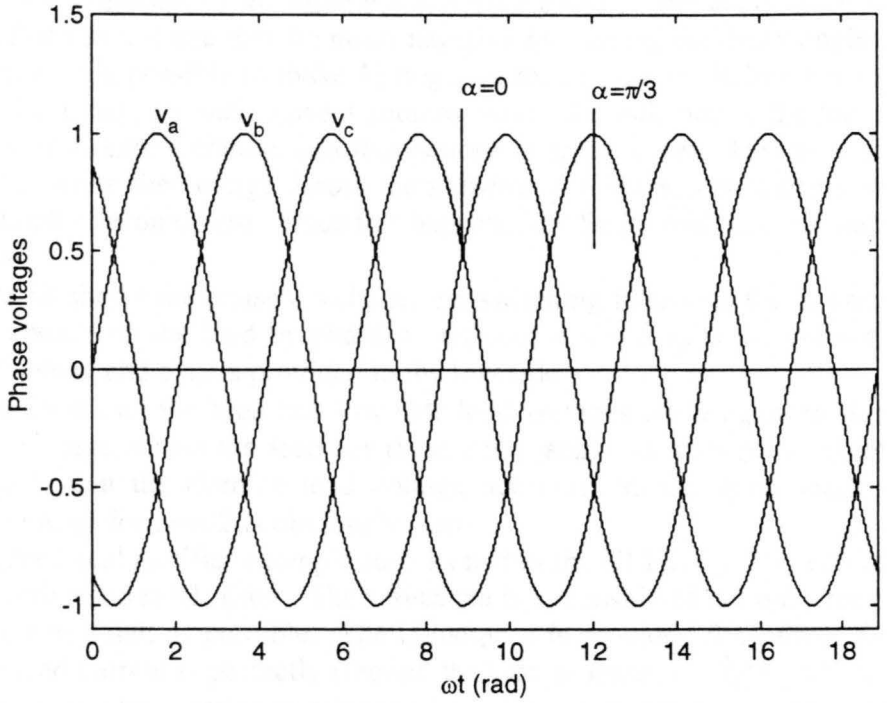

Figure 37: Rectifier input phase voltages.

As mentioned above, it is necessary to for the load voltage to have a dc component in order to transfer power to the dc current source. For this simplified rectifier, it is easy to demonstrate that this dc component exists. The average load voltage may be calculated by realizing that each SCR comes on at α and stays on for $2\pi/3$ radians. The average voltage on the high side of the load is

$$\langle v_{high} \rangle = \frac{3V_0}{2\pi} \int_{\alpha}^{\alpha+2\pi/3} \sin\left(\theta + \tfrac{\pi}{6}\right) d\theta = \frac{3\sqrt{3}V_0}{2\pi} \cos(\alpha)$$

where $\theta = \omega t$ and V_0 is the amplitude of the phase voltages, in this case one. The average voltage of the low side is evaluated in a similar manner.

$$\langle v_{low} \rangle = \frac{3V_0}{2\pi} \int_{\alpha}^{\alpha+2\pi/3} \sin\left(\theta + \tfrac{\pi}{6} + \pi\right) d\theta = -\frac{3\sqrt{3}V_0}{2\pi} \cos(\alpha)$$

The dc component of the load voltage is

$$V_L = \langle v_{high} \rangle - \langle v_{low} \rangle = \frac{3\sqrt{3}V_0}{\pi}\cos(\alpha) \tag{90}$$

for $0 \le \alpha \le \pi$. This shows that the load voltage has a dc component whose amplitude is dependent on the amplitude of the input phase voltages and on the delay angle α. Equation (90) even implies that this voltage may be made negative by making the delay angle greater than 90°. For this example, it is possible to make V_L negative for as long as desired because of the current source load. In reality, no such current sources exist. An inductor in the load can emulate the characteristics of a current source, and this is done in many cases. However, in contrast to the example above, when the voltage across the inductor is reversed, the current will begin to fall, and will eventually become zero. Once this happens, the SCRs will turn-off and the load voltage will fall to zero.

Figure 38 shows the phase *a* voltage, the switching functions for S_1 and S_2 for α=0, and the voltage imposed on the load by phase *a*. Of course, the $S_1 v_a$ is the voltage provided to the high side of the load and $S_2 v_a$ is provided to the low side.

Figure 39 shows the high and low side load voltages for α equal to 0, $\pi/6$, $\pi/3$ and $\pi/2$ radians. The voltage across the load for these delay angles is shown in Figure 40. It is clear from these plots that the average load voltage decreases as the delay angle increases. The average load voltage for $\alpha=\pi/2$ is obviously zero.

Consider a real rectifier example such as that in the UI HEV. The rectifier load is a is the battery pack with a series RL filter. The resistance is a parasitic of the inductor and batteries and should be made as small as possible. The inductance is provided for current filtering to reduce losses. If the load current is perfectly filtered, the system losses are $I_L^2 R_t$, where I_L is the dc load current and R_t is the total series resistance of the RL combination and the battery pack. The largest unwanted frequency component of the load voltage for the rectifier discussed above is six times the input frequency. There are also additional, higher frequency components as well. These voltage components create current components of the same frequency in the load. If they are not filtered, the losses become

$$P_{loss} = \left(I_L^2 + \sum_j I_{Lj}^2 \right) R_t$$

where I_{Lj} are the additional current components. This loss is obviously greater than $I_L^2 R_t$. Since the only power transferred to load is due to the zero component, it is desirable to eliminate the I_{Lj} components. The largest and hardest to filter component is I_{L6}, and usually the filter is chosen with the reduction of this component in mind.

In a real world application, the delay angle must be calculated and translated into a real time quantity that may be used to trigger the SCRs. Consider the expression for the load voltage in eq. (90). This equation is non-linear in the control variable α making the control issue difficult. However, if we define the control variable to be $\kappa=\cos(\alpha)$, the problem becomes linear [6]. A possible control strategy is then to sense the average load voltage, compare it to the desired load voltage, and use the error, possibly with a PI controller, to adjust κ.

The calculation of the arccosine can be done in a very simple way. Let κ be the control input which varies between zero and the amplitude of the phase voltages, in this case, one. Let v_{ar} be a cosine function of the same frequency as the phase voltages that is equal to one at α=0

for phase *a* as illustrated in Figure 41. The SCR S_1 is to be turned on at $\alpha=\omega t_{on}$. The time t_{on} is exactly the point where κ and v_{ar} meet. The trigger for S_1 is derived by comparing κ and v_{ar}. As v_{ar} crosses and falls below κ, the comparator triggers S_1. The remaining high side SCRs S_3 and S_5 are triggered in a similar fashion. The low side SCR S_2 can be triggered by comparing $-\kappa$ to v_{ar}. The only difference is that the comparator must detect when v_{ar} cross and goes above $-\kappa$. The remaining low side SCRs are triggered similarly.

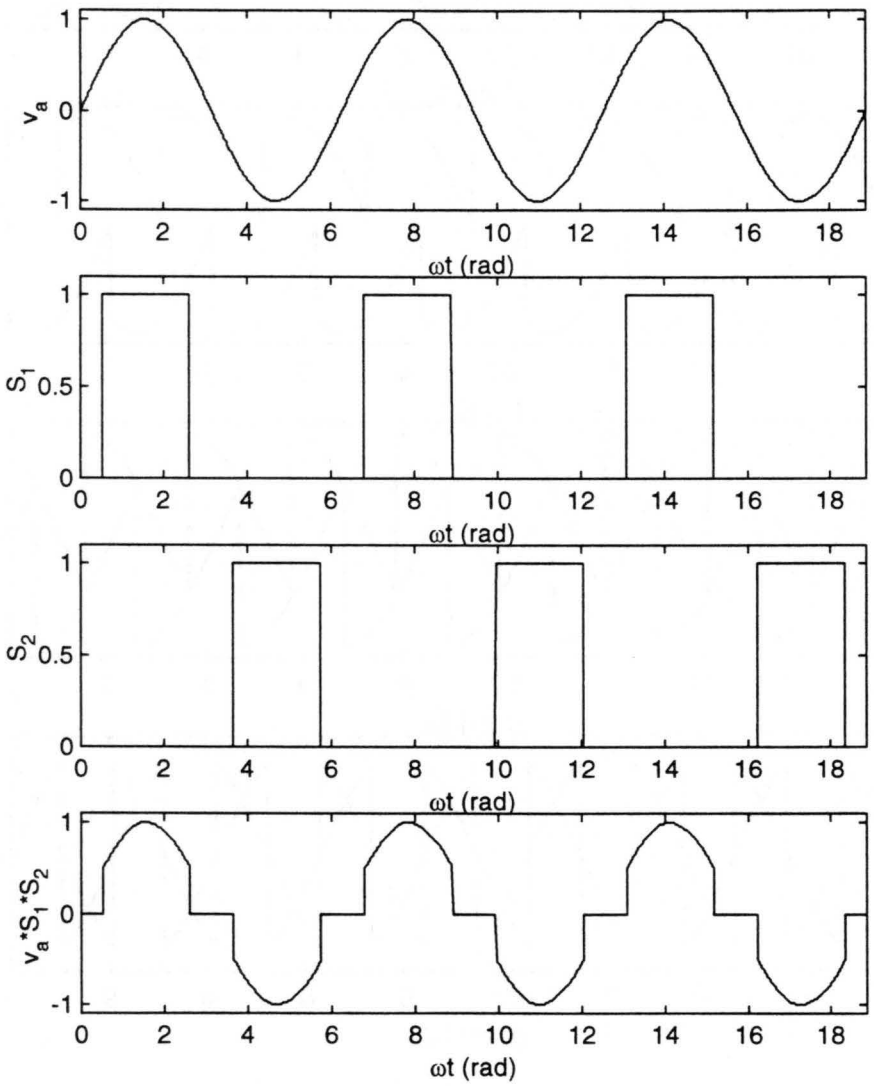

Figure 38: Phase *a* voltage, switching functions and voltage imposed on load.

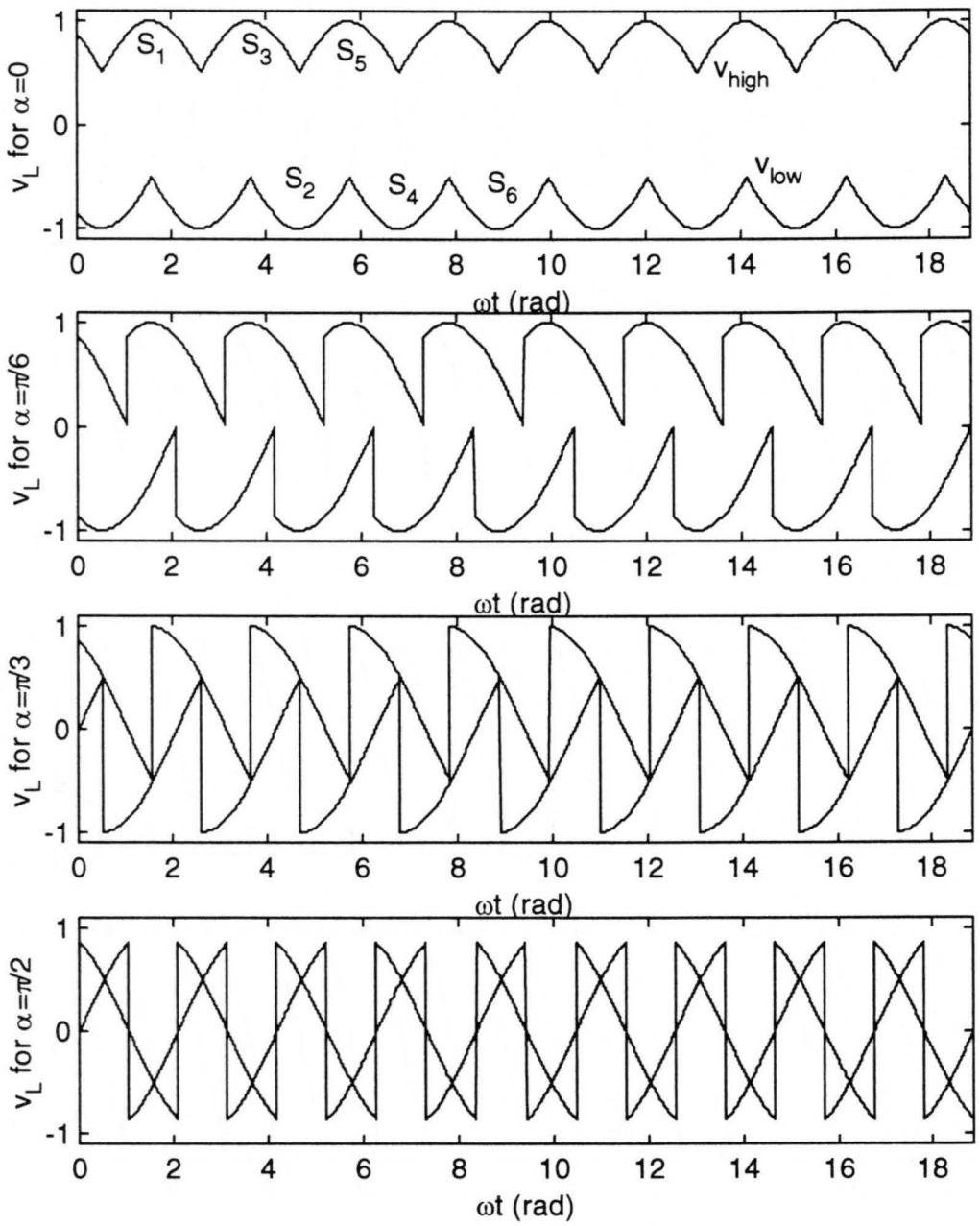

Figure 39: High and low side load voltages for various values of α.

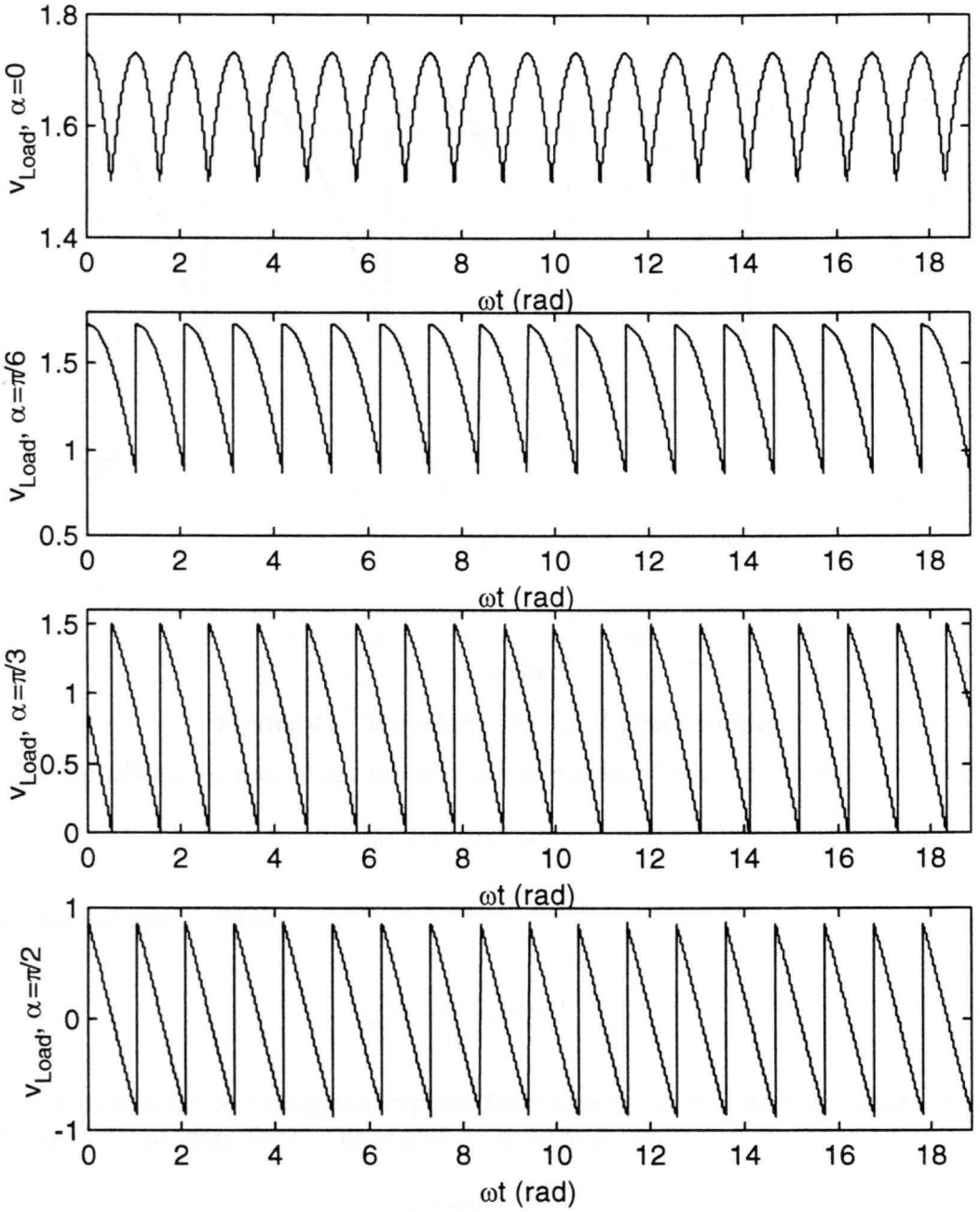

Figure 40: Voltage across the load for various values of α.

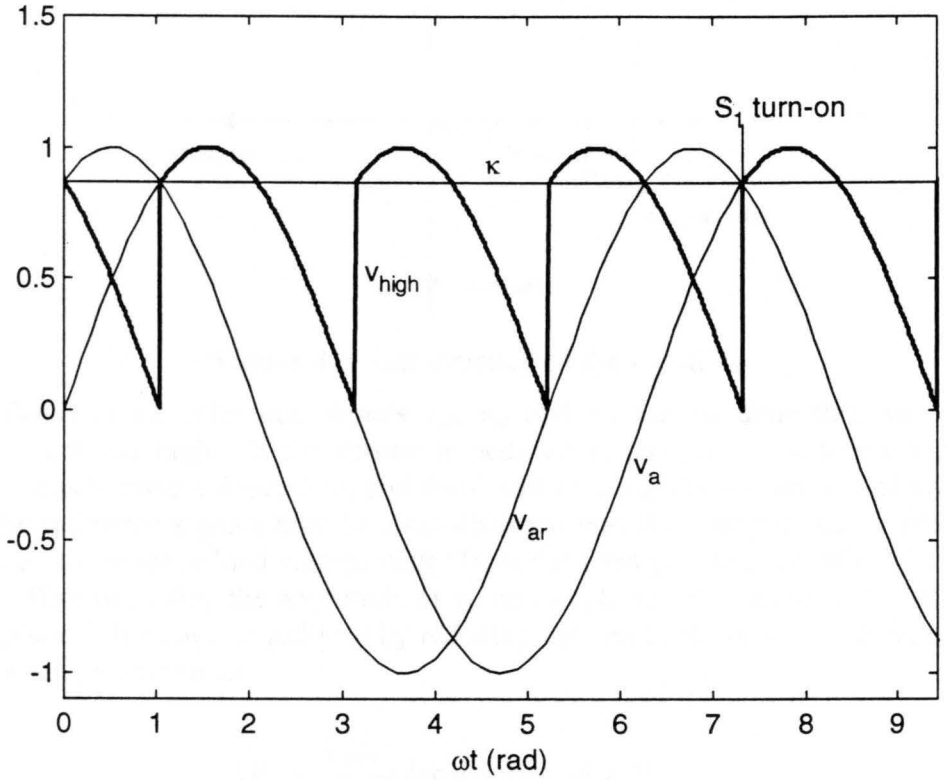

Figure 41: Waveforms for SCR phase control.

The signals v_{ar}, v_{br} and v_{cr} are not difficult to obtain. Consider the phase *a* voltage

$$v_a = V_0 \sin(\omega t)$$

Integrate this voltage to obtain

$$v_{ax} = -\frac{V_0}{\omega}\cos(\omega t) \tag{91}$$

and we now have a set of orthogonal signals from which v_{ar} may be synthesized by using, for example, operational amplifiers. The signal we need to create is

$$v_{ar} = \cos(\omega t - \tfrac{\pi}{6}) \tag{92}$$

The construction of this signal is shown graphically in Figure 42. From the figure, v_{ar} is given by

$$v_{ar} = \sin(\tfrac{\pi}{6})\sin(\omega t) + \cos(\tfrac{\pi}{6})\cos(\omega t) \tag{93}$$

The signals v_{br} and v_{cr} are constructed in a similar manner.

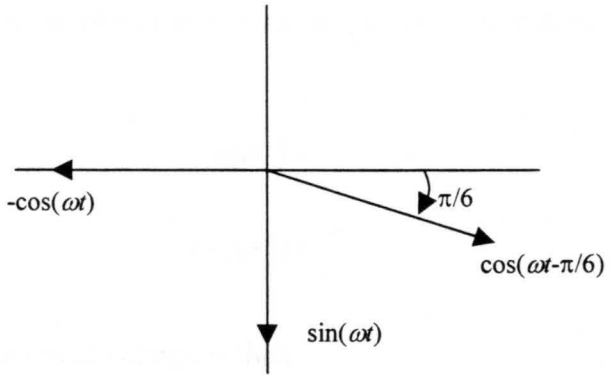

Figure 42: Construction of the signal v_{ar}.

Synthesis of the reference signals v_{ar}, v_{br} and v_{cr} can be done this way if the source impedance is not too high. If the source impedance is too great, the terminal voltages will become very much current dependent, and there will be a significant amount of switching noise present. The reference signals may become distorted and their amplitudes or phases changed. This will make the average load voltage differ from the form given in eq. (90).

The effect of scaling the amplitude of v_{ar} on the phase delay angle is shown in Figure 43. The actual phase delay angle is reduced by reducing the amplitude of v_{ar}. The change in average load voltage can be written as

$$\Delta V_L = \frac{3\sqrt{3}V_0}{\pi}\left(\cos(\alpha_1) - \cos(\alpha_2)\right)$$

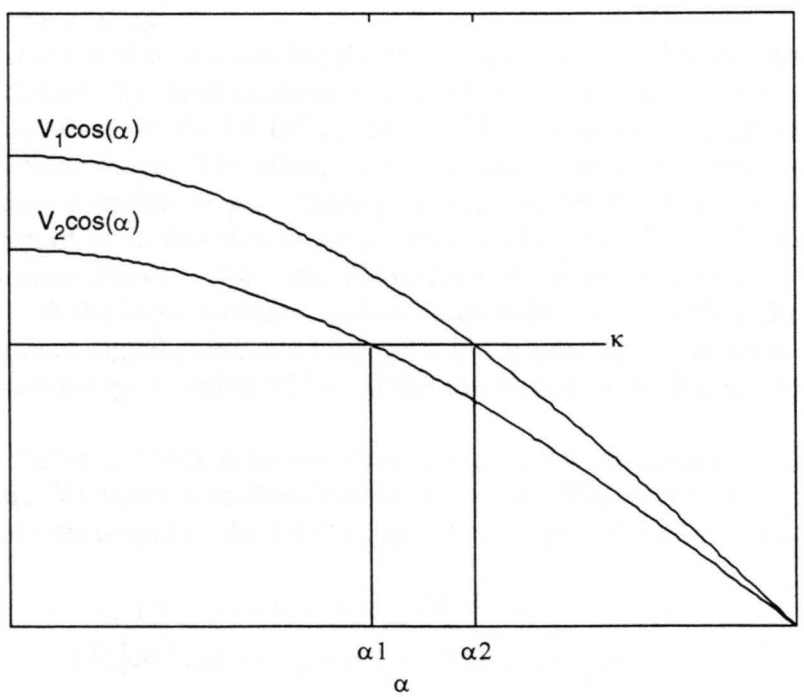

Figure 43: Effect of scaling the amplitude of v_{ar} on the delay angle.

The cosine function can be eliminated from the previous equation substituting the following expressions

$$\cos(\alpha_1) = \frac{\kappa}{V_1}$$

$$\cos(\alpha_2) = \frac{\kappa}{V_2}$$

The change in the average load voltage is then

$$\Delta V_L = \frac{3\sqrt{3}V_0}{\pi}\left(\frac{V_1 - V_2}{V_1 V_2}\right)\kappa$$

Now, let V_1=1, which is the desired value, and let V_2<1. The expression for the average load voltage is

$$\Delta V_L = \frac{3\sqrt{3}V_0}{\pi}\left(\frac{1 - V_2}{V_2}\right)\kappa \tag{94}$$

which shows that the average load voltage increases as the amplitude of the reference signal v_{ar} decreases.

The second problem of v_{ar} having phase error is simpler. The delay angle varies linearly with changes in the phase of v_{ar}.

The last difficulty is that of obtaining the line frequency needed to construct the reference signals. There is a division by input frequency in eq. (91). If the line frequency is constant, this is not a problem. However, in the UI HEV, the rectifier is coupled to a generator which may vary its speed over a wide range. Therefore, there is a need to sense the input frequency in some way. This can be done in several ways, including sensing the generator shaft speed.

The generation of v_{ar} in this simulation program and in the UI HEV is done in a different way from the discussion above. They use Phase-Locked-Loops (PLLs) to synthesize signals which are in phase with the input voltages, and of magnitude one. The PLL does a good job of maintaining the reference signal phase and amplitude in the presence of rectifier input distortion. There is a slight disadvantage to using PLLs. If the input frequency changes too fast, they will fail.

The PLL is shown in block diagram form in Figure 44. It consists of a mixer, lowpass filter, integrator, and a Voltage Controlled Oscillator (VCO). The mixer used is a multiplier that has as inputs $v_{in}(t)$ and the output of the VCO $v_{vco}(t)$. The output of the mixer is given by

$$\begin{aligned} v_m(t) &= v_{in}(t)v_{vco}(t) = V_0\cos(\omega_{in} + \theta_{in})\cos(\omega_{in}t + \theta_{vco}) \\ &= V_0\left[\cos(2\omega_{in}t + \theta_{in} + \theta_{vco}) + \cos(\theta_{in} + \theta_{vco})\right] \end{aligned} \tag{95}$$

where

$$v_{in}(t) = V_0 \cos(\omega_{in} t + \theta_{in})$$
$$v_{vco}(t) = \cos(\omega_0 t + \theta_{vco})$$

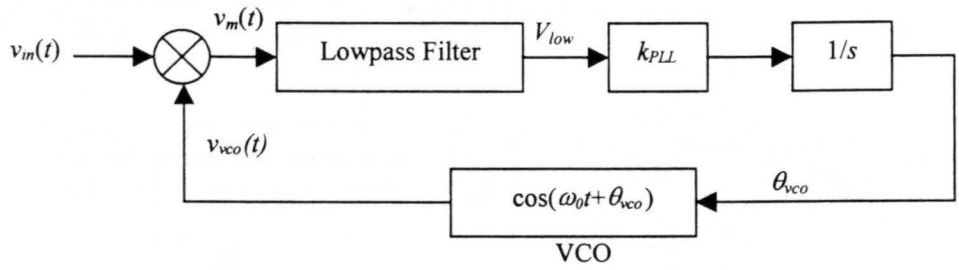

Figure 44: Block diagram of the Phase-Locked-Loop.

The mixer output frequency components are the sum and difference of the input voltage and the VCO frequencies. This signal is then passed through a lowpass filter to attenuate the higher frequency component. The output of the lowpass filter is approximately

$$v_{low} \cong k \cos(\theta_{in} - \theta_{vco})$$

This signal is then scaled by k_{PLL} and integrated, and the result used to control the VCO. The loop attempts to minimize this value. At the minimum, the VCO voltage is

$$v_{vco}(t) = \cos(\omega_{in} t - \tfrac{\pi}{2}) = \sin(\omega_{in} t) \qquad (96)$$

Even though the VCO was shown here to have the same frequency as the input source, this process will still work even if it is not. If there is a frequency difference between v_{in} and v_{vco}, then there is a corresponding increase in phase error with time. As the phase is corrected, the frequencies will become the same.

The input to the rectifier is provided by the synchronous generator. Therefore, the input frequency is dependent directly on the generator shaft speed. The fact that this speed is not constant requires the filter in the PLL to be second order with two free integrators. This will allow the PLL to track a ramp in frequency [8].

The PLL delivers a signal with a set amplitude of one that lags the input signal by 90°. Adding a PLL to each phase gives a balanced three-phase set of signals from which v_{ar}, v_{br} and v_{cr} can be constructed.

The SIMULINK block diagram of a PLL is shown in Figure 45. Saturation has been added to the input and VCO signals that effectively squares the sinusoids. This eliminates distortion present in the input signal. The PLL process works in much the same way, however. The t_out signal is the width of the gate pulse. In a real rectifier, the SCR may be initially reverse biased when the gate pulse arrives. This prevents the SCR from coming on. This problem is alleviated by extending the gate pulse to a length of $\pi/2$ radians. If the SCR is initially reverse biased, it will come on at the instant it becomes forward biased.

Construction of the timing signals v_{ar}, v_{br} and v_c is shown in Figure 46. These signals are constructed directly from the three-phase balanced set delivered by the PLLs. If unbalanced

operation, such as the loss of a generator phase, is required, the signals may be constructed as described above by using integration to create an orthogonal set of signal vectors for each phase.

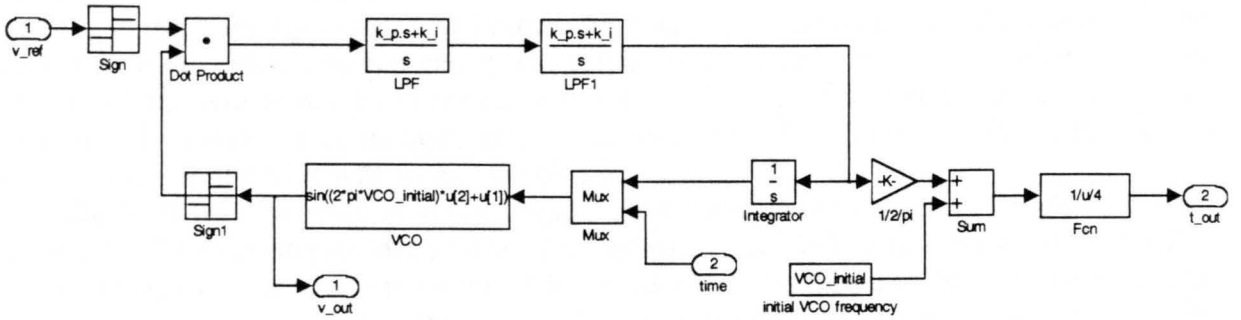

Figure 45: Block diagram of Phase-Locked-Loop.

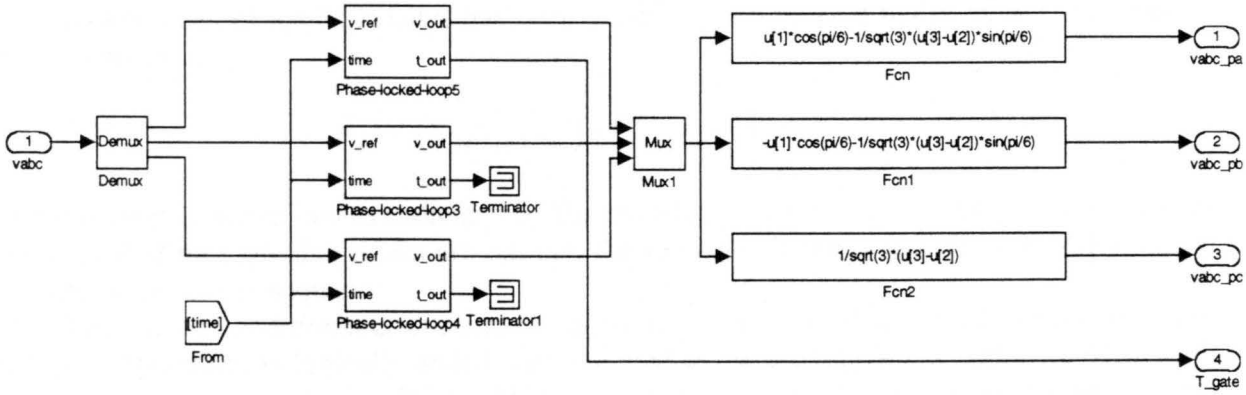

Figure 46: Construction of the reference signals v_{ar}, v_{br}, and v_c.

The SIMULINK block diagram for generation of the trigger pulses used to turn on the individual SCRs is shown Figure 47. The reference signals v_{ar}, v_{br} and v_{cr} are compared with κ to detect when the reference signals fall below κ and trigger the high side SCRs. The low side SCRs are triggered by comparing the reference signals to $-\kappa$. The signals SCR_a, SCR_b, and SCR_c are used to control the high and low side phase *a*, *b*, and *c* SCR pairs, respectively.

These trigger signals activate the gate drivers for each SCR as shown in Figure 48. The gate drivers are positive edge-triggered D flip-flops. The Q-output of each flip-flop is used to trigger its respective SCR. This output is held high for the length of time specified by T_gate. Ideally, the trigger should be held high for $\pi/2$ radians as mentioned above.

Figure 49 shows the block diagram model for each SCR. The state of the SCR, either on or off, is modeled by a positive edge-triggered D flip-flop. The flip-flop output Q is equal to one when the SCR is in the on-state. The output $!Q$ is equal to 1-Q. The clock signal for the flip-flop is state with boolean operations as follows

$$CLK = V_{bias} V_{gate}(!Q) + V_{gate}(!Q_d)$$

where $!Q_d$ is a delayed version of $!Q$, V_{bias} is equal to one when the SCR is forward biased, and V_{gate} is equal to one when the gate signal is active. If the SCR is initially off and the gate signal is made active, the clock input will become high until the flip-flop changes state, and the clock will then go low. The gate signal remains high for $\pi/2$ radians, but the clock signal will stay low. If the SCR is reset, the $!Q$ output will become high again. If the gate signal is still active, the second term in the clock equation above will cause the flip-flop to be clocked again. In other words, an attempt will be made to once again turn the SCR on. This mimics the action of a real rectifier which provides a continuous gate pulse train for $\pi/2$ radians. If the SCR terminal conditions allow it, the SCR will go into the on-state again.

The SCR may be reset in several ways. The most obvious reset is the phase current crossing zero. This action provides a reset signal given that the SCR was in the on-state initially. The second way to cause a reset is for the SCR current to be less than a value i_eps after the gate signal has become inactive, given that the SCR was initially in the on-state. This prevents the SCR from remaining on indefinitely with zero phase current. The last way to reset the SCR is provided by the Reset Logic block in Figure 52. This reset prevents two SCRs on the same side, high or low, from being active when there are no active SCRs on the other side. This situation can occur when one of the SCR gates has been disabled to simulate a faulty SCR. The reset for phase *a* is given by

$$\overline{R}_{AL} = \left(S_{HA} S_{HB} S_{HC}\right) + \left(\overline{S}_{LA} + \overline{S}_{LB}\right)$$

where this reset is active low as indicated by the over-bar. This equation says reset the low-side phase a SCR if no high-side SCRs are on, and the low-side phase *a* and phase *b* SCRs are on. This applies for an *abc* sequence.

There is one additional constraint, but is not really a reset. A control line from each low side SCR's $!Q$ output is logically anded with the enable for the respective high-side SCR. The same is true for each high-side SCR. This prevents both SCRs belonging to one phase from coming on simultaneously. Once again, this problem arises when simulating fault conditions.

Figure 50 shows the SCR pair for phase *a*, the gate driver block, and the check for forward bias. The check for forward bias is done by comparing the phase voltage with either V_H, the high side load voltage, or V_L, the low side load voltage.

Figure 51 shows how the high and low side load voltages, and the load current are determined. Define the following vectors

$$\mathbf{S}_H = \begin{bmatrix} S_1 & S_3 & S_5 \end{bmatrix}^T$$
$$\mathbf{S}_L = \begin{bmatrix} S_2 & S_4 & S_6 \end{bmatrix}^T$$
$$\mathbf{v}_{abc} = \begin{bmatrix} v_a & v_b & v_c \end{bmatrix}^T$$
$$\mathbf{i}_{abc} = \begin{bmatrix} i_a & i_b & i_c \end{bmatrix}^T$$

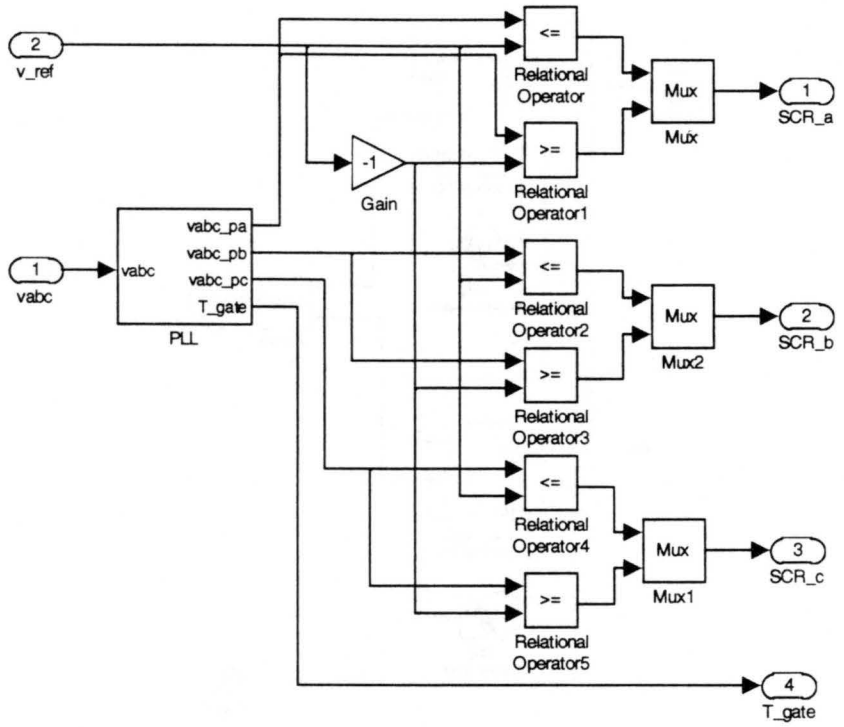

Figure 47: Generation of SCR gate trigger pulses.

The high and low side load voltages are given by

$$v_H = \left[\frac{\mathbf{S}_H^T \mathbf{v}_{abc}}{\mathbf{S}_H^T \mathbf{S}_H + \overline{Z}_H} + \overline{Z}_H (V_b + v_L) \right] (Z_H + Z_L) \tag{97}$$

$$v_L = \left[\frac{\mathbf{S}_L^T \mathbf{v}_{abc}}{\mathbf{S}_L^T \mathbf{S}_L + \overline{Z}_L} + \overline{Z}_L (v_H - V_b) \right] (Z_H + Z_L) \tag{98}$$

where

$$Z_H = \begin{cases} 1 & \mathbf{S}_H^T \mathbf{S}_H > 0 \\ 0 & \mathbf{S}_H^T \mathbf{S}_H = 0 \end{cases}$$

$$Z_L = \begin{cases} 1 & \mathbf{S}_L^T \mathbf{S}_L > 0 \\ 0 & \mathbf{S}_L^T \mathbf{S}_L = 0 \end{cases}$$

and $\overline{Z}_H = 1 - Z_H$, $\overline{Z}_L = 1 - Z_L$, and V_b is a dc voltage source in series with the load. Z_H and Z_L are logical variables, therefore the sum in Z_H+Z_L in eqs. (97) and (98) is equal to zero or one.

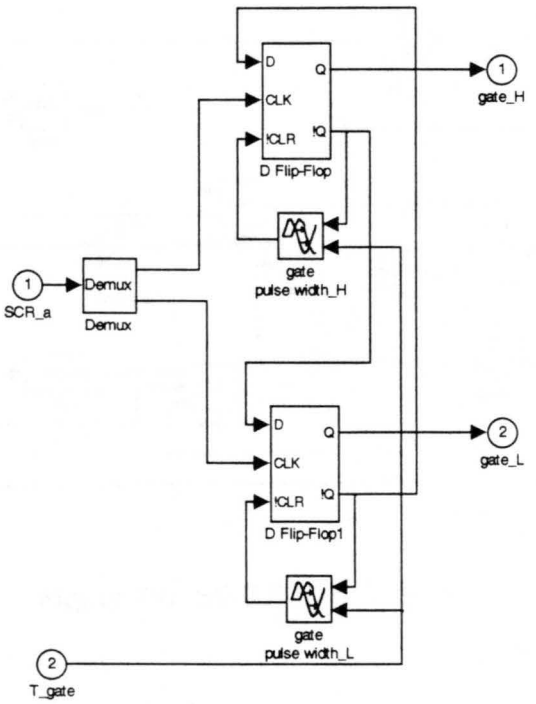

Figure 48: SCR gate drive pair for the phase *a* SCRs.

The expressions for the high and low side load voltages do not define exactly the load voltage. They are used to determine if the SCRs are forward biased or not. For instance, if no SCRs are on, $\mathbf{S}_H$=0 and $\mathbf{S}_L$=0, the by eqs. (97) and (98), v_H=0 and v_L=0. This does not mean that the voltage across the load is zero. It means that the load voltage is floating with respect to the rectifier. Either a high or low side SCR may be turned on at this point. However, as soon as any of the SCRs are turned, the load voltage is then well defined with respect to the rectifier.

Consider the case where S_1 is in the on-state. The high side load voltage, as given by eq. (97) is v_a. This is correct because the high side of the load is connected directly to phase *a*. The low side load voltage, as given by eq. (98) is v_a-V_b. This is confirmed by summing the voltages from phase *a* to the low side of the load. In order for a low side SCR to be turned on, its respective phase voltage must be lower than v_L.

When two high side SCRs are on, the high side load voltage, from eq. (97), is equal to the average of the two phases connected to the high side. This the commutation process in which one SCR is turning off and another is turning on. The fact that the load voltage is equal to the average of the connected phase voltages will be shown later.

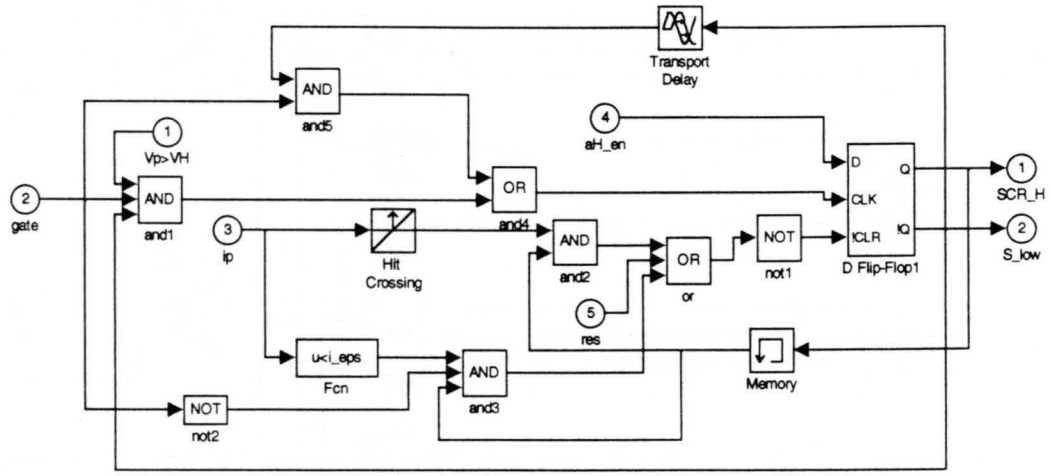

Figure 49: SIMULINK SCR model.

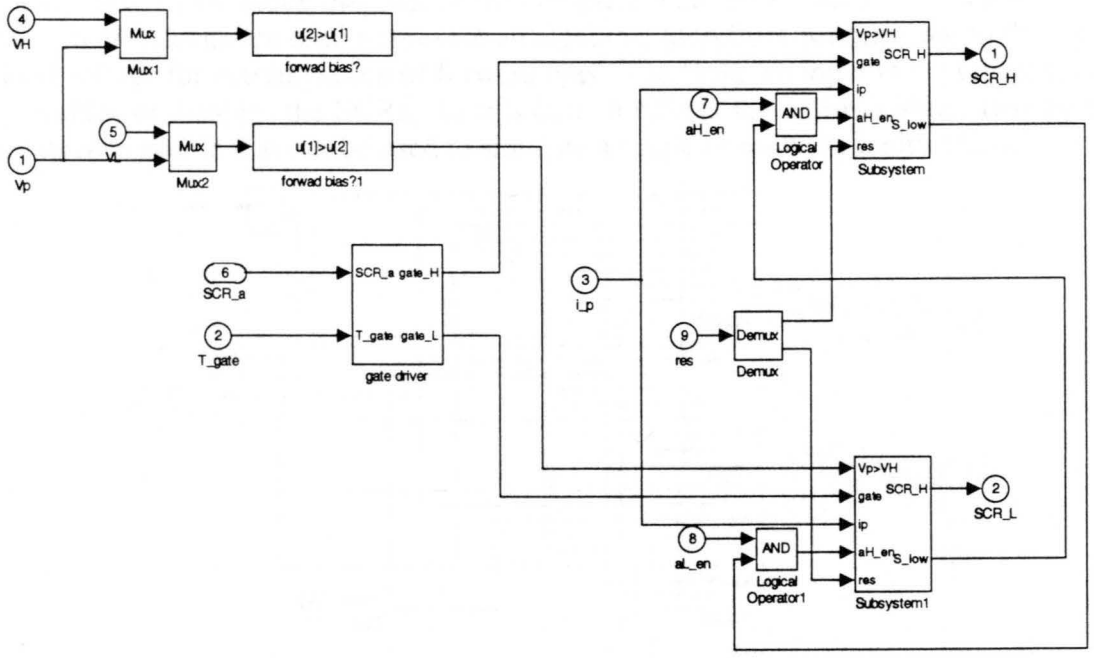

Figure 50: Phase *a* SCR pair with gate driver.

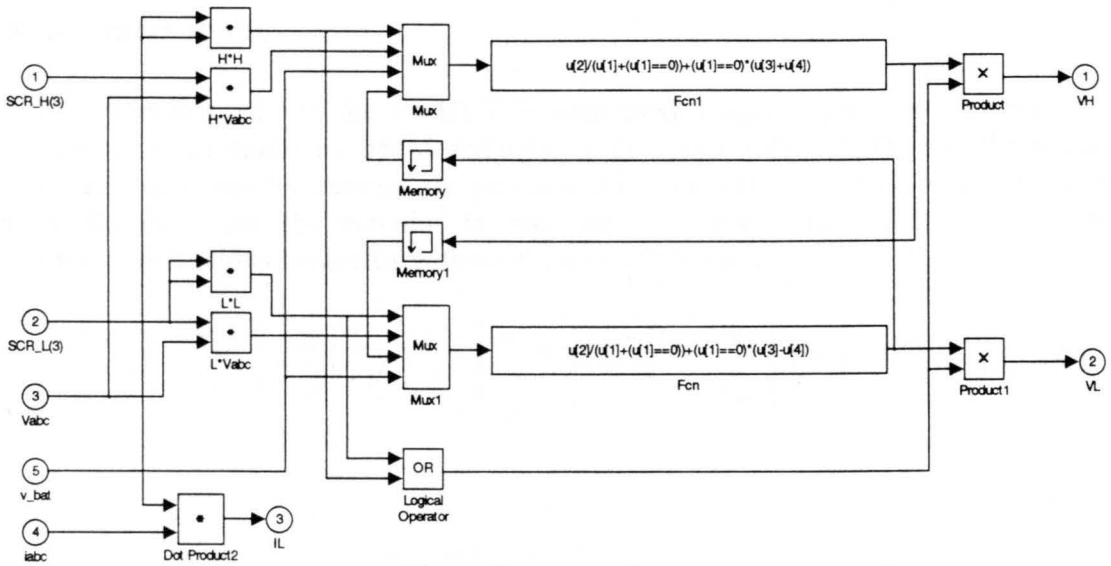

Figure 51: Determination of the high and low side load voltages and the load current.

The SIMULINK block diagram of the complete SCR bridge rectifier is shown in Figure 52. The memory blocks are used to prevent an algebraic loop from forming due to the feed back of the load voltage for determination of forward bias. The Brdg_en input is the bridge enable. It directly enables or disables the SCRs. In this case, it affects the entire bridge. However, each SCR has its own enable that can be used to simulate a single or multiple faulty SCRs.

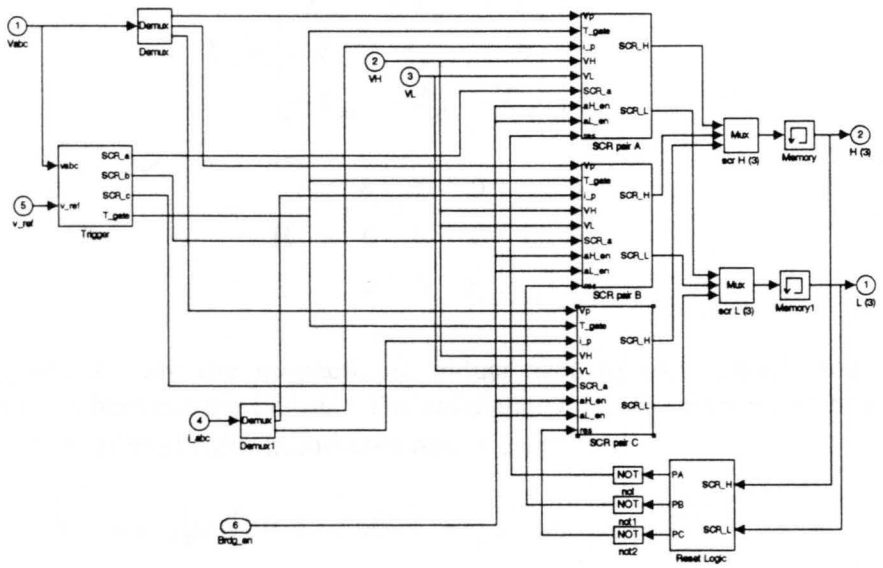

Figure 52: SIMULINK block diagram of SCR bridge.

2.8 Generator Model

The generator used in the UI HEV is permanent magnet synchronous generator. The model is presented in stationary *abc* coordinates to be compatible with the rectifier model. The model contains no damper windings, the permanent magnets are simulated by a constant current applied to the field, and the machine is assumed to be round rotor [9]. The model for a conventional synchronous generator with no damper windings is

$$\begin{bmatrix} \mathbf{v}_{abc} \\ v_{fd} \end{bmatrix} = \frac{d}{dt}\begin{bmatrix} \mathbf{L}_s & \mathbf{L}'_{sr} \\ \mathbf{L}'^{T}_{sr} & L_r \end{bmatrix}\begin{bmatrix} -\mathbf{i}_{abc} \\ i_{fd} \end{bmatrix} + \begin{bmatrix} -\mathbf{R}_s & \mathbf{0} \\ \mathbf{0} & R_{fd} \end{bmatrix}\begin{bmatrix} \mathbf{i}_{abc} \\ i_{fd} \end{bmatrix} \tag{99}$$

where

$$\mathbf{v}_{abc} = \begin{bmatrix} v_a & v_b & v_c \end{bmatrix}^T$$

are the stator voltages, and

$$\mathbf{i}_{abc} = \begin{bmatrix} i_a & i_b & i_c \end{bmatrix}^T$$

are the stator currents. The matrices $\mathbf{L}_s$ and $\mathbf{R}_s$ are

$$\mathbf{L}_s = \begin{bmatrix} L_{aa} & -L_{ab} & -L_{ac} \\ -L_{ba} & L_{bb} & -L_{bc} \\ -L_{ca} & -L_{cb} & L_{cc} \end{bmatrix}$$

$$\mathbf{R}_s = \begin{bmatrix} r_s & 0 & 0 \\ 0 & r_s & 0 \\ 0 & 0 & r_s \end{bmatrix}$$

where L_{aa}, L_{bb}, and L_{cc} are the magnetizing inductances of each phase, and the others are coupling inductances between the phases. The resistance r_s is the series resistance of each phase. The vector L_{sr}' is the referred rotor inductance and is given by

$$\mathbf{L}'_{sr} = L_{md}\left[\sin\left(\tfrac{P}{2}\theta_r\right) \quad \sin\left(\tfrac{P}{2}\theta_r - \tfrac{2\pi}{3}\right) \quad \sin\left(\tfrac{P}{2}\theta_r + \tfrac{2\pi}{3}\right)\right]^T \tag{100}$$

where

$$\theta_r = \int_0^t \omega_r dt$$

is the machine rotor position. In this case, the machine contains permanent magnets, so $i_{fd}=I_{fd}$ is constant, and the rotor equation can be neglected. The stator equation can be written as

$$\mathbf{v}_{abc} = -\mathbf{R}_s \mathbf{i}_{abc} - \mathbf{L}_s \frac{d\mathbf{i}_{abc}}{dt} + \tfrac{P}{2}\omega_r I_{fd} L_{md} \begin{bmatrix} \cos\left(\tfrac{P}{2}\theta_r\right) \\ \cos\left(\tfrac{P}{2}\theta_r - \tfrac{2\pi}{3}\right) \\ \cos\left(\tfrac{P}{2}\theta_r + \tfrac{2\pi}{3}\right) \end{bmatrix} \tag{101}$$

The constant $I_{fd}L_{md}$ can be evaluated from open circuit data. The terminal voltage of the unloaded generator is related to the speed by constant. Call this constant k_g in units of V•s/rad. The rms phase voltage of the unloaded generator is given by

$$V_{phase} = k_g \omega_r \tag{102}$$

The quantity $I_{fd}L_{md}$ is then

$$I_{fd} L_{md} = \frac{2\sqrt{2}}{P} k_g \tag{103}$$

Since the machine is round rotor, the shaft torque is given by

$$T_{em} = L_{md} i'_{fd} \frac{P}{2}\left[\left(i_a - \frac{1}{2}i_b - \frac{1}{2}i_c\right)\cos\left(\tfrac{P}{2}\theta_r\right) + \frac{\sqrt{3}}{2}(i_b - i_c)\sin\left(\tfrac{P}{2}\theta_r\right)\right] \tag{104}$$

The rotor speed equation is

$$J_T \frac{d\omega_r}{dt} = \frac{N_{sm}}{N_{ICE}} T_{ICE} - T_{em} \tag{105}$$

where the ICE torque has been scaled by the belt drive ratio between the ICE and the generator. The inertia J_T is the total inertia of the generator, ICE and belt drive.

The SIMULINK block diagram of the generator is shown in Figure 53. The block labeled SM solves the machine equations for the various terminal constraints imposed by the rectifier and will be discussed in the next section when the rectifier and generator are considered together. The block T_generator determines the generator shaft torque and the block V_abc gives the terminal voltages of the motor. The shaft torque is determined directly from eq. (104) and the terminal voltages are provided by eq. (101). The rotor speed block is not shown here, but is implemented directly from eq. (105).

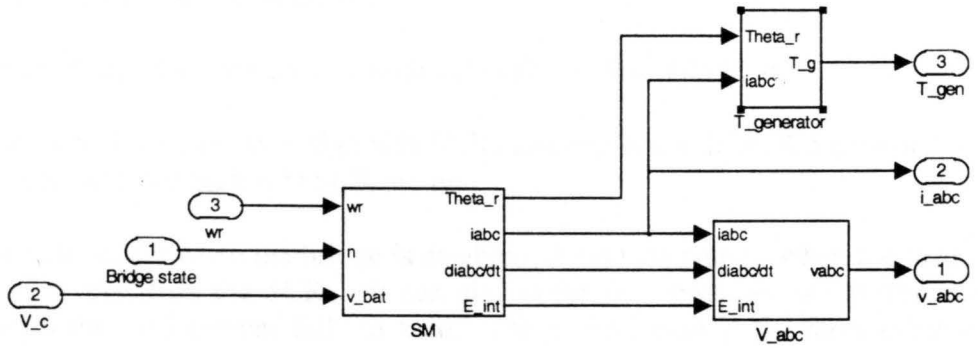

Figure 53: Block diagram of the synchronous generator.

2.9 Generator and Rectifier Interface

The schematic of the generator and rectifier is shown in Figure 54. The load is comprised of an inductance L_L, a resistance R_L, and a dc source V_b. The voltage V_b represents the battery pack voltage, the inductance is used as a current filter, and R_L is the inductance and connection resistance. The six SCRs model the rectifier. The generator is modeled by three ac sources with a series resistance and inductance. The phase currents and voltages are labeled i_a, i_b and i_c, and v_a, v_b and v_c, respectively. The generator internal sources and cross coupling terms are represented by v_{aa}, v_{bb}, and v_{cc}.

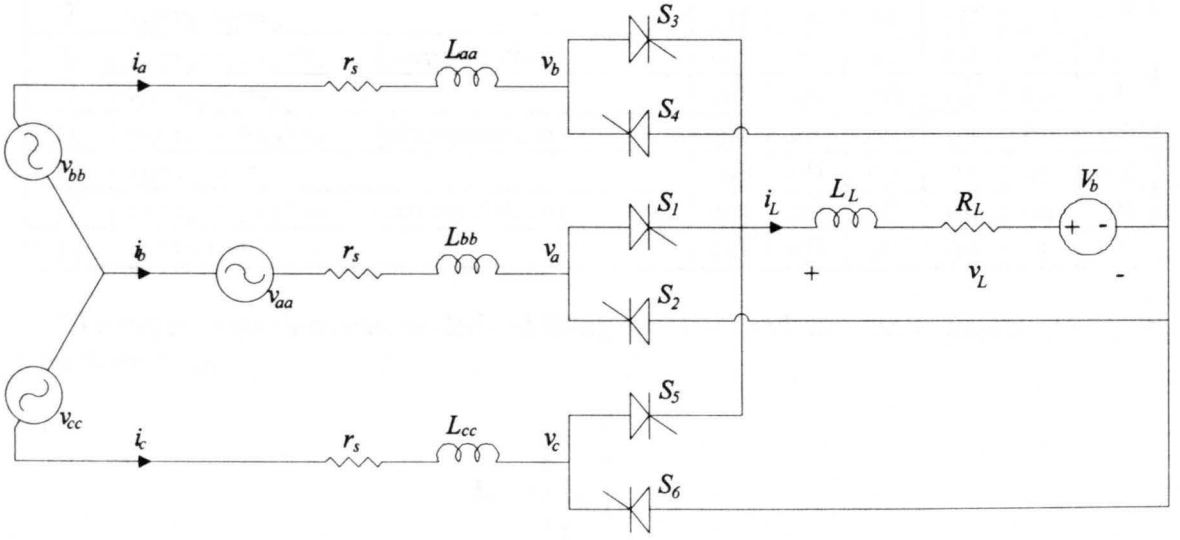

Figure 54: Generator and rectifier diagram.

There are three basic configurations which the are possible within the bridge structure:

1. all SCRs in the bridge are off

2. two of the SCRs are on, one high side and one low side SCR

3. three SCRs are on, two high side SCRs and one low side SCR are on or two low side SCRs and one high side SCR are on

The first case occurs when the bridge is disabled, during start-up or when the load voltage is high enough to reverse bias the SCRs. It can also occur in a situation called discontinuous current mode when the load current falls to zero. The second case is the most common. Current is flowing to the load through a high side SCR and from the load through a low side SCR. The third case happens during switch commutation when the load current is shifted from one generator phase to another. During this time, two SCRs on the same side share the load current. This commutation time is dependent on the generator series phase inductance.

Thirteen bridge configurations can be constructed this way and are listed in Table 6 where v_H and v_L refer to the high and low side load voltages, respectively. Equations describing each of these bridge configurations are created and used by the simulator. The bridge configuration is determined from external controls and the generator and load voltages. The configuration is then used to select the proper set of equations to describe the system.

Table 6: Rectifier bridge configurations.

	Bridge Configuration	S_1	S_2	S_3	S_4	S_5	S_6
1	$v_H=v_a$, $v_L=v_b$	on	off	off	on	off	off
2	$v_H=v_a$, $v_L=v_b=v_c$ (commutation)	on	off	off	on	off	on
3	$v_H=v_a$, $v_L=v_c$	on	off	off	off	off	on
4	$v_H=v_a=v_b$, $v_L=v_c$ (commutation)	on	off	on	off	off	on
5	$v_H=v_b$, $v_L=v_c$	off	off	on	off	off	on
6	$v_H=v_b$, $v_L=v_a=v_c$ (commutation)	off	on	on	off	off	on
7	$v_H=v_b$, $v_L=v_a$	off	on	on	off	off	off
8	$v_H=v_b=v_c$, $v_L=v_a$ (commutation)	off	on	on	off	on	off
9	$v_H=v_c$, $v_L=v_a$	off	on	off	off	on	off
10	$v_H=v_c$, $v_L=v_a=v_b$ (commutation)	off	on	off	on	on	off
11	$v_H=v_c$, $v_L=v_b$	off	off	off	on	on	off
12	$v_H=v_a=v_c$, $v_L=v_b$ (commutation)	on	off	off	on	on	off
13	$v_H=0$, $v_L=0$	off	off	off	off	off	off

The system equations can be derived using eq. (101) and the circuit diagram in Figure 54. First, partition $\mathbf{L}_s$ as

$$\mathbf{L}_s = \begin{bmatrix} \mathbf{L}_a \\ \mathbf{L}_b \\ \mathbf{L}_c \end{bmatrix}$$

where $\mathbf{L}_a$, $\mathbf{L}_b$, and $\mathbf{L}_c$ are row vectors. Now, assume that SCRs S_2 and S_4 are in the on-state and using eq. (101), write the loop equation as follows

$$v_a - v_b = R_L i_a + L_L \frac{di_a}{dt} + V_b$$

$$-r_s i_a - \mathbf{L}_a \frac{d\mathbf{i}_{abc}}{dt} + \tfrac{P}{2}\omega_r L_{md} I_{fd} \cos\left(\tfrac{P}{2}\theta_r\right) + r_s i_b + \mathbf{L}_b \frac{d\mathbf{i}_{abc}}{dt} - \tfrac{P}{2}\omega_r L_{md} I_{fd} \cos\left(\tfrac{P}{2}\theta_r - \tfrac{2\pi}{3}\right)$$
$$= R_L i_a + L_L \frac{di_a}{dt} + V_b$$

$$-(r_s + R_L) i_a + r_s i_b + (\mathbf{L}_b - \mathbf{L}_a)\frac{d\mathbf{i}_{abc}}{dt} - L_L \frac{di_a}{dt} + \tfrac{P}{2}\omega_r L_{md} I_{fd}\left[\cos\left(\tfrac{P}{2}\theta_r\right) - \cos\left(\tfrac{P}{2}\theta_r - \tfrac{2\pi}{3}\right)\right] = V_b$$

Define $\mathbf{L}_x$ as $\mathbf{L}_x = \mathbf{L}_b - \mathbf{L}_a$ and use a subscripted numeral to indicate a particular component of a vector. The above equation may now be written as

$$(L_{x1} - L_L)\frac{di_a}{dt} + L_{x2}\frac{di_b}{dt} + L_{x3}\frac{di_c}{dt} = (r_s + R_L) i_a - r_s i_b + \tfrac{P}{2}\omega_r L_{md} I_{fd}\left[\cos\left(\tfrac{P}{2}\theta_r\right) - \cos\left(\tfrac{P}{2}\theta_r - \tfrac{2\pi}{3}\right)\right] + V_b \tag{106}$$

This is one state equation for the system. Since there are three state variables, three equations are needed. The second equation is found by applying KCL at the load

$$i_a + i_b = 0$$

After taking derivatives, the second state equation is

$$\frac{di_a}{dt} + \frac{di_b}{dt} = 0 \tag{107}$$

The final equation is found by noting that the phase c current is zero since it is open circuited. Hence, the third equation is

$$\frac{di_c}{dt} = 0 \tag{108}$$

Placing these state equations in matrix form yields

$$\begin{bmatrix} L_{x1} - L_L & L_{x2} & 0 \\ 1 & 1 & 0 \\ 0 & 0 & 1 \end{bmatrix} \frac{d\mathbf{i}_{abc}}{dt} = \begin{bmatrix} r_s + R_L & -r_s & 0 \\ 0 & 0 & 0 \\ 0 & 0 & 0 \end{bmatrix} \mathbf{i}_{abc} - \tfrac{P}{2}\omega_r L_{md} I_{fd} \begin{bmatrix} \cos\left(\tfrac{P}{2}\theta_r\right) - \cos\left(\tfrac{P}{2}\theta_r - \tfrac{2\pi}{3}\right) \\ 0 \\ 0 \end{bmatrix} + \begin{bmatrix} V_b \\ 0 \\ 0 \end{bmatrix}$$

(109)

This equation may now be put into standard form by inverting the matrix on the left and multiplying. The solution for the commutation configuration is similar.

Assume that SCRs S_1, S_4 and S_6 are in the on-state. Here, the load current is being shifted from phase b to phase c. Equation (106) also holds in this case and doesn't need to be modified. The second equation is KCL at the load and in this case is

$$i_a + i_b + i_c = 0 \Rightarrow \frac{di_a}{dt} + \frac{di_b}{dt} + \frac{di_c}{dt} = 0 \tag{110}$$

The phase c current is no longer zero. The last equation is found by noting that $v_b=v_c$.

$$-r_s i_b - \mathbf{L}_b \frac{d\mathbf{i}_{abc}}{dt} + \tfrac{P}{2}\omega_r L_{md} I_{fd} \cos\left(\tfrac{P}{2}\theta_r - \tfrac{2\pi}{3}\right) + r_s i_c + \mathbf{L}_c \frac{d\mathbf{i}_{abc}}{dt} - \tfrac{P}{2}\omega_r L_{md} I_{fd} \cos\left(\tfrac{P}{2}\theta_r + \tfrac{2\pi}{3}\right) = 0$$

$$(\mathbf{L}_c - \mathbf{L}_b)\frac{d\mathbf{i}_{abc}}{dt} = r_s(i_b - i_c) - \tfrac{P}{2}\omega_r L_{md} I_{fd}\left[\cos\left(\tfrac{P}{2}\theta_r - \tfrac{2\pi}{3}\right) - \cos\left(\tfrac{P}{2}\theta_r + \tfrac{2\pi}{3}\right)\right] \tag{111}$$

Defining $\mathbf{L}_y=\mathbf{L}_c-\mathbf{L}_b$, these equations are put in matrix form as follows

$$\begin{bmatrix} L_{x1} - L_L & L_{x2} & L_{x3} \\ L_{y1} & L_{y2} & L_{y3} \\ 1 & 1 & 1 \end{bmatrix} \frac{d\mathbf{i}_{abc}}{dt} = \begin{bmatrix} r_s + R_L & -r_s & 0 \\ 0 & r_s & -r_s \\ 0 & 0 & 0 \end{bmatrix} i_{abc} - \tfrac{P}{2}\omega_r L_{md} I_{fd} \begin{bmatrix} \cos\left(\tfrac{P}{2}\theta_r\right) - \cos\left(\tfrac{P}{2}\theta_r - \tfrac{2\pi}{3}\right) \\ \cos\left(\tfrac{P}{2}\theta_r - \tfrac{2\pi}{3}\right) - \cos\left(\tfrac{P}{2}\theta_r + \tfrac{2\pi}{3}\right) \\ 0 \end{bmatrix} + \begin{bmatrix} V_b \\ 0 \\ 0 \end{bmatrix} \tag{112}$$

As with the previous equation, this equation can be placed in standard form by inverting the matrix on the left and multiplying through. The other configurations are found in a similar fashion and all thirteen are listed in the Appendix I.

Each of the configurations above are of the form

$$\mathbf{A}_j \frac{d\mathbf{i}_{abc}}{dt} = \mathbf{B}_j \mathbf{i}_{abc} - \tfrac{P}{2}\omega_r L_{md} I_{fd} \mathbf{U}_j(\theta_r) + \begin{bmatrix} V_b \\ 0 \\ 0 \end{bmatrix}$$

where the index j indicates that these matrices are for a specific configuration. These equations may be put into standard state space form by multiplying by $\mathbf{A}^{-1}$. Multiplying yields

$$\frac{d\mathbf{i}_{abc}}{dt} = \mathbf{A}_j^{-1}\mathbf{B}_j \mathbf{i}_{abc} - \tfrac{P}{2}\omega_r L_{md} I_{fd} \mathbf{A}_j^{-1}\mathbf{U}_j(\theta_r) + \mathbf{A}_j^{-1}\begin{bmatrix} V_b \\ 0 \\ 0 \end{bmatrix} \tag{113}$$

This is the form of the state equations used by the simulation program. This is only one of thirteen equations, however. Define the row vector of switching functions **Q** as

$$\mathbf{Q} = \begin{bmatrix} q_1 & q_2 & \cdots & q_{12} & q_{13} \end{bmatrix} \tag{114}$$

where the switching functions q_j take on values of one or zero, and are constrained in the following manner

$$\sum_{j=1}^{13} q_j = 1 \tag{115}$$

These switching functions are also a function of the state of the SCRs contained within the rectifier bridge.

$$q_j = q_j(S_1, S_2, S_3, S_4, S_5, S_6) \tag{116}$$

Let $\mathbf{U}_j(\theta_r)=\mathbf{M}_j\mathbf{W}(\theta_r)$ where $\mathbf{M}_j$ is matrix of scalars and $\mathbf{W}(\theta_r)$ is defined as

$$\mathbf{W}(\theta_r) = \begin{bmatrix} \cos(\frac{P}{2}\theta_r) \\ \cos(\frac{P}{2}\theta_r - \frac{2\pi}{3}) \\ \cos(\frac{P}{2}\theta_r + \frac{2\pi}{3}) \end{bmatrix}, \text{ and } \mathbf{V}_b = \begin{bmatrix} V_b \\ 0 \\ 0 \end{bmatrix}.$$

The system state equations can now be written as

$$\frac{d\mathbf{i}_{abc}}{dt} = q_1\mathbf{A}_1^{-1}\left[\mathbf{B}_1\mathbf{i}_{abc} - \tfrac{P}{2}\omega_r L_{md} I_{fd}\mathbf{M}_1\mathbf{W}(\theta_r) + \mathbf{V}_b\right] + q_2\mathbf{A}_2^{-1}\left[\mathbf{B}_2\mathbf{i}_{abc} - \tfrac{P}{2}\omega_r L_{md} I_{fd}\mathbf{M}_2\mathbf{W}(\theta_r) + \mathbf{V}_b\right] + \cdots$$
$$+ q_{13}\mathbf{A}_{13}^{-1}\left[\mathbf{B}_{13}\mathbf{i}_{abc} - \tfrac{P}{2}\omega_r L_{md} I_{fd}\mathbf{M}_{13}\mathbf{W}(\theta_r) + \mathbf{V}_b\right]$$

and simplified to give

$$\frac{d\mathbf{i}_{abc}}{dt} = \mathbf{Q}\mathbf{A}^{-1}\left[\mathbf{B}\mathbf{i}_{abc} - \tfrac{P}{2}\omega_r L_{md} I_{fd}\mathbf{M}\mathbf{W}(\theta_r) + \mathbf{V}_b\right] \tag{117}$$

where **Q** is defined as in eq. (114) and the matrices **A**, **B**, and **M** are defined as

$$\mathbf{A} = \begin{bmatrix} \mathbf{A}_1 & 0 & \cdots & 0 \\ 0 & \mathbf{A}_2 & & \\ \vdots & & \ddots & \\ 0 & & & \mathbf{A}_{13} \end{bmatrix} \qquad \mathbf{B} = \begin{bmatrix} \mathbf{B}_1 \\ \mathbf{B}_2 \\ \vdots \\ \mathbf{B}_{13} \end{bmatrix} \qquad \mathbf{M} = \begin{bmatrix} \mathbf{M}_1 \\ \mathbf{M}_2 \\ \vdots \\ \mathbf{M}_{13} \end{bmatrix}$$

The state of a single SCR is determined by the external control and the terminal conditions of that SCR. The collection of the six SCR states is used to determine the system configuration used. The SIMULINK block used to determine the system configuration is shown in Figure 55. The two inputs SCR_H and SCR_L are vectors who's components are S_1, S_3, and S_5 and S_2, S_4, and S_6, respectively. These values are converted to a unique index by the following transformation

$$Index = 1 + S_6 + 2S_5 + 4S_4 + 8S_3 + 16S_2 + 32S_1 \tag{118}$$

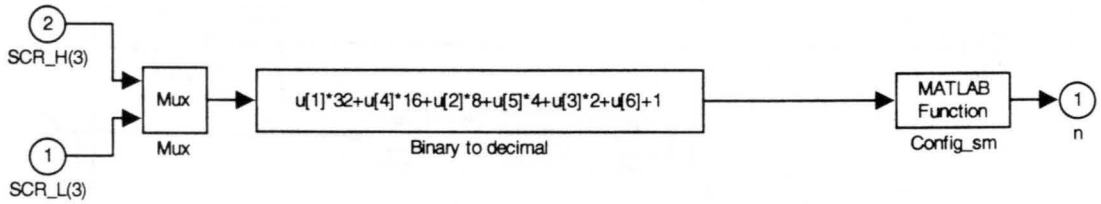

Figure 55: SIMULINK configuration block.

The MATLAB function Config_sm translates the index of eq. (118) to an index ranging from 1 to 13. This index is supplied to generator model to select the proper configuration.

The generator block that calculates the phase currents and current derivatives is shown in Figure 56. The three integrators provide the phase currents by integrating the right-hand-side of eq. (117). The current derivatives are simply the inputs to these integrators. The MATLAB function A_smf1 is used to calculated the first term of eq. (117) $\mathbf{QA}^{-1}\mathbf{Bi}_{abc}$. The function takes as inputs the configuration number and the three phase currents.

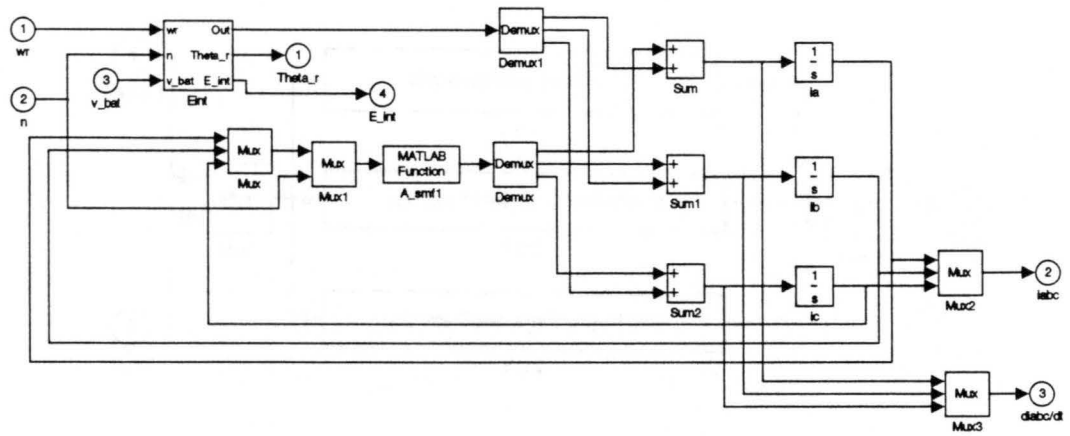

Figure 56: Determination of synchronous machine currents and current derivatives.

The Eint block is used to calculate the remaining terms in eq. (117), the motor shaft speed, and the generator internal voltages. The SIMULINK block diagram of Eint is shown in Figure 57. The integrator labeled theta_r integrates the shaft speed and provides θ_r on the

interval [0,2π]. The MATLAB function phi_sm implements the matrix function $\mathbf{W}(\theta_r)$. The MATLAB function A_smf2 computes the terms $\mathbf{QA}^{-1}\left(\frac{P}{2}\omega_r L_{md} I_{fd}\mathbf{MW}(\theta_r) + \mathbf{V}_b\right)$ in eq. (117).

The block labeled Eabc in Figure 57 computes the internal phase voltages of the generator. The SIMULINK block diagram for Eabc is shown in Figure 58. Computation of the internal voltages is done using eq. (101) with the currents and current derivatives set equal to zero.

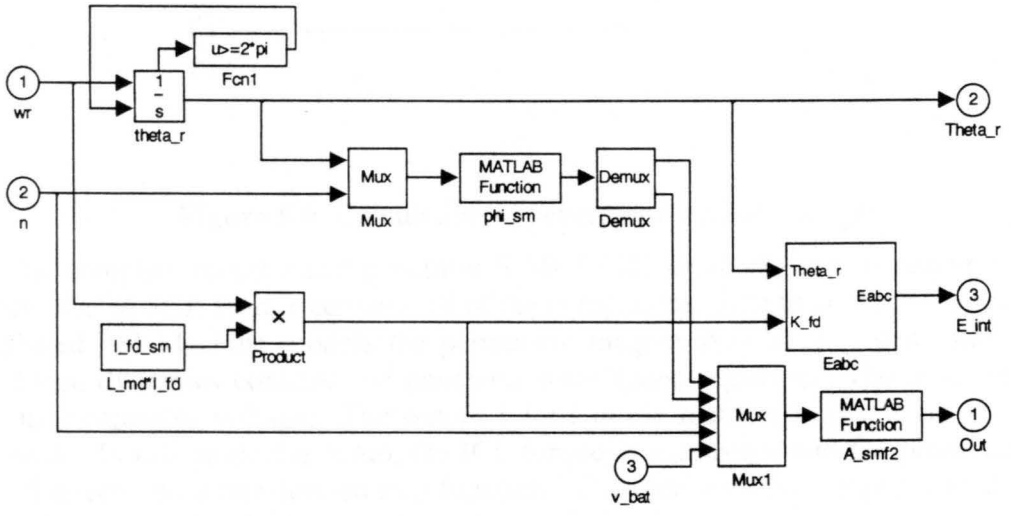

Figure 57: SIMULINK block Eint.

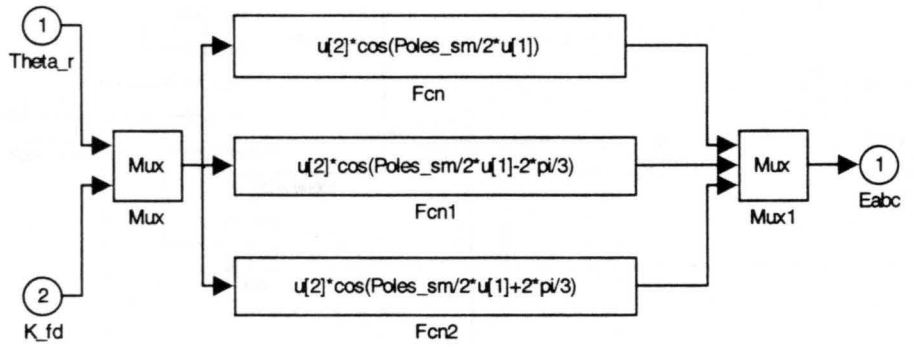

Figure 58: Computation of generator no-load phase voltages.

The block used to calculate the generator terminal voltages is labeled V_abc and is shown in Figure 53. The blocks contained in this subsystem block are shown in Figure 59. The terminal voltages are calculated using the internal generator internal voltages and eq. (101).

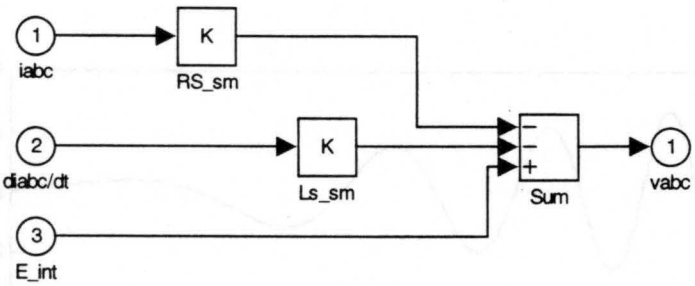

Figure 59: Calculation of generator terminal voltages.

The complete rectifier and generator SIMULINK block diagram is shown in Figure 60. The block labeled SCR Bridge contains all of the components used to construct the rectifier. The block labeled PM Machine models the permanent magnet synchronous generator. The block labeled Mech dynamics contains the generator rotor speed equation. The input port vc is the battery pack capacitor voltage. The output i_load is the rectifier load current supplied to the battery pack. In this particular setup, the ICE torque is a constant and the phase delay angle is controlled directly by a rate-limited step function. The rectifier enable input is made active only after the PLLs have gained a lock on the generator frequency.

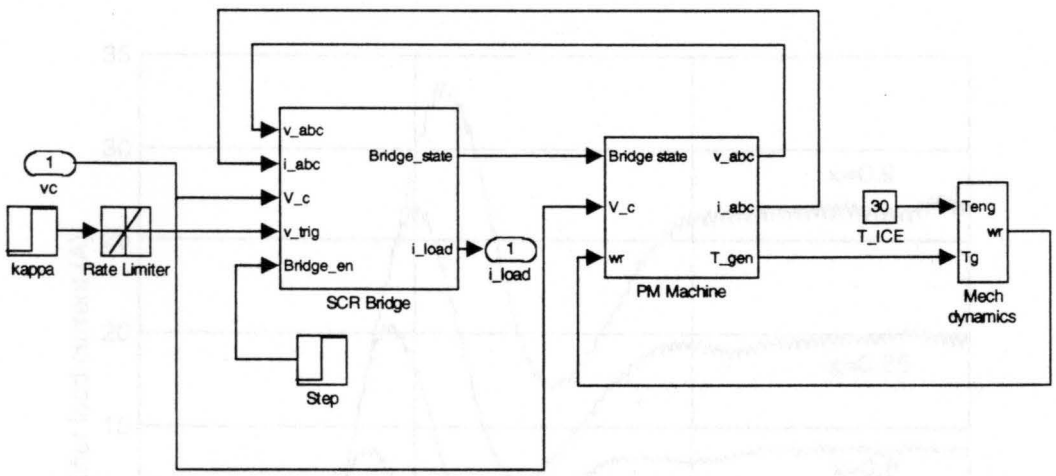

Figure 60: Generator and rectifier block diagram.

In the remainder of this section, several generator and rectifier simulations are examined. The first is a simulation of free acceleration of the generator. This is done by directly disabling the rectifier via the Brige_en input. Figure 61 shows the generator phase *a* voltage and shaft speed during free acceleration. The phase voltage magnitude and frequency vary linearly with the shaft speed of the generator.

Figure 62 shows the rectifier load current for various values of κ. The steady-state load current is close to being a linear function of κ. Since the load is not a perfect current source, this

relation is not exactly linear. These plots display the dynamic response of the rectifier load current to a step in κ.

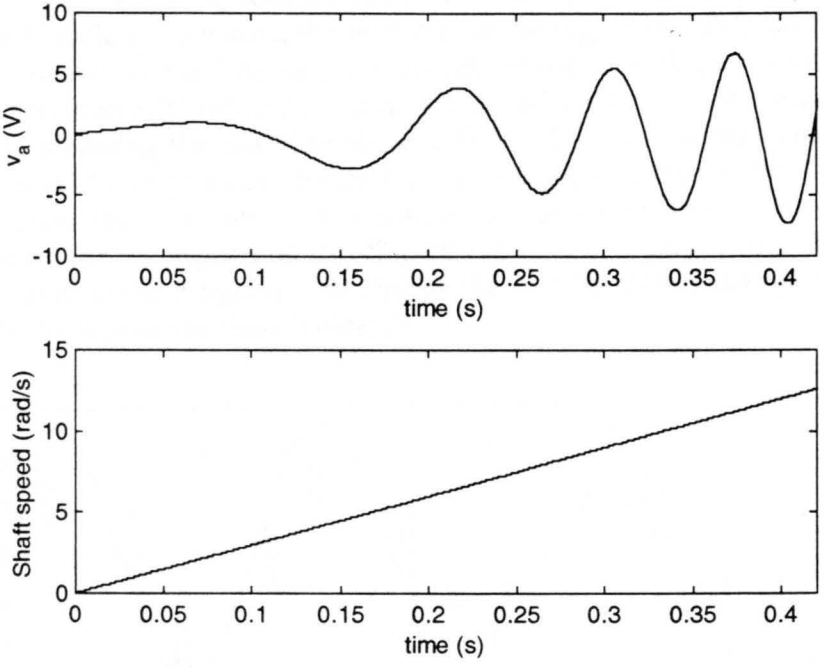

Figure 61: Generator phase *a* voltage and shaft speed.

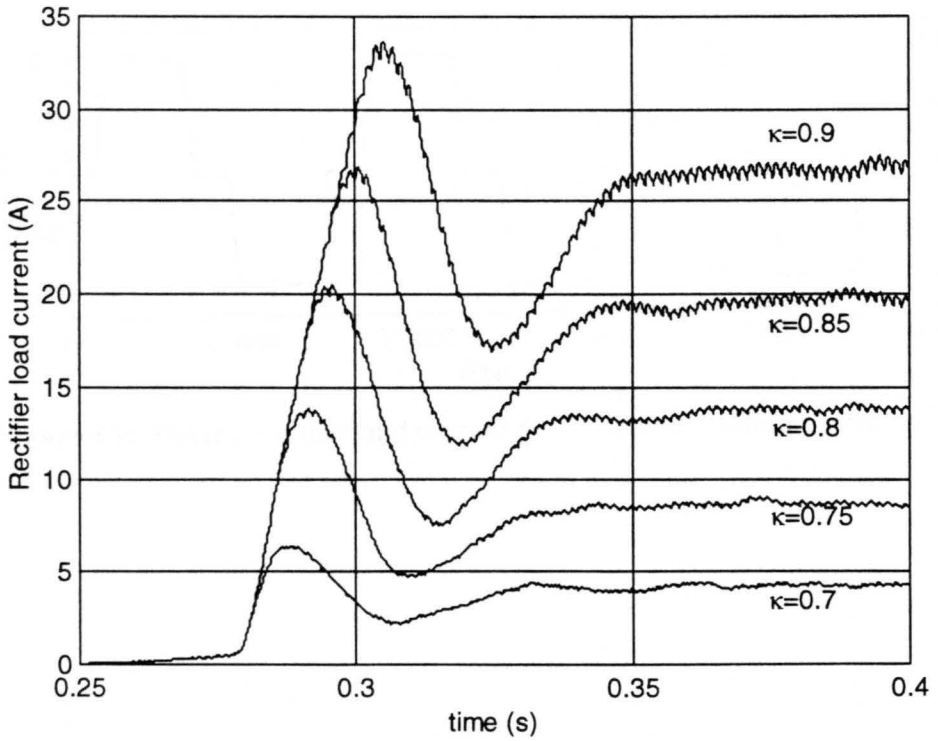

Figure 62: Rectifier load current for various values of κ.

Figure 63 shows the rectifier phase *a* voltage current. Switch commutation is very apparent in this figure. Figure 64 shows the rectifier phase *a*,*b*, and *c* voltages and the bridge configuration number. It can be seen from this plot that the commutating phase voltages are equal. During each cycle of operation, the bridge steps through each configuration in sequence.

Figure 65 illustrates the loss of the high-side phase *a* SCR gate drive at time t=0.3 s. Note that the bridge can still function, but at a reduced capacity. The remaining SCRs still function properly, including the low-side phase *a* SCR. The load current falls of dramatically. This can be corrected to some extent by decreasing the bridge delay angle. This setup can be modified to simulate faults as well. For instance, a situation with a shorted SCR can be simulated by forcing the corresponding flip-flop output to remain high during the fault condition. The real modification to the program is to change the rectifier commutation resistance simulate the opening of the SCR after the fault is cleared.

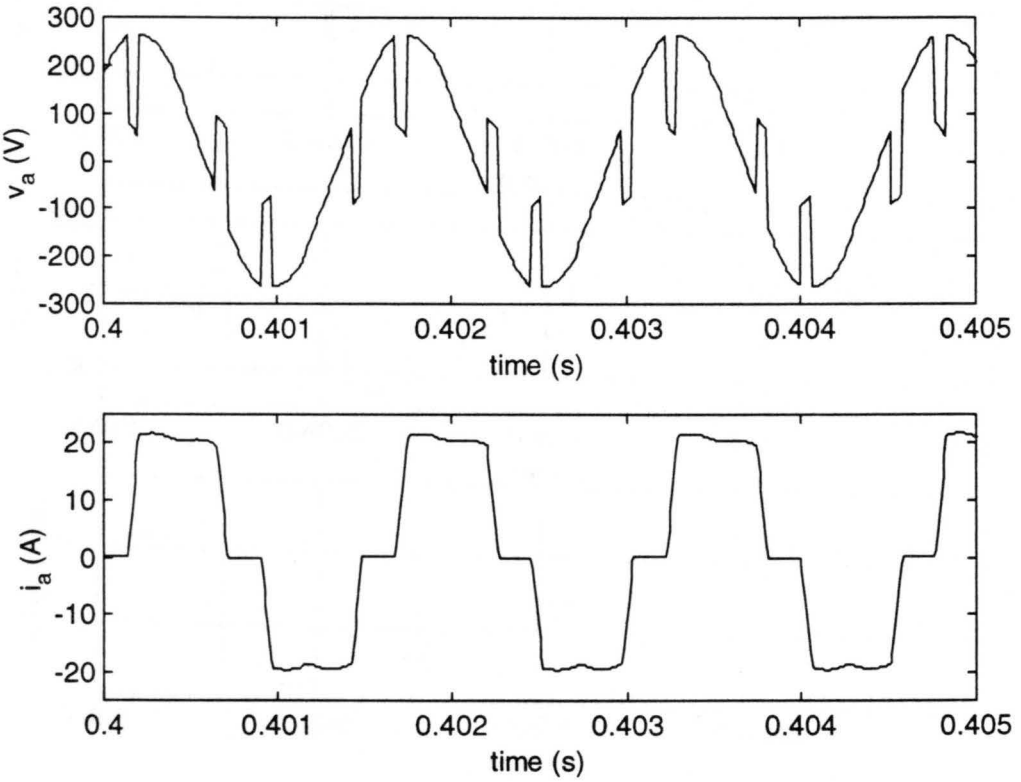

Figure 63: Phase *a* voltage and current demonstrating switch commutation.

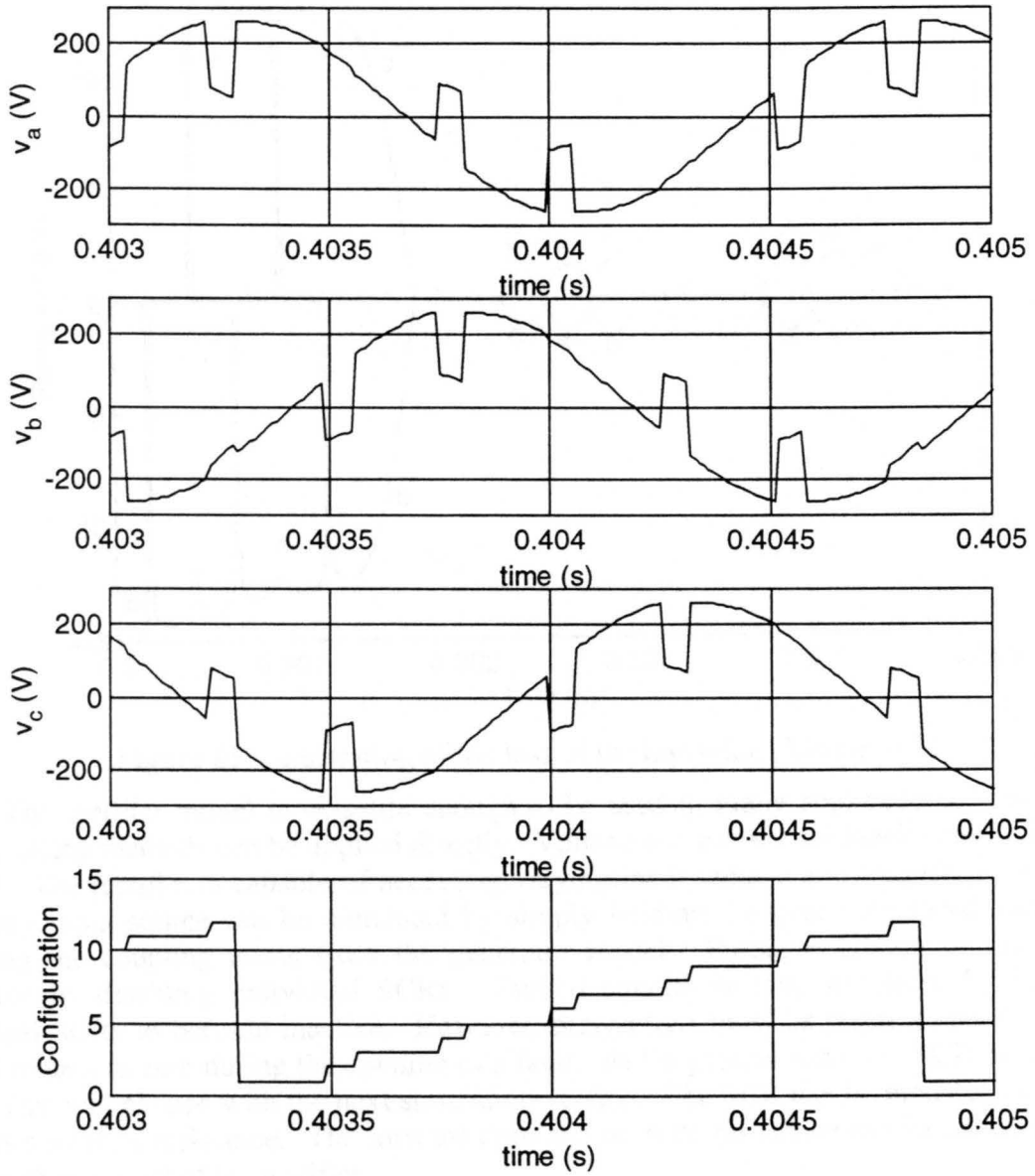

Figure 64: Rectifier phase *a*,*b* and *c* voltages and the bridge configuration.

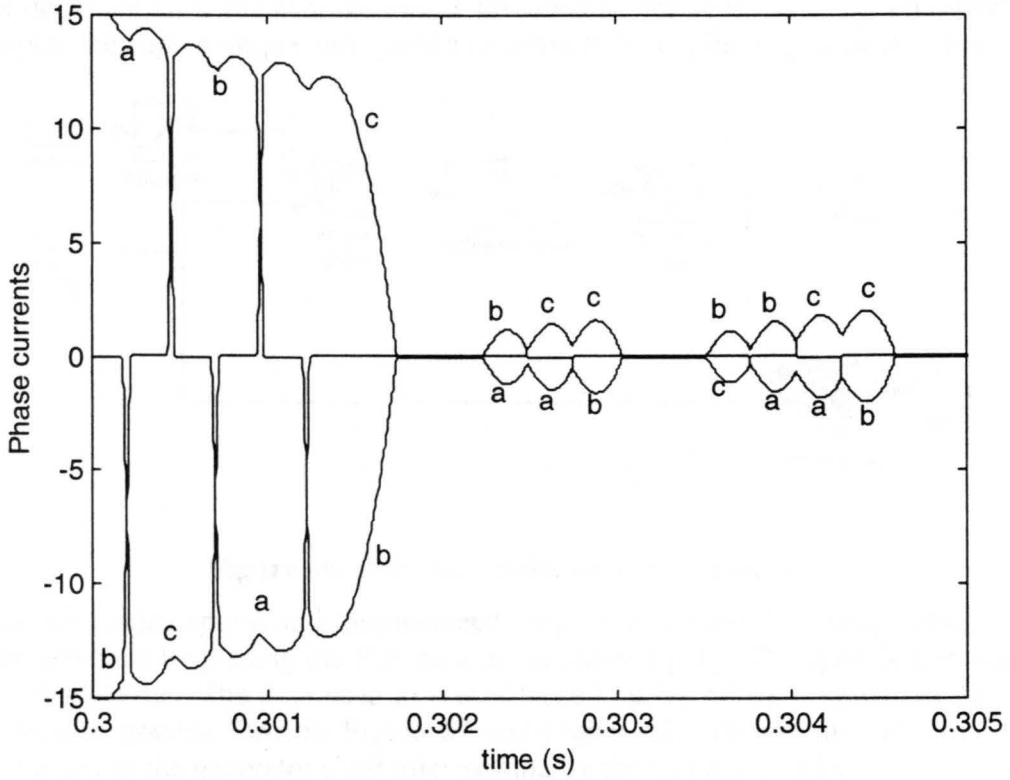

Figure 65: Illustration of the loss of the high-side phase *a* SCR.

The rectifier model is versatile enough to be used in many applications. For instance, varying gating methods can be applied directly. Voltage and current feedback control are readily applied. The rectifier is capable of accepting varying input voltage and frequency. A constant frequency input source can be simulated by simply holding the generator speed constant and removing the coupling terms from the generator model. Partial operation of the bridge is simulated by disabling individual SCRs. Faulted conditions may simulated by forcing the individual SCRs to become inactive. However, precautions must be taken to ensure the phase current returns to zero during the opening of a fault. At the present time, the SCR model used is ideal. This will change with the next simulation version. The SCR can be modeled as a forward drop with a series resistance. The forward drop and on-state resistance can be added directly in series with the input of the rectifier.

2.10Internal Combustion Engine Model

The ICE is modeled from steady-state data obtained from testing at the University of Illinois. The model includes steady-state torque vs. speed maps for various values of throttle opening. A specific fuel consumption map is also used to provide efficiency data. The fuel consumption is computed from the engine torque and speed. The ICE model is shown in Figure 66. The input gamma is the throttle position and w_eng is the ICE shaft speed. The saturation block is used to limit the throttle from 0 to 100% opening. The throttle position and the engine speed are used to determine the shaft torque. The Throttle response block models the dynamic

response of the throttle actuator. The pure time delay simulates the delay for fuel combustion [10]. The delay output is the average torque provided by the ICE. The fuel consumption block takes as inputs the engine torque and speed and delivers the engine's specific fuel consumption.

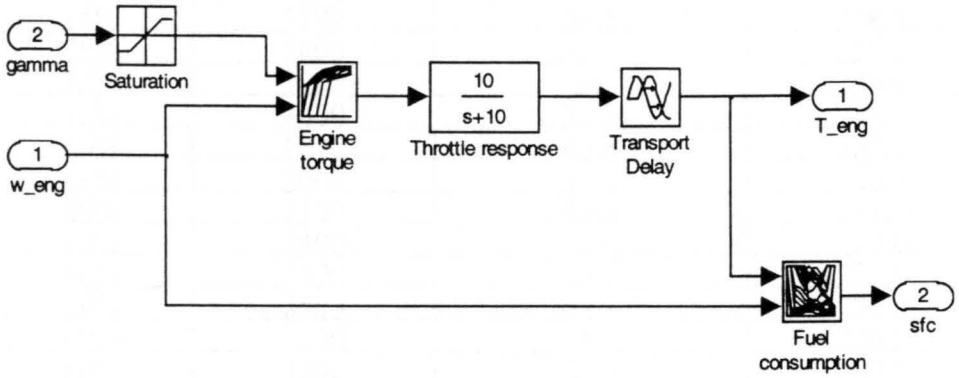

Figure 66: Internal combustion engine model.

The fuel consumption and torque-speed maps were created by extrapolating steady-state engine data obtained by placing the ICE on a dynamometer [11]. The specific fuel consumption is in units of g/kW-hr. The data used to create these look-up tables is shown in Table 7. This data is shown in graphic form in Figure 67 and Figure 68. The torque output of the ICE is provided directly to the generator shaft after scaling by the belt drive ratio.

Table 7: ICE engine data.

Thottle	Speed (RPM)	Shaft Torque (N•m)	SFC (g/kW•hr)
100%	1800	42.5	249.8
100%	2000	47	222.7
100%	2200	47.7	221.5
100%	2400	48.8	218.6
100%	2600	47.3	224.5
100%	2800	47.5	225.7
100%	3000	46.6	228.9
100%	3200	45	234.8
100%	3400	41	256.5
100%	3500	41.2	250.3
100%	3600	41.1	249.7
100%	3700	40.9	248.4
100%	3800	40.8	242.8
100%	3900	40.3	245.8
100%	4000	39.8	246.3
75%	1800	42.8	236.2
75%	2000	46.2	218.8
75%	2200	47.1	220.0
75%	2400	48	223.3
75%	2600	47.8	223.2
75%	2800	47.4	227.2
75%	3000	46.1	227.0
75%	3200	44	233.2

Thottle	Speed (RPM)	Shaft Torque (N•m)	SEC (g/kW•hr)
75%	3400	38.4	261.9
75%	3500	39	256.6
75%	3600	39.3	250.8
75%	3700	39.1	248.1
75%	3800	38.6	250.0
75%	3900	38	245.9
75%	4000	37.3	243.7
60%	1800	43.8	233.1
60%	2000	45.7	223.4
60%	2200	45.8	221.8
60%	2400	45	228.0
60%	2600	43.6	233.0
60%	2800	42.3	234.2
60%	3000	40	240.0
60%	3200	35.6	262.5
60%	3400	35.1	253.2
60%	3500	35	252.5
60%	3600	34.7	248.8
60%	3700	34	252.4
60%	3800	33.3	251.6
60%	3880	32.8	257.0
60%	1800	43.6	248.2
60%	2000	45.1	229.8
60%	2200	45.2	220.3
60%	2400	44.1	216.5
60%	2600	42.8	218.4
60%	2800	41.1	220.0
60%	3000	38.6	230.3
60%	3200	34.5	254.7
60%	3400	34.5	241.4
60%	3500	34.1	242.7
60%	3600	34	239.0
60%	3700	33	238.5
60%	3800	32.6	239.8
50%	1800	40.2	237.5
50%	2000	42.4	220.4
50%	2200	42	226.2
50%	2400	41.5	227.7
50%	2600	39.9	229.1
50%	2800	38.4	228.8
50%	3000	36.2	232.9
50%	3200	34.2	242.0
50%	3280	30.6	260.5
25%	2000	27.4	224.1
25%	2200	27	218.9
25%	2370	26.2	221.7

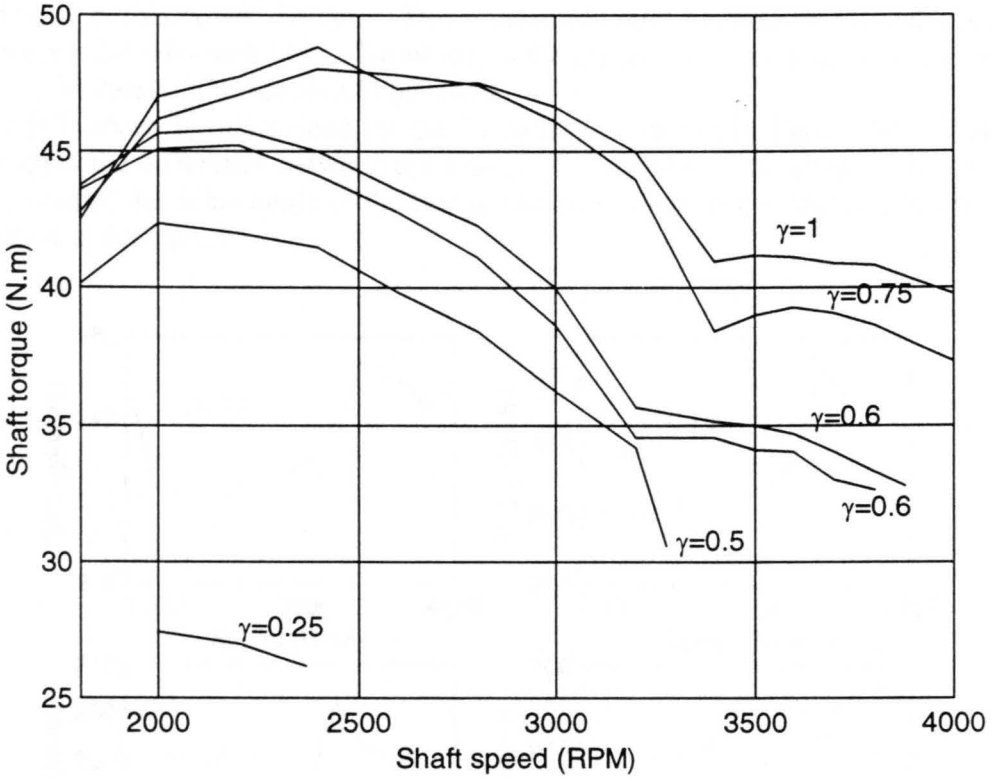

Figure 67: ICE shaft torque vs. shaft speed for various throttle openings.

The APU is controlled by the power controller shown in Figure 69. This controller is very basic and can be made more sophisticated if the need arises. The flip-flop gives the state of the APU. When the flip-flop is active, the APU is active. The APU can be turned on in two ways. The APU is activated when the average power load exceeds a value called P_APU_low. P_APU_low is the lower limit on the power the APU can provide and is about 6 kW. This limit is imposed due to the power range of the ICE. The average power is obtained by filtering the power load imposed on the battery pack.

The APU can also be turned if the battery pack SOC falls below a limit called SOC_low. A battery pack SOC lower than this is inefficient and could cause battery damage. The activation of the APU is delayed by the block called ICE starting delay. This delay models the time it takes to start the APU and bring it up to speed. The APU is brought into the inactive state whenever the battery pack SOC rises above a limit called SOC_high.

Once the APU is activated, the power reference block, shown in Figure 70, provides a power reference as follows

$$P_{ref} = k_{soc}\left(SOC_{ref} - soc\right) + P_{load} \tag{119}$$

where SOC_{ref} lies between SOC_high and SOC_low and is the reference SOC we wish the APU to maintain. P_{load} is the average power load of the battery pack.

The power reference is used by a look-up table to determine the desired generator shaft speed. The reference is also compared to the APU output power and the result provided to a PI controller which controls the ICE throttle position. This, in effect, maintains the ICE shaft

torque at the appropriate level. The ICE speed is set by the power reference, and the ICE torque is adjusted to meet this power demand. This controller could be modified by adding another PI loop to maintain the reference SOC. However, in the present case, so long as k_{soc} in eq. (119) is large, the steady state SOC error should be small.

The ICE speed is maintained by the PI controller shown in Figure 69. This controller takes as an input the difference between the desired ICE speed and the actual ICE speed and uses this error to control the delay angle of the bridge rectifier. Note that to increase the rectifier load, the delay angle is decreased.

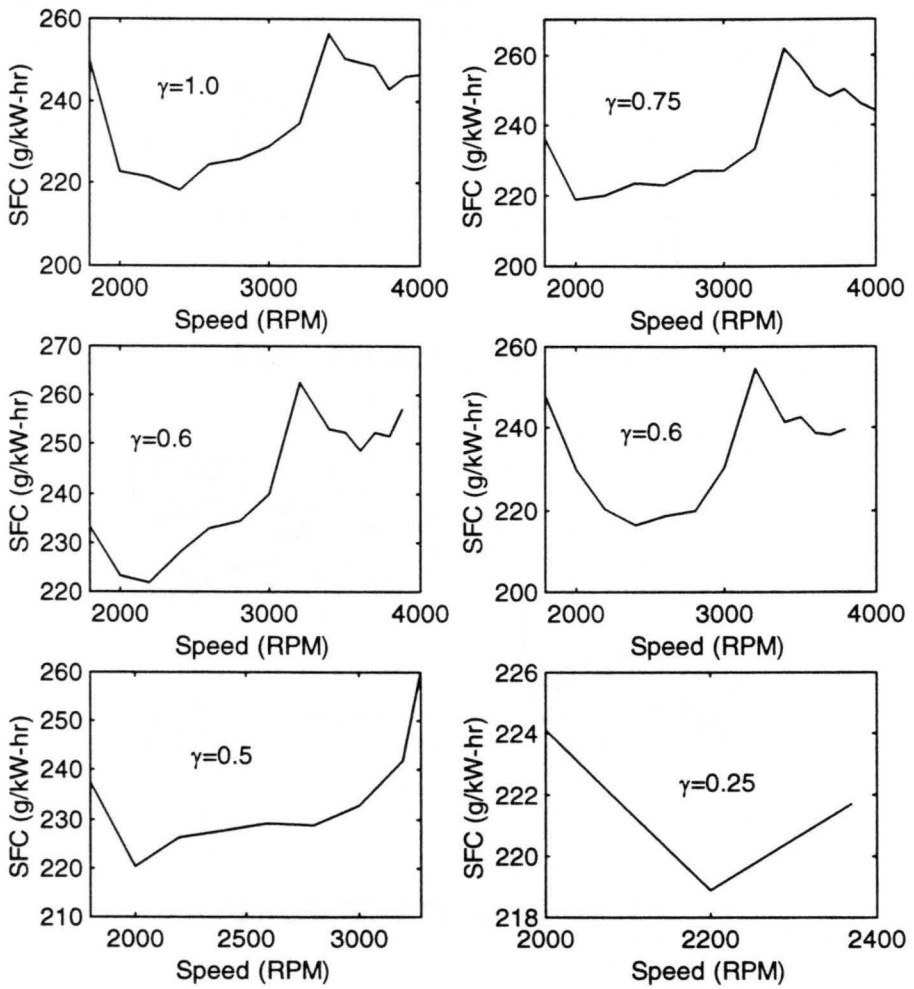

Figure 68: ICE specific fuel consumption vs. speed for various throttle openings.

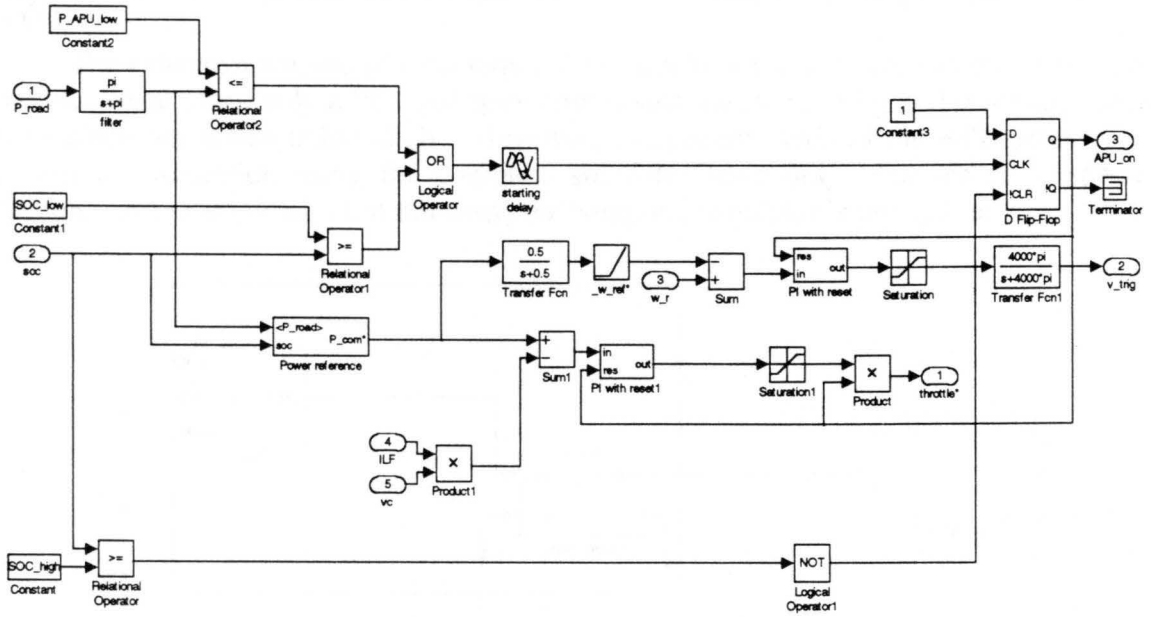

Figure 69: APU power controller.

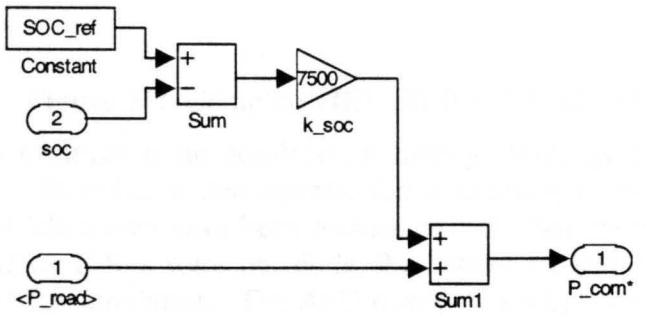

Figure 70: APU power reference.

2.11 HEV Simulator

The complete block diagram of the HEV simulator is shown in Figure 71. The three main components are the APU, battery pack and the traction system. As demonstrated in the previous sections, the simulator is very complex and contains many components. The simulation time is dependent on the number of system components that are active during the simulation. For instance, if the APU is inactive, the simulation will run faster. As a benchmark, the simulator, with all components active, requires approximately one hour of computation time to

complete one second of real time simulation on a 300 Mhz PC platform with 128 MB of user RAM.

The extensive amount of time required for simulation places constraints on testing of the simulator when using only a PC. All components such as the rectifier and electronic drive have been sufficiently tested individually. However, components such as the APU power controller that require evaluation using the complete simulator have only been tested in special case situations. An example of a test run using the complete simulator is now given.

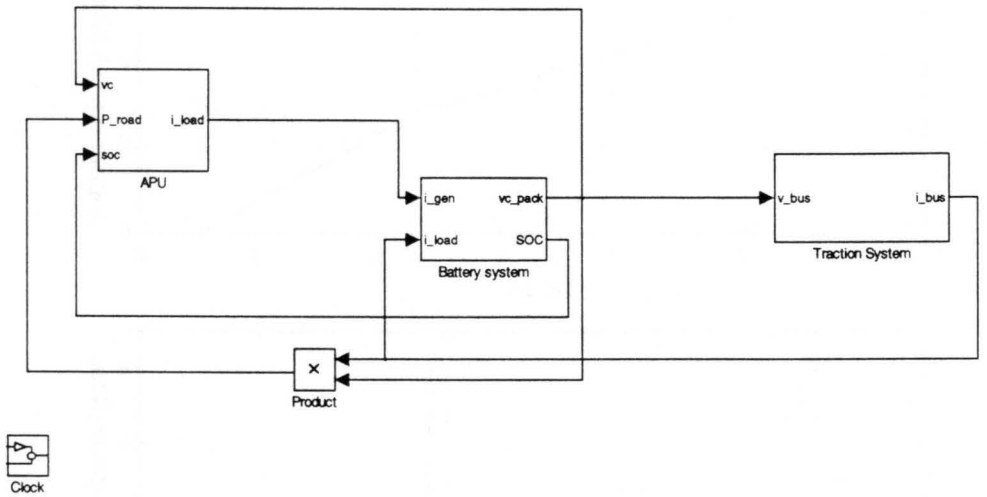

Figure 71: Complete HEV SIMULINK model.

The simulation example is an acceleration through three gears followed by a sudden braking of the vehicle. In order to demonstrate the interaction between components, several modifications to the vehicle model have been performed. The battery pack size has been scaled down by a factor of fifty. If this were not done, the battery pack SOC would vary very little during the short time of the simulation. The APU power controller response is much faster than it would be in the actual vehicle. The power tracking response is on the order of seconds for this simulation. In a practical HEV it would be much longer. Finally, in order to observe shifting of the transmission, the shift speeds are made lower than they would be otherwise.

For this example, the road grade is set to zero. The transmission shifts from first to second gear at a speed of 2.5 m/s, and from second to third gear at 5 m/s. The induction motor torque is initially set to 75 N•m, and at time equal to 6.2 s is reduced to –75 N•m for braking of the vehicle. The lower limit SOC_{low} on the battery pack SOC is set at 40% and the initial SOC is set to 40.2%. This allows start-up the APU to be illustrated.

Figure 72 shows the vehicle velocity in m/s and the transmission gear vs. time for this example. Remember that gear six represents the transmission neutral. At time equal to 6.2 s, the drive motor torque is made negative, and the vehicle speed starts decreasing.

The induction drive motor shaft speed and torque are shown in Figure 73. Since the vehicle is shifting up through the gears in an acceleration, the motor speed decreases during shifting synchronization as explained in section 2.2. The initial oscillation of the motor torque is due to the rotor not having enough time to build. The electronic drive requires a period of time

to build the rotor field before FOC is completely effective as explained in section 2.5. In this example, 0.5 s of idling time has been allowed for the field build up and the lock-in of the PLLs of the rectifier. If the idle time were slightly longer, the ripple on the motor torque waveform would not exist. At about 2.5 s and 5.5 s the motor becomes negative during synchronization of the transmission gears during shifting. At 6.2 s the motor torque is brought to –75 N•m to simulate braking of the vehicle.

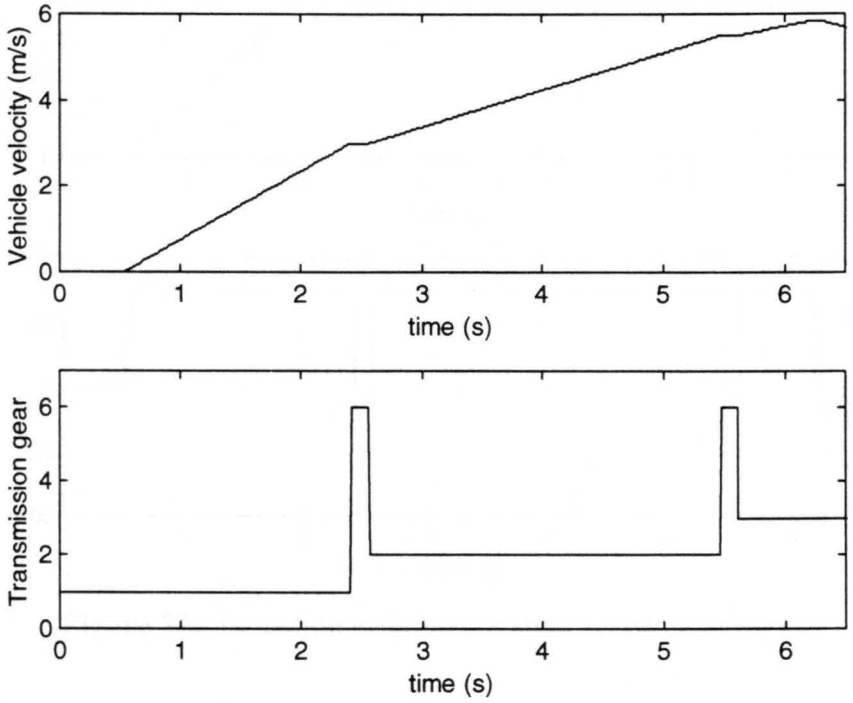

Figure 72: Vehicle velocity and transmission gear.

Figure 74 shows the battery pack SOC and the APU status. As the battery pack SOC falls below the lower limit SOC_{low}=0.4, the APU becomes active. The APU power reference, APU output power, and the power supplied to the electronic drive are shown in Figure 75. As mentioned above, the power controller speed is very fast compared to what it would be in normal operation. The APU output power does not track the power reference exactly because the integral portion of the PI controller does not have time to act. This would be fine for simulating the actual vehicle, but error is apparent over this very short simulation. The shape of the output power is correct due to the proportional component of the PI controller. The power supplied from the battery pack to the electronic drive is also shown in the figure. Note that this power becomes negative during up-shifting of the transmission and during braking of the vehicle. This power return represents extraction of kinetic energy from the rotating parts in the transmission and the vehicle's motion.

The rectifier load current and the voltage of the battery pack parallel capactitance are shown in Figure 76. The reason that the rectifier current decreases during shifting is, as mentioned above, the APU power controller is much fast than it would be in practice. During shifting, the induction motor load is reduced significantly. In fact, during up-shifting, there is some regeneration. The APU power controller responds to this reduction in load by reducing its output. The voltage of the parallel capacitance contained within the battery pack is also shown

in this figure. The voltage is reduced during acceleration and is increasing during shifting and braking.

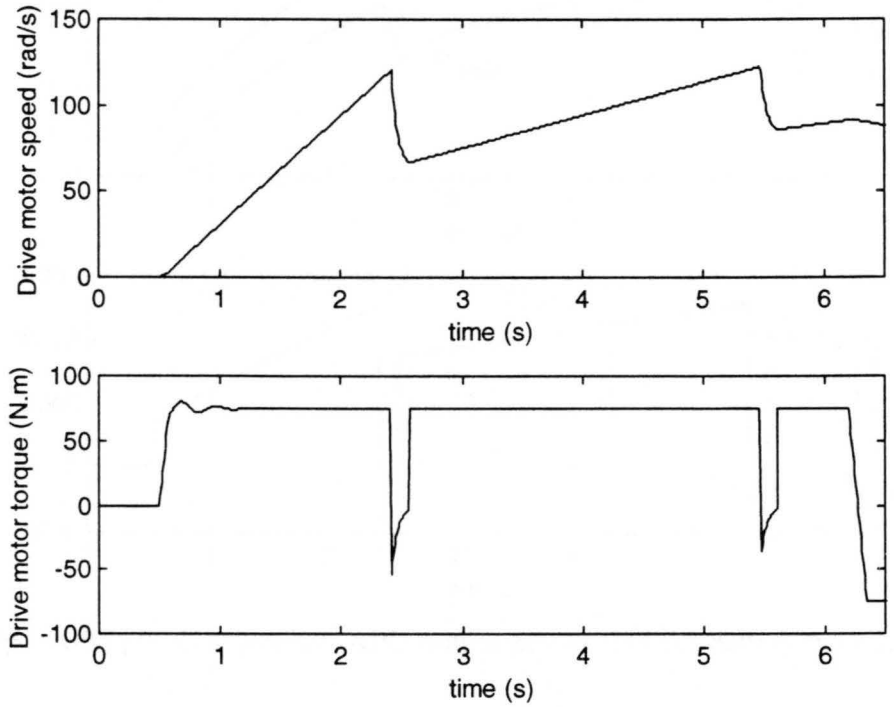

Figure 73: Induction drive motor shaft speed and torque.

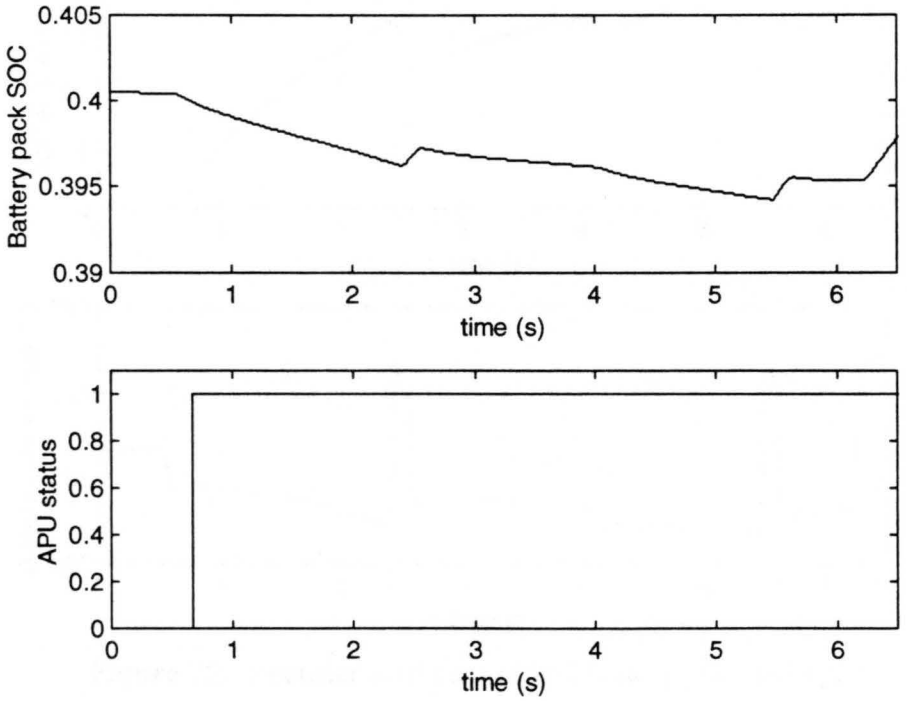

Figure 74: Battery pack SOC and APU status (1=on, 0=off).

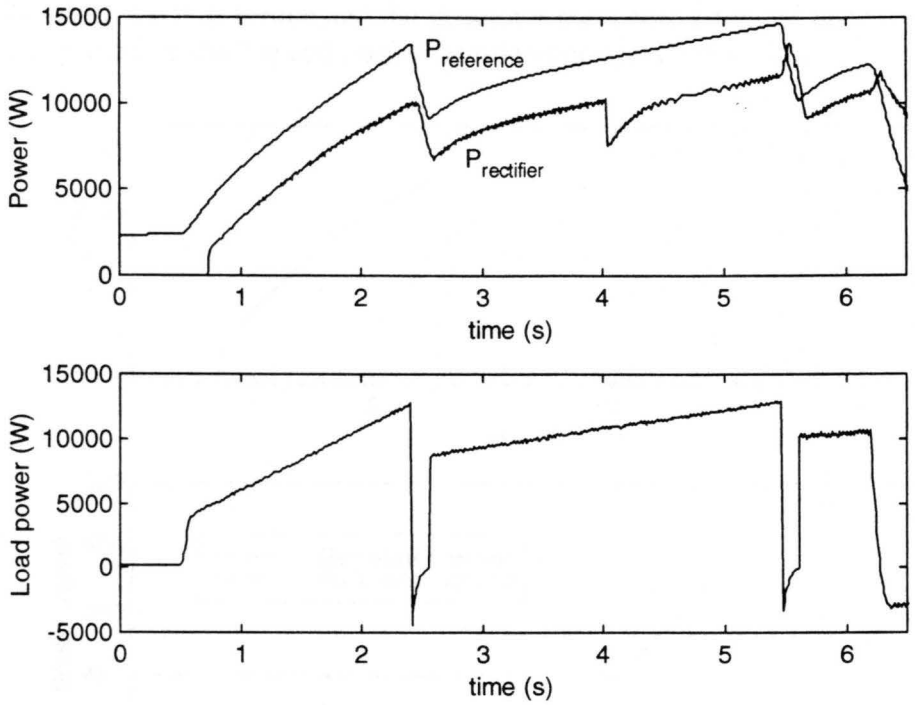

Figure 75: APU power reference, APU output power, and the battery pack load power.

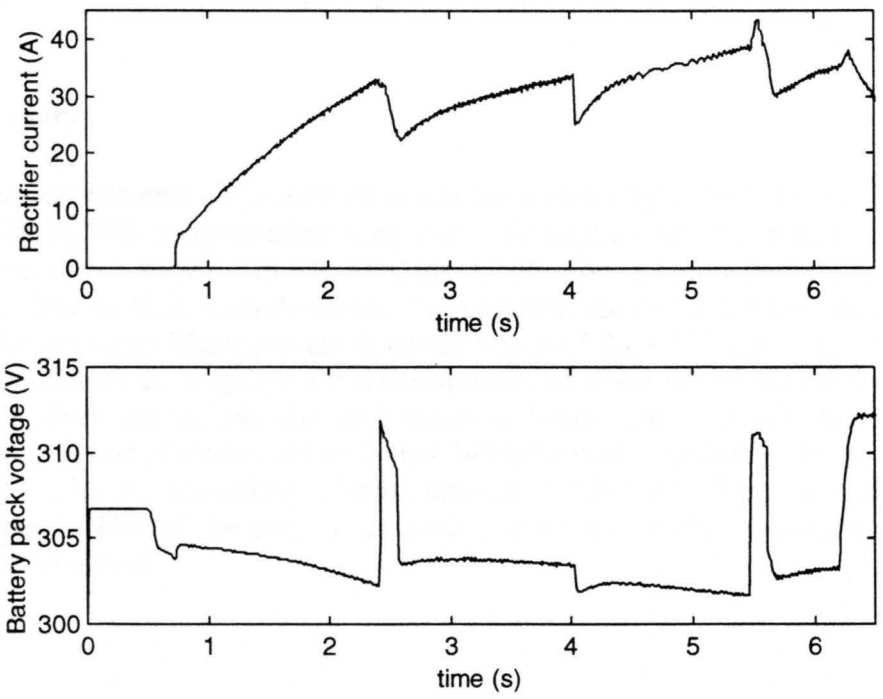

Figure 76: Rectifier load current and battery pack voltage.

The ICE shaft torque and the generator reference speed and actual shaft speed are shown in Figure 77. Both the ICE torque and the generator shaft speed change faster than they would in practice. The generator shaft speed tracks the reference speed very well.

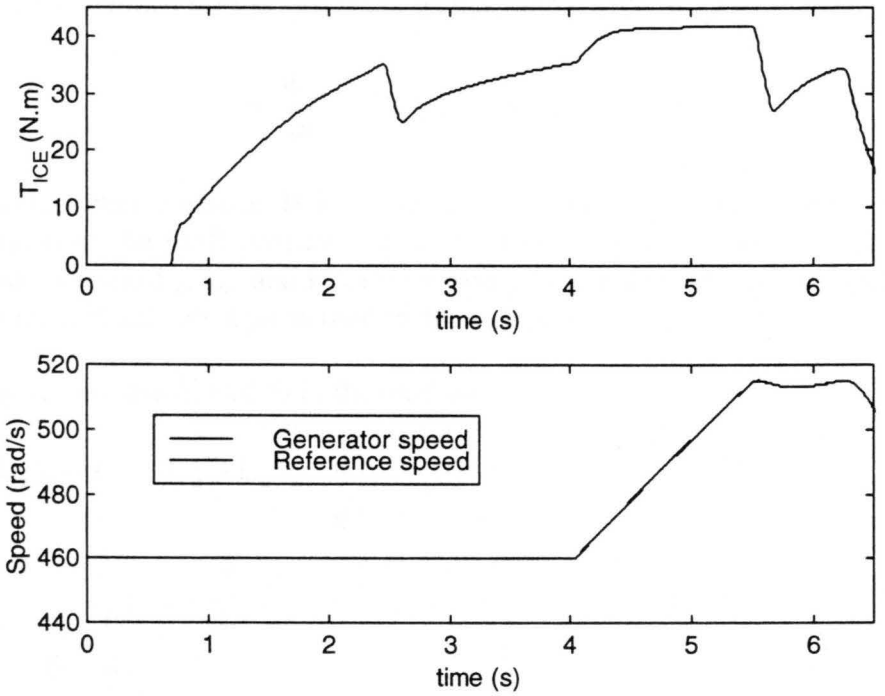

Figure 77: ICE shaft torque, and generator reference speed and actual shaft speed.

2.12 Summary

This report presents a dynamic simulator for a series hybrid electric vehicle written in the MATLAB/SIMULINK programming language. Simulation results from each of the vehicle subsystems have been shown. In addition, the results from a complete vehicle simulation have been shown. Due to time considerations, the complete model simulation had to be modified. The simulation provided illustrates the dynamic action of the HEV very well. However, further testing and evaluation are required for determination of some model parameters. In particular, the ICE model does not include the shaft torque pulsation due to combustion. Also, the APU power controller is one of many, and will most likely be modified in the future.

There is also the possibility of compiling the SIMULINK file to C-code to increase the simulation speed. Use of the present dynamic models to validate averaged or reduced order models is also an option.

3 Appendix I: System Configuration Matrices

The state equations for the synchronous machine variables take the form of

$$\mathbf{A}\frac{d\mathbf{i}_{abc}}{dt} = \mathbf{B}\mathbf{i}_{abc} - \tfrac{P}{2}\omega_r L_{md} I_{fd}\mathbf{U}(\theta_r)$$

where **A** is an inductance matrix, **B** is a resistance matrix, and **U**(θ_r) is the driving input vector and is a function of the shaft position. The matrices for each switch configuration are listed below. The row vectors $\mathbf{L}_a$, $\mathbf{L}_b$, and $\mathbf{L}_c$ are the rows of $\mathbf{L}_s$, and ϕ_a=0, ϕ_b=-2π/3, and ϕ_c=2π/3. The subscripted numerals indicate a particular vector component.

Configuration 1: switches S_1 and S_4 in the on-state.

$$\mathbf{A} = \begin{bmatrix} (\mathbf{L}_b - \mathbf{L}_a)_1 - L_L & (\mathbf{L}_b - \mathbf{L}_a)_2 & 0 \\ 1 & 1 & 0 \\ 0 & 0 & 1 \end{bmatrix}$$

$$\mathbf{B} = \begin{bmatrix} r_s - R_L & -r_s & 0 \\ 0 & 0 & 0 \\ 0 & 0 & 0 \end{bmatrix}$$

$$\mathbf{U} = \begin{bmatrix} \cos(\theta_r + \phi_a) - \cos(\theta_r + \phi_b) \\ 0 \\ 0 \end{bmatrix}$$

Configuration 2: switches S_1, S_4, and S_6 in the on-state.

$$\mathbf{A} = \begin{bmatrix} (\mathbf{L}_b - \mathbf{L}_a)_1 - L_L & (\mathbf{L}_b - \mathbf{L}_a)_2 & (\mathbf{L}_b - \mathbf{L}_a)_3 \\ (\mathbf{L}_b - \mathbf{L}_c)_1 & (\mathbf{L}_b - \mathbf{L}_c)_2 & (\mathbf{L}_b - \mathbf{L}_c)_3 \\ 1 & 1 & 1 \end{bmatrix}$$

$$\mathbf{B} = \begin{bmatrix} r_s - R_L & -r_s & 0 \\ 0 & -r_s & r_s \\ 0 & 0 & 0 \end{bmatrix}$$

$$\mathbf{U} = \begin{bmatrix} \cos(\theta_r + \phi_a) - \cos(\theta_r + \phi_b) \\ \cos(\theta_r + \phi_c) - \cos(\theta_r + \phi_b) \\ 0 \end{bmatrix}$$

Configuration 3: switches S_1 and S_6 in the on-state.

$$\mathbf{A} = \begin{bmatrix} (\mathbf{L_c} - \mathbf{L_a})_1 - L_L & 0 & (\mathbf{L_c} - \mathbf{L_a})_3 \\ 1 & 0 & 1 \\ 0 & 1 & 0 \end{bmatrix}$$

$$\mathbf{B} = \begin{bmatrix} r_s + R_L & 0 & -r_s \\ 0 & 0 & 0 \\ 0 & 0 & 0 \end{bmatrix}$$

$$\mathbf{U} = \begin{bmatrix} \cos(\theta_r + \phi_a) - \cos(\theta_r + \phi_c) \\ 0 \\ 0 \end{bmatrix}$$

Configuration 4: switches S_1, S_3, and S_6 in the on-state.

$$\mathbf{A} = \begin{bmatrix} (\mathbf{L_c} - \mathbf{L_a})_1 - L_L & (\mathbf{L_c} - \mathbf{L_a})_2 & (\mathbf{L_c} - \mathbf{L_a})_3 \\ (\mathbf{L_a} - \mathbf{L_b})_1 & (\mathbf{L_a} - \mathbf{L_b})_2 & (\mathbf{L_a} - \mathbf{L_b})_3 \\ 1 & 1 & 1 \end{bmatrix}$$

$$\mathbf{B} = \begin{bmatrix} r_s & R_L - r_s & 0 \\ -r_s & 0 & r_s \\ 0 & 0 & 0 \end{bmatrix}$$

$$\mathbf{U} = \begin{bmatrix} \cos(\theta_r + \phi_a) - \cos(\theta_r + \phi_c) \\ \cos(\theta_r + \phi_c) - \cos(\theta_r + \phi_a) \\ 0 \end{bmatrix}$$

Configuration 5: switches S_3 and S_6 in the on-state.

$$\mathbf{A} = \begin{bmatrix} 0 & (\mathbf{L_c} - \mathbf{L_b})_2 - L_L & (\mathbf{L_c} - \mathbf{L_b})_3 \\ 0 & 1 & 1 \\ 1 & 0 & 0 \end{bmatrix}$$

$$\mathbf{B} = \begin{bmatrix} 0 & r_s + R_L & -r_s \\ 0 & 0 & 0 \\ 0 & 0 & 0 \end{bmatrix}$$

$$\mathbf{U} = \begin{bmatrix} \cos(\theta_r + \phi_b) - \cos(\theta_r + \phi_c) \\ 0 \\ 0 \end{bmatrix}$$

Configuration 6: switches S_2, S_3, and S_6 in the on-state.

$$\mathbf{A} = \begin{bmatrix} (\mathbf{L_c} - \mathbf{L_b})_1 & (\mathbf{L_c} - \mathbf{L_b})_2 - L_L & (\mathbf{L_c} - \mathbf{L_b})_3 \\ (\mathbf{L_c} - \mathbf{L_a})_1 & (\mathbf{L_c} - \mathbf{L_a})_2 & (\mathbf{L_c} - \mathbf{L_a})_3 \\ 1 & 1 & 1 \end{bmatrix}$$

$$\mathbf{B} = \begin{bmatrix} 0 & R_L + r_s & -r_s \\ r_s & 0 & -r_s \\ 0 & 0 & 0 \end{bmatrix}$$

$$\mathbf{U} = \begin{bmatrix} \cos(\theta_r + \phi_b) - \cos(\theta_r + \phi_c) \\ \cos(\theta_r + \phi_a) - \cos(\theta_r + \phi_c) \\ 0 \end{bmatrix}$$

Configuration 7: switches S_2 and S_3 in the on-state.

$$\mathbf{A} = \begin{bmatrix} (\mathbf{L}_a - \mathbf{L_b})_1 & (\mathbf{L}_a - \mathbf{L_b})_2 - L_L & 0 \\ 1 & 1 & 0 \\ 0 & 0 & 1 \end{bmatrix}$$

$$\mathbf{B} = \begin{bmatrix} -r_s & r_s + R_L & 0 \\ 0 & 0 & 0 \\ 0 & 0 & 0 \end{bmatrix}$$

$$\mathbf{U} = \begin{bmatrix} \cos(\theta_r + \phi_b) - \cos(\theta_r + \phi_a) \\ 0 \\ 0 \end{bmatrix}$$

Configuration 8: switches S_2, S_3, and S_5 in the on-state.

$$\mathbf{A} = \begin{bmatrix} (\mathbf{L_a} - \mathbf{L_b})_1 - L_L & (\mathbf{L_a} - \mathbf{L_b})_2 & (\mathbf{L_a} - \mathbf{L_b})_3 \\ (\mathbf{L_b} - \mathbf{L_c})_1 & (\mathbf{L_b} - \mathbf{L_c})_2 & (\mathbf{L_b} - \mathbf{L_c})_3 \\ 1 & 1 & 1 \end{bmatrix}$$

$$\mathbf{B} = \begin{bmatrix} R_L - r_s & r_s & 0 \\ 0 & r_s & -r_s \\ 0 & 0 & 0 \end{bmatrix}$$

$$\mathbf{U} = \begin{bmatrix} \cos(\theta_r + \phi_b) - \cos(\theta_r + \phi_a) \\ \cos(\theta_r + \phi_c) - \cos(\theta_r + \phi_b) \\ 0 \end{bmatrix}$$

Configuration 9: switches S_2 and S_5 in the on-state.

$$\mathbf{A} = \begin{bmatrix} (\mathbf{L}_a - \mathbf{L}_c)_1 & 0 & (\mathbf{L}_a - \mathbf{L}_c)_2 - L_L \\ 1 & 0 & 1 \\ 0 & 1 & 0 \end{bmatrix}$$

$$\mathbf{B} = \begin{bmatrix} -r_s & 0 & r_s + R_L \\ 0 & 0 & 0 \\ 0 & 0 & 0 \end{bmatrix}$$

$$\mathbf{U} = \begin{bmatrix} \cos(\theta_r + \phi_c) - \cos(\theta_r + \phi_a) \\ 0 \\ 0 \end{bmatrix}$$

Configuration 10: switches S_2, S_4, and S_5 in the on-state.

$$\mathbf{A} = \begin{bmatrix} (\mathbf{L}_a - \mathbf{L}_c)_1 & (\mathbf{L}_a - \mathbf{L}_c)_2 & (\mathbf{L}_a - \mathbf{L}_c)_3 - L_L \\ (\mathbf{L}_a - \mathbf{L}_b)_1 & (\mathbf{L}_a - \mathbf{L}_b)_2 & (\mathbf{L}_a - \mathbf{L}_b)_3 \\ 1 & 1 & 1 \end{bmatrix}$$

$$\mathbf{B} = \begin{bmatrix} -r_s & 0 & r_s + R_L \\ -r_s & r_s & 0 \\ 0 & 0 & 0 \end{bmatrix}$$

$$\mathbf{U} = \begin{bmatrix} \cos(\theta_r + \phi_c) - \cos(\theta_r + \phi_a) \\ \cos(\theta_r + \phi_b) - \cos(\theta_r + \phi_a) \\ 0 \end{bmatrix}$$

Configuration 11: switches S_4 and S_5 in the on-state.

$$\mathbf{A} = \begin{bmatrix} 0 & (\mathbf{L}_b - \mathbf{L}_c)_1 & (\mathbf{L}_b - \mathbf{L}_c)_2 - L_L \\ 0 & 1 & 1 \\ 1 & 0 & 0 \end{bmatrix}$$

$$\mathbf{B} = \begin{bmatrix} 0 & -r_s & r_s + R_L \\ 0 & 0 & 0 \\ 0 & 0 & 0 \end{bmatrix}$$

$$\mathbf{U} = \begin{bmatrix} \cos(\theta_r + \phi_c) - \cos(\theta_r + \phi_b) \\ 0 \\ 0 \end{bmatrix}$$

Configuration 12: switches S_1, S_4, and S_5 in the on-state.

$$\mathbf{A} = \begin{bmatrix} (\mathbf{L_b} - \mathbf{L_a})_1 & (\mathbf{L_b} - \mathbf{L_a})_2 - L_L & (\mathbf{L_b} - \mathbf{L_a})_3 \\ (\mathbf{L_a} - \mathbf{L_c})_1 & (\mathbf{L_a} - \mathbf{L_c})_2 & (\mathbf{L_a} - \mathbf{L_c})_3 \\ 1 & 1 & 1 \end{bmatrix}$$

$$\mathbf{B} = \begin{bmatrix} r_s & R_L - r_s & 0 \\ -r_s & 0 & r_s \\ 0 & 0 & 0 \end{bmatrix}$$

$$\mathbf{U} = \begin{bmatrix} \cos(\theta_r + \phi_a) - \cos(\theta_r + \phi_b) \\ \cos(\theta_r + \phi_c) - \cos(\theta_r + \phi_a) \\ 0 \end{bmatrix}$$

Configuration 13: all switches in the off-state.

$\mathbf{B} = \mathbf{0}$

$\mathbf{U} = \mathbf{0}$

The state derivatives are zero. The value for **A** is irrelevant.

4 Appendix II: HEV Parameters

The following table gives the HEV parameters setup in the m-file named hev_setup.m. These are not the same parameters used in the simulations. Several changes were made for the simulation examples in order to speed up the subsystem processes.

Table 8: HEV simulation parameters.

Description	Variable name	Value
Workspace variable sampling interval	T_sample	0.0001 s
Rectifier current error	i_eps	0.01 A
Rectifier gate pulse train period	T_gate_osc	1e-4 s
Generator and ICE rotational inertia	J_sm	0.1103 kg m^2
Generator base frequency	wb_sm	376 rad/s
Magnetizing inductance	X_md	300 μH
Generator poles	Poles_sm	18
Generator phase resistance	Rs_sm	0.25 Ω
Rectifier load inductance	L_load_sm	0.01 H
Rectifier series resistance	R_load_sm	0.1 Ω
Number of battery pack batteries	Battery_number	26
Battery pack parallel capacitance	C_pack	0.01 F
Maximum W-hr rating of single battery	E_pack_max_W_hr	302 W-hr
Maximum total pack energy	E_pack_max	28.27 MJ
Initial pack energy	E_pack_initial	11.32 MJ
Lower SOC limit	SOC_low	0.4
Upper SOC limit	SOC_high	0.8
Reference SOC	SOC_ref	0.7
Lower APU power limit	P_APU_low	6 kW
APU starting delay	APU_starting_delay	0.01 s
Induction motor base frequency	IM_wb	1257 rad/s
Rated induction motor voltage	V_rated	132.8 $V_{l\text{-}n}$
Induction motor referred rotor leakage inductance	IM_Lpr	114 μH
Induction motor stator leakage inductance	IM_Ls	114 μH
Induction motor magnetizing inductance	IM_Lm	0.0036 H
Induction motor stator series resistance	IM_rs	0.0248 Ω
Induction motor referred rotor series resistance	IM_rrp	0.01438 Ω
Induction motor poles	IM_Poles	4
Electronic drive current regulator gain	CR_gain	500
IGBT forward drop	V_IGBT	1.1 V
IGBT on-state resistance	R_IGBT	4.2e-3 Ω
Road grade	Grade	0
Ambient air density	Rho	1.2 kg/m^3
Vehicle drag coefficient	C_drag	0.36

Description	Variable name	Value
Wheel radius	r_wheel	0.30 m
Vehicle frontal area	frontal_area	2.323 m^2
Gravitational constant	grav_const	9.81 m/s^2
Tire resistance coefficient	R_tire	0.00993
Vehicle total mass	Total_mass	1577 kg
Transmission marginal efficiency	Tran_efficiency	0.95

5 References

[1] D. L. Logue, "Hybrid electric vehicle simulation," University of Illinois, Tech. Rep. PAP-TR-97-9, October 1997.

[2] S. A. Splater, "Power consumption analysis of a practical series hybrid electric vehicle," University of Illinois, Tech. Rep. PAP-TR-96-10, December 1996.

[3] Data sheets shipped with motor XK6151000, Magnetek, McMinnville, TN, 1993.

[4] P. C. Krause, O. Wasynczuk, S. D. Sudhoff, *Analysis of Electric Machinery*. New York, NY: IEEE, 1995.

[5] C. Ong, *Dynamic Simulation of Electric Machinery using MATLAB/SIMULINK*. Upper Saddle River, NJ: Prentice Hall, 1998.

[6] P. T. Krein, *Elements of Power Electronics*. New York: Oxford University Press, Inc., 1998.

[7] D. W. Novotny and T. A. Lipo, *Vector Control and Dynamics of AC Drives*. New York: Oxford University Press, Inc., 1997.

[8] D. R. Stephens, *Phase-Locked Loops for Wireless Communications, Digital and Analog Implementations*. Norwell, Massachusetts: Kluwer Academic Publishers, 1998.

[9] Correspondence with Unique Machines, Inc.

[10] A. C. Dalton, "Engine simulation control of an induction motor," University of Illinois, Tech. Rep. PAP-TR-98-4, October 1998.

[11] C. H. H. Chavez, "Implementation of a multi-port fuel injection system and stoichiometry in a small V-twin engine," University of Illinois, Tech. Rep. PAP-TR-96-8, August 1996.